

Electronic Thesis and Dissertation Repository

---

5-2-2014 12:00 AM

## Design and Development of Magneto-Rheological Actuators with Application in Mobile Robotics

Wenjun Li, *The University of Western Ontario*

Supervisor: Dr. Mehrdad R. Kermani, *The University of Western Ontario*

A thesis submitted in partial fulfillment of the requirements for the Master of Engineering Science degree in Electrical and Computer Engineering

© Wenjun Li 2014

Follow this and additional works at: <https://ir.lib.uwo.ca/etd>



Part of the [Controls and Control Theory Commons](#)

---

### Recommended Citation

Li, Wenjun, "Design and Development of Magneto-Rheological Actuators with Application in Mobile Robotics" (2014). *Electronic Thesis and Dissertation Repository*. 2073.  
<https://ir.lib.uwo.ca/etd/2073>

This Dissertation/Thesis is brought to you for free and open access by Scholarship@Western. It has been accepted for inclusion in Electronic Thesis and Dissertation Repository by an authorized administrator of Scholarship@Western. For more information, please contact [wlsadmin@uwo.ca](mailto:wlsadmin@uwo.ca).

DESIGN AND DEVELOPMENT OF MAGNETO-RHEOLOGICAL  
ACTUATORS WITH APPLICATION IN MOBILE ROBOTICS

(Thesis format: Integrated Article)

by

Wenjun Li

Graduate Program in Electrical and Computer Engineering

A thesis submitted in partial fulfillment  
of the requirements for the degree of  
Master of Engineering Science

The School of Graduate and Postdoctoral Studies  
The University of Western Ontario  
London, Ontario, Canada

© Wenjun Li 2014

# Abstract

In recent years, Magneto-Rheological (MR) fluids devices are widely studied and used for various purposes. Among these MR fluids devices, the MR actuator has attracted increasing attention for last two decades. An MR actuator is usually made of an active component (motor) and MR clutches. Compared with the regular actuators, the MR actuator features compliance due to the existence of MR fluids, which is commonly consider as benefits at the aspect of safety. On the other hand, the MR actuator has advantages on controllable bandwidth, torque-mass and torque-inertia ratios compared with the other compliant actuators.

In this study, a new closed-loop, Field-Programable-Gate-Array (FPGA) based control scheme to linearize an MR clutch's input-output relationship is presented. The feedback signal used in this control scheme is the magnetic field acquired from hall sensors within the MR clutch. The FPGA board uses this feedback signal to compensate for the nonlinear behavior of the MR clutch using an estimated model of the clutch magnetic field. The local use of an FPGA board will dramatically simplify the use of MR clutches for torque actuation. The effectiveness of the proposed technique is validated using an experimental platform that includes an MR clutch as part of a compliant actuation mechanism. The results clearly demonstrate that the use of the FPGA based closed-loop control scheme can effectively eliminate hysteretic behaviors of the MR clutch, allowing to have linear actuators with predictable behaviors. Moreover, a novel optimization design of MR clutches is proposed. Based on the optimization, the characteristics of MR clutches in three common configurations are discussed and compared. People can select suitable configuration of MR clutch before design. Lastly, a lightweight mobile robot is developed by using MR actuators. This mobile robot also has large driving force and can stop at any positions without running the motor.

**Keywords:** Magneto-Rheological actuator, Hall sensor, Optimization, mobile robot

–

## **Co-Authorship Statement**

The work presented in this thesis involved in part collaboration with Peyman Yadmelat and Alex Shafer who shared their knowledge of the Magneto-Rheological clutches. I would also like to acknowledge the contribution of University Machine Services staffs Ian J. Vinkenleugel in the manufacturing of the MR clutches and mobile robot.

## **Dedication**

I would like to dedicate this thesis to my family, especially to my mother and grandfather.

## **Acknowledgments**

I would like to express my sincere appreciation and gratitude to Dr. Mehrdad Kermani for supervising my research during my M.E.Sc. studies. I would like to thank his patience and understanding throughout the last two and half years. I would also like to thank my lab-mates, Peyman Yadmellat, Alex Shafer, Vahid Setoudeh Nejad, Nima Najmaei, and Dr. Ali Asadian for sharing their experience and guidance for me.

# Contents

<b>Abstract</b>	<b>ii</b>
<b>Co-Authorship Statement</b>	<b>iii</b>
<b>Dedication</b>	<b>iv</b>
<b>Acknowledgments</b>	<b>v</b>
<b>List of Figures</b>	<b>ix</b>
<b>List of Tables</b>	<b>xii</b>
<b>List of Appendices</b>	<b>xiii</b>
<b>1 Introduction</b>	<b>1</b>
1.1 Background . . . . .	1
1.2 Motivations . . . . .	4
1.3 Main Contributions . . . . .	6
1.4 Thesis Outlines . . . . .	8
<b>Bibliography</b>	<b>9</b>
<b>2 Linearized Torque Actuation using FPGA-Controlled Magneto-Rheological Actuators</b>	<b>14</b>
2.1 Introduction . . . . .	15
2.2 MR Clutch . . . . .	18
2.2.1 Placement of hall sensors . . . . .	19

2.3	Torque Control in the MR Clutch . . . . .	22
2.3.1	Control Scheme . . . . .	24
2.3.2	Static Model . . . . .	25
2.3.3	Dynamic Model . . . . .	27
2.3.4	Implementation on an FPGA Board . . . . .	29
2.4	Experimental Results . . . . .	29
2.4.1	Validation of the Proposed Model . . . . .	30
2.4.2	Torque Control Experiments . . . . .	32
2.5	Conclusion . . . . .	40
	<b>Bibliography</b>	<b>42</b>
<b>3</b>	<b>Design Optimization and Comparison of Magneto-Rheological Actuators</b>	<b>45</b>
3.1	Introduction . . . . .	46
3.2	MR clutch . . . . .	48
3.2.1	Drum MR clutch . . . . .	49
3.2.2	Single-Disk MR clutch . . . . .	51
3.2.3	Multi-Disk MR clutch . . . . .	52
3.3	Design Optimization . . . . .	54
3.3.1	Material Selection . . . . .	54
3.3.2	Optimal design of MR clutches . . . . .	56
3.4	Results and Discussions . . . . .	58
3.4.1	Validation of the model in COMSOL Multiphysics . . . . .	60
3.4.2	Analysis Results . . . . .	62
3.5	Conclusion . . . . .	70
	<b>Bibliography</b>	<b>71</b>
<b>4</b>	<b>Design, Development, and Validation of a Mobile Robot Actuated by Magneto-Rheological (MR) Actuators</b>	<b>74</b>
4.1	Introduction . . . . .	75
4.2	Development of the MR actuator . . . . .	77

4.2.1	Optimization design of the MR clutch . . . . .	78
4.2.2	Mechanical Design of the MR clutch . . . . .	81
4.3	Development of Mobile Robot . . . . .	83
4.4	Conclusion . . . . .	85
	<b>Bibliography</b>	<b>87</b>
<b>5</b>	<b>Conclusion and Future Works</b>	<b>89</b>
5.1	Conclusion . . . . .	89
5.2	Future Works . . . . .	91
	<b>Curriculum Vitae</b>	<b>94</b>

# List of Figures

1.1	The behavior of MR and ER fluids. . . . .	2
2.1	Block diagram of the proposed control scheme. . . . .	18
2.2	2D MR clutch model and the magnetic field distribution. . . . .	20
2.3	Applying different input currents, the magnetic field distribution on output disks. . . . .	20
2.4	Cross-section of a multi-disk MR clutch. . . . .	21
2.5	The position of hall sensors in an MR clutch. . . . .	21
2.6	Rate-dependent hysteresis for an MR clutch. . . . .	23
2.7	MR clutch current-torque model. . . . .	23
2.8	Applying a sinusoidal current to an MR clutch: (a) output torque vs. magnetic field; (b) yield stress vs. magnetic field for MR fluids and the piecewise linear function. . . . .	24
2.9	Closed-loop control configuration using embedded hall sensors. . . . .	25
2.10	Proposed model for output torque estimation. $B(t)$ is the magnetic field, and $T_s(t)$ and $\hat{T}(t)$ are static and dynamic estimations of the output torque, respectively. . . . .	25
2.11	Output torque of the MR clutch in response to a step input current; (a) measured and estimated torques, (b) error between the measured and estimated torques. . . . .	27
2.12	Schematic architecture of the experimental setup. . . . .	30
2.13	Multi-Sine input current, (a) estimated and measured torques, (b) error between measured and estimated torques . . . . .	33

2.14 Swept-Sine input current, (a) estimated and measured torques, (b) error between measured and estimated torques . . . . .	33
2.15 Closed-loop control scheme for: (a) 1st configuration, (b) 2nd configuration.	34
2.16 Closed-loop tracking of a square reference torque using hall sensor vs ex- ternal force/ torque sensor; (a) generated torques, (b) error signal, (c) input current, and (d) magnetic field inside MR clutch. . . . .	35
2.17 Closed-loop tracking of a 1 Hz sinusoid reference torque using hall sensor vs external force/ torque sensor; (a) generated torques, (b) error signal, (c) input current, and (d) magnetic field inside MR clutch. . . . .	36
2.18 Closed-loop tracking of a 5 Hz sinusoid reference torque using hall sensor vs external force/ torque sensor; (a) generated torques, (b) error signal, (c) input current, and (d) magnetic field inside MR clutch. . . . .	37
2.19 Closed-loop tracking of a 10 Hz sinusoid reference torque using hall sensor vs external force/ torque sensor; (a) generated torques, (b) error signal, (c) input current, and (d) magnetic field inside MR clutch. . . . .	38
2.20 Closed-loop tracking of a Multi-Sine reference torque using hall sensor vs external force/ torque sensor; (a) generated torques, (b) error signal, (c) input current, and (d) magnetic field inside MR clutch. . . . .	39
2.21 Embedded FPGA board inside MR clutches. . . . .	41
3.1 Use of MR clutch to an actuator. . . . .	47
3.2 Cross section of the drum-type MR clutch. . . . .	49
3.3 Cross section of a single-disk-type MR clutch. . . . .	52
3.4 Cross section of the multi-disk-type MR clutch. . . . .	53
3.5 Shear stress versus magnetic field intensity for MRF-140CG. . . . .	55
3.6 Relative permeability versus magnetic flux density for MRF-140CG. . . . .	56
3.7 Relative permeability versus magnetic flux density for AISI steel 1018. . . . .	56
3.8 Cross section of the coil. . . . .	58
3.9 Magnetic flux density contour map in drum configuration with 2 W input power. . . . .	59

3.10	Magnetic flux density contour map in single-disk configuration with 2 $W$ input power. . . . .	60
3.11	Magnetic flux density contour map in 3-disk configuration with 2 $W$ input power. . . . .	61
3.12	Magnetic flux density contour map in corresponding model of MR clutch with 1 $A$ input current. . . . .	62
3.13	Cross section of the coil circuit. . . . .	65
3.14	Torque-mass ratio versus input power for three configurations. . . . .	66
3.15	Torque-mass ratio versus input power for different output disks configurations. . . . .	68
3.16	Torque-mass ratio versus to input power for different gap sizes. . . . .	69
4.1	Cross section of the MR clutch without outer part. . . . .	78
4.2	Cross section of the coil. . . . .	80
4.3	Cross section of the MR clutch. . . . .	82
4.4	The optimal designed MR clutch. . . . .	83
4.5	Schematic architecture of the mobile robot. . . . .	84
4.6	Design of the mobile robot. . . . .	85

# List of Tables

1.1	ER fluids versus MR fluids . . . . .	4
2.1	RMSE of Dynamic Model . . . . .	32
2.2	RMSE for torque control experiments . . . . .	40
2.3	RMSE for torque control experiments with different models . . . . .	40
3.1	Optimized dimensional variables in Drum configuration . . . . .	59
3.2	Optimized dimensional variables in Single-Disk configuration . . . . .	60
3.3	Optimized dimensional variables in Multi-Disk configuration . . . . .	61
3.4	Specifications of the developed MR clutch for the 2-DOF manipulator . . .	62
3.5	Comparison between measured results and simulation . . . . .	63
3.6	Comparison among MR clutches in different configurations . . . . .	64
3.7	Comparison among disk-type MR clutches with different number of output disks . . . . .	67
3.8	Comparison among disk-type MR clutches with different MR fluids gap sizes	68
3.9	Conclusion of comparisons among different configurations . . . . .	69
4.1	Optimized dimensional parameters of the MR clutch . . . . .	79
4.2	Maximum current density for different gauge copper wires . . . . .	80
4.3	Specifications of the MR clutch . . . . .	82
4.4	Specifications of the mobile vehicle . . . . .	85
5.1	Comparison of output torque among MR clutches with different MR-fluid gaps sizes. . . . .	92

# List of Appendices

# Chapter 1

## Introduction

### 1.1 Background

Magneto-Rheological (MR) and Electro-Rheological (ER) fluids are a class of smart material with variable viscosity in response to external magnetic or electric excitations. Both fluids act as suspension medium carrying micrometer or nanometer scale particles. Under normal circumstances, these particles are located randomly inside carrier fluids, making MR and ER fluids behave as liquids. However, once subjected to a external (magnetic or electric) excitations, the particles within respective fluids join into columns in the direction of the applied fields (see the Fig. 1.1). Due to this characteristic change, MR and ER fluids become viscoelastic solid and the yield stress of fluid is increased dramatically. More importantly, this kind of process is rapid and reversible, which means that MR and ER fluids can change from liquid to solid and back to liquid within milliseconds. In other words, the viscosity of the MR and ER fluids can be accurately controlled by modulating the strength of the corresponding fields. It is due to these properties of the fluids that MR and ER fluids have increasingly considered and used in various applications in recent years.

While ER fluids were first reported in 1940s [1, 2], they did not attract much attentions for commercial purposes for the first few decades after their discovery. In 1990s, the use of silicon oil as the carrier fluid in ER fluids [3] improved the tolerance of the fluid to high temperature[4], enabling its commercial applications; of which ER dampers and clutches are the most well-known applications. In 1992, Petek considered an ER damper as a

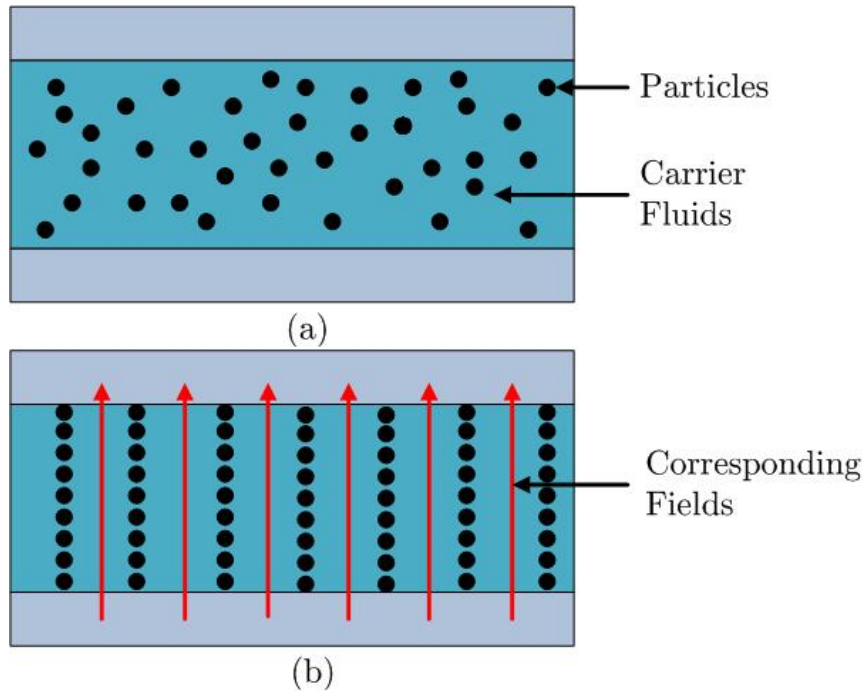


Figure 1.1: The behavior of MR and ER fluids.

shock absorber [5] and experimentally proved that ER dampers had advantages over other dampers. Three years later, the same author ER dampers were used in a car suspension system [6]. In 1995, a small-size, high-voltage ER damper was developed again as car suspension system [7]. ER fluids have also been widely used to viscously couple components as in ER clutches and brakes. The experimental results in [8] demonstrate that the output torque of an ER clutch is dependent on the strength of the electric field, the temperature, and the input velocity. By using these characteristics, a 2 degrees-of-freedom (DOF) passive force display using ER brakes was developed in [9]. One main advantage of ER clutches within the class of devices with similar functionality is the ability of ER clutches to control the impedance as reported in [10]. Another interesting study on ER fluids was conducted by Kenaley [11] in which ER fluids were used in order to simulate the behavior of a human's finger. In this study ER fluids were placed between two component: "skin" and "bone". The stiffness of ER fluids was changed by controlling the magnitude of the electrical field applied between "skin" and "bone" allowing for the grippers that were built using such fingers to lift lightweight objects with small grasping force. ER dampers have also been used in the field of civil engineering [12, 13, 14].

Similar to ER fluids, the initial discovery of MR fluids can be traced back to the 1940s. Jacob Rabinow published a paper [15] about MR fluids and patented the initial MR fluids devices [16]. Not unlike ER fluids, MR fluids did not receive much attention until the early 1990s. In 1993, a mathematic model that described the MR effect was proposed by Kordonsky [17]. In the same year, a high-strength MR fluids was proposed [18]. In 1994, MR fluid dampers with magnetic valves for controlling the flow parameters of the MR fluids were developed [19]. With further enhancement of the MR fluids, MR fluids devices became commercial successes in the late 1990s [20]. A controllable MR damper was applied to a track suspension [21]. In another example, an MR clutch was used to control the fan speed of an engine in a cooling system [22]. The use of MR fluid dampers for building earthquake-proof structure with millisecond response time was explored by mechanical and civil engineers [23]. More recently, MR fluids devices were applied to different fields and achieved a huge success.

MR fluids also offer advantages as actuators. A simple MR actuator was developed in [24]. The experimental results proved that the MR actuators featured high torque to mass and torque to inertia ratios, simple interfaces and safe actuation. The response time of this actuator was later improved by replacing the aluminum connections in the actuators with plastic connections and applying a closed-loop torque control scheme [25].

MR actuators were employed in exoskeleton legs [26] as well as assistive knee braces [27]. In these applications, the MR actuator acts as an MR clutch to augment the human's motions while acting as an MR brake when the motion required to be limited. The characteristics of MR actuators also make them an ideal candidate for applications involving human-robot interactions. To this end, Shafer and Kermani proposed a new actuation concept called, Distributed Active Semi-Active (DASA) actuation and experimentally validated it [28]. Using this concept, the same research group developed a 1-DOF, 2-DOF, and 3-DOF antagonistically actuated manipulators [29], [30], and [31]. It was shown that these manipulators were not only capable of enhancing the safety of the robots towards their human counterparts but also maintaining the desired performance of operations in demanding tasks.

While ER and MR fluids can both offer advantages, each fluid may best suit a particular

application given their differences in their characteristics [20, 32, 33, 34, 35]. Table 1.1 lists the main differences between the types of fluids. As observed, MR fluids feature much higher maximum yield stress than ER fluids. Hence, in a similar configuration MR fluid can generate larger output torque than ER fluids. Moreover MR fluids are less sensitive to thermal variations and have better stability. On the other hand, the excitation of ER fluids using external electric fields are mechanically less complex and less heavy and the particles in ER fluids are less prone to settling, although these particles require longer time to relax than the time for aligning themselves with the direction of external electric field [36].

Given the subject of the study of this thesis, the focus will be on MR fluids and MR fluids actuation.

Table 1.1: ER fluids versus MR fluids

Representative feature	ER fluids	MR fluids
Maximum yield stress	2-5 kPa	50-100 kPa
Power supply	2-5 kV @ 1-10 mA	2-24 V @ 1-2 A
Response time	Some millisecond	Some millisecond
Operational field	4 kV/mm	250 kA/m
Energy density	0.001 J/cm <sup>3</sup>	0.1 J/cm <sup>3</sup>
Stability	Poor for most impurities	Good for most impurities
Operational temperature	-25 °C up to +125 °C	-40 °C up to +150 °C

## 1.2 Motivations

In recent years, the use of Magneto-Rheological (MR) fluids for realizing compliant actuation has received increasing attentions. In comparison to other compliant actuators, MR actuators can provide larger controllable bandwidth and safe actuation inherent in the design. To this effect, a compliant actuator using an MR clutch for variable coupling of the input and output was studied in [24]. This actuator provided a maximum torque of 5 Nm. Later, the transient response of the actuator was improved to near 30Hz by replacing Alu-

minum with an engineering plastic in all connecting parts of the MR clutch [25]. An MR actuator with a locking mechanism was used as an assistive knee brace in [27]. The MR device acted as a brake when the lock was on and as a clutch when the lock was off. The locking mechanism was used to interlock the shaft of the MR actuator to the brace. Dual Differential Rheological Actuator (DDRA) is another MR fluids based compliant actuator [37]. DDRA couples two different MR brakes, each of which moved at the same speed but in opposite directions. The coupled MR brakes generate an output torque with an applied magnetic field. The controllable bandwidth of DDRA is limited to 4Hz and the hysteresis of the MR brakes have not been addressed.

In our previous body of work, we developed a new actuation concept known as Distributed Active Semi-Active (DASA) Actuator using MR clutches [29]. In this actuation mechanism an electric motor (active component) can be coupled to (theoretically) unlimited number of MR clutches (semi-active component), where all clutches receive their power from the motor (through distributed actuations). The electric motor provides a rather constant power and each MR clutch controls transmission of the torque to its output shaft independently. DASA actuator has high torque-to-mass and torque-to-inertia ratios and in comparison to similar actuation concepts features a more compact structure [28]. The performance of the actuator in terms of the controllable bandwidth and time response competes with servo motors within the same torque range [29]. The use of MR clutches in DASA actuation, however, presents a nonlinear hysteretic relationship between the input current and output torque of the actuator. This nonlinear relationship poses a challenge in controlling the actuator. In order to overcome this shortcoming, a new hysteresis model to replicate the nonlinear relationship of the actuator's input and output was developed [38, 39]. This nonlinearity is mainly manifested between the input current to the actuator and the developed magnetic field inside the actuator and it has been shown that the shear stress of MR fluids has a one-to-one and nearly linear relationship with the applied magnetic field [29]. In other words, the output torque of DASA actuation is almost linearly proportional to the intensity of the applied magnetic field and the nonlinear behavior of the actuator is mainly due to the hysteretic relationship between the input current of the actuator and the developed magnetic field.

The design of MR devices for optimum performance is not a trivial task and Finite Element Analysis (FEA) and other optimization techniques have been increasingly employed to design more performance MR devices recently. A rotary MR brake was designed in [40] for a prosthetic knee optimized for maximum output torque and minimum off-state torque. The number of turns for a electromagnetic coil inside an MR brake was optimized in [41]. Multi objectives optimization techniques were employed in [42, 43], to design an MR brake with large output torque and small weight. The geometrical parameters of a disk-type MR brake were optimized in [44]. The objective of the optimization was to maximize the output torque of an MR brake which was constrained with a certain space. Achieving maximum magnetic flux density on MR fluids was selected as the objective of the optimization in [45]. A T-shape MR brake that used magnetic field in the axial and radial directions was proposed in [46]. The geometrical parameters of this brake were optimized considering the output torque, the mass of the brake, and the temperature caused by friction. Unlike the design of MR devices mentioned above, achieving as large output torque as possible in designing MR clutches is not the primary concern. A larger output torque in an MR clutch may lead to more power consumption or lower control resolution. The output torque of an MR clutch can be controlled using two inputs, namely the input current and the input mechanical power. In practice, the input mechanical power is often kept as a constant and an MR clutch is mainly controlled using the input current. The value of the input current is determined by the resistance of the coil inside the MR clutch and the electrical components outside the MR clutch. The resistance of the coil is dependent on the dimensions of the coil which can be optimized. Yet, the electrical components are normally determined prior to designing the MR clutch.

### **1.3 Main Contributions**

The main contributions of this dissertation are listed as follows:

#### **The Linearization of the MR Actuator**

A novel closed-loop control scheme to control the output torque of the MR actuator is pro-

posed. In this control scheme, the feedback signal is the magnetic flux intensity acquired by a Hall sensor within the MR clutch. Moreover, an embedded circuit board based on Field Programmable Gate Array (FPGA) is designed. This FPGA circuit board uses the feedback signal to compensate for the nonlinear behavior of the MR clutch using an estimated model of the clutch magnetic field. The local use of an FPGA board will dramatically simplify the use of MR clutches for torque actuation. The effectiveness of the proposed technique is validated using an experimental platform that includes an MR clutch as part of a compliant actuation mechanism. The results clearly demonstrate that the use of the proposed FPGA based closed-loop control scheme can effectively eliminate hysteretic behaviors of the MR clutch, allowing linear actuators with predictable behaviors.

### **Design Optimization and Comparison of MR Actuators**

An optimization method for designing MR clutches is studied. The proposed method optimizes the geometrical dimensions of an MR clutch, hence its mass, for given output torque and electrical input power. The main idea behind this optimization is that the input power and output torque are two parameters that are normally known to the designer prior to the design of an MR clutch and considering these parameters in the optimization as fixed values has a practical significance. Having presented the optimization method, we compare the characteristics of three different MR clutch configurations in order to demonstrate the effectiveness of the proposed method. A comparison between the drum, single-disk and multi-disk configurations of MR clutches is performed. Using the proposed method one can select a suitable configuration as well as the geometrical dimensions for an MR clutch that best suits the requirements of each individual design.

### **Implementation MR Actuators on the Mobile Robot**

A lightweight mobile robot prototype is designed and developed by using MR actuators as actuation. Due to the one active-multi semi-active structure of the MR actuator, the prototype is able to move omni-directionally only through applying one motor and two MR clutches which are also designed as the wheel components. The MR clutches used in the prototype are optimized by considering the input power and the weight. To this end, the

prototype can generate high drive force as well as keep small weight and low power consumption. Moreover, the control of the mobile robot can be obtained in two ways. One is to control the rotating speed/circles of wheels (MR clutches) by using the embedded encoders. The other way is to command the output torque of wheels (MR clutches), because the output torque of the MR actuator is able to be controlled without any torque sensors. Meanwhile, the MR clutches on the prototype can also function as brakes when the motor is turned off. Last but not the least, the existence of compliance in the MR actuator theoretically provides infinite gear ratio to the robot and also prevents damages to core component such as motor, motion-transmit shaft and electronic control devices.

## 1.4 Thesis Outlines

Chapter 2 firstly reviews the structure and the hysterical input-output relationship of MR clutches. Different methods to overcome this control challenge are analyzed and a novel FPGA based closed-loop control scheme is proposed. A model that estimates the output torque is also presented in this chapter. Moreover, experimental results for torque control using estimated torque values are reported and compared with those obtained using actual torque measurements.

In Chapter 3, a brief introduction to different configurations of MR clutches such as single-disk, multi-disk and drum is given. The characteristics of different configurations are analyzed which includes a detailed analysis of output torques among configurations. Chapter 3 also reviews some proposed optimization and reports a new optimization method that considers the input power and output torque. Lastly, a detailed comparison among different configurations of MR clutches is reported by using the new proposed optimization.

Chapter 4 discusses the structure of a new-designed MR clutch and a mobile robot using MR clutches as actuation. The discussion includes mechanical structure, optimization design, material selection and electronics devices design. Chapter 4 also reports the advantages of this MR clutch-driven mobile robot.

Chapter 5 concludes this thesis and discusses the future work.

## Bibliography

- [1] W. M. Winslow, "Method and means for translating electrical impulses into mechanical force," Mar. 25 1947. US Patent 2,417,850.
- [2] W. M. Winslow, "Induced fibrillation of suspensions," *Journal of applied physics*, vol. 20, no. 12, pp. 1137–1140, 2004.
- [3] J. D. Carlson, "Electrorheological fluids," Sept. 20 1988. US Patent 4,772,407.
- [4] W. E. Armstrong and F. E. Filisko, "Electric field dependent fluids," May 17 1988. US Patent 4,744,914.
- [5] N. K. Petek, "An electronically controlled shock absorber using electrorheological fluid," tech. rep., SAE Technical Paper, 1992.
- [6] N. K. Petek, D. J. Romstadt, M. B. Lizell, and T. R. Weyenberg, "Demonstration of an automotive semi-active suspension using electrorheological fluid," *SAE PUBLICATION SP 1074. NEW DEVELOPMENTS IN VEHICLE DYNAMICS, SIMULATION, AND SUSPENSION SYSTEMS (SAE TECHNICAL PAPER 950586)*, 1995.
- [7] M. Sturk, X. Wu, and J. Wong, "Development and evaluation of a high voltage supply unit for electrorheological fluid dampers," *Vehicle System Dynamics*, vol. 24, no. 2, pp. 101–121, 1995.
- [8] C. A. Papadopoulos, "Brakes and clutches using er fluids," *Mechatronics*, vol. 8, no. 7, pp. 719–726, 1998.
- [9] M. Sakaguchi, J. Furusho, and N. Takesue, "Passive force display using er brakes and its control experiments," in *Virtual Reality, 2001. Proceedings. IEEE*, pp. 7–12, IEEE, 2001.
- [10] T. Nakamura, N. Saga, and M. Nakazawa, "Impedance control of a single shaft-type clutch using homogeneous electrorheological fluid," *Journal of intelligent material systems and structures*, vol. 13, no. 7-8, pp. 465–469, 2002.

- [11] G. L. Kenaley and M. R. Cutkosky, “Electrorheological fluid-based robotic fingers with tactile sensing,” in *Robotics and Automation, 1989. Proceedings., 1989 IEEE International Conference on*, pp. 132–136, IEEE, 1989.
- [12] R. Ehrgott and S. Masri, “Modeling the oscillatory dynamic behaviour of electrorheological materials in shear,” *Smart Materials and Structures*, vol. 1, no. 4, p. 275, 1992.
- [13] H. P. Gavin and R. D. Hanson, “Characterization of an er active member,” in *Structures Congress XII*, pp. 863–868, ASCE, 1994.
- [14] H. P. Gavin, *Electrorheological dampers for structural vibration suppression*. No. 35, University of Michigan, 1994.
- [15] J. Rabinow, “The magnetic fluid clutch,” *Electrical Engineering*, vol. 67, no. 12, p. 1167–1167, 1948.
- [16] J. Rabinow, “Rabinow,” Nov. 20 1951. US Patent 2,575,360.
- [17] W. Kordonsky, “Magnetorheological effect as a base of new devices and technologies,” *Journal of Magnetism and Magnetic Materials*, vol. 122, no. 1, pp. 395–398, 1993.
- [18] K. D. Weiss, T. G. Duclos, J. D. Carlson, M. J. Chrzan, and A. J. Margida, “High strength magneto-and electro-rheological fluids,” tech. rep., SAE Technical Paper, 1993.
- [19] J. D. Carlson and M. J. Chrzan, “Magnetorheological fluid dampers,” Jan. 11 1994. US Patent 5,277,281.
- [20] M. R. Jolly, J. W. Bender, and J. D. Carlson, “Properties and applications of commercial magnetorheological fluids,” in *5th Annual International Symposium on Smart Structures and Materials*, pp. 262–275, International Society for Optics and Photonics, 1998.

- [21] J. Carlson and B. Spencer Jr, "Magneto-rheological fluid dampers for semi-active seismic control," in *Proc. of the 3rd Int. Conf. on Motion and Vibr. Control*, pp. 35–40, 1996.
- [22] X. Xu and C. Zeng, "Design of a magneto-rheological fluid clutch based on electromagnetic finite element analysis," in *Computer Engineering and Technology (ICCET), 2010 2nd International Conference on*, vol. 5, pp. V5–182, IEEE, 2010.
- [23] H. S. Works, "How smart structures will work."
- [24] N. Takesue, H. Asaoka, J. Lin, M. Sakaguchi, G. Zhang, and J. Furusho, "Development and experiments of actuator using mr fluid," in *Industrial Electronics Society, 2000. IECON 2000. 26th Annual Conference of the IEEE*, vol. 3, pp. 1838–1843, IEEE, 2000.
- [25] N. Takesue, J. Furusho, and Y. Kiyota, "Fast response mr-fluid actuator," *JSME International Journal Series C*, vol. 47, pp. 783–791, 2004.
- [26] J. Chen and W.-H. Liao, "Design and control of a magnetorheological actuator for leg exoskeleton," in *Robotics and Biomimetics, 2007. ROBIO 2007. IEEE International Conference on*, pp. 1388–1393, IEEE, 2007.
- [27] J. Chen and W. Liao, "Design, testing and control of a magnetorheological actuator for assistive knee braces," *Smart Materials and Structures*, vol. 19, no. 3, p. 035029, 2010.
- [28] A. S. Shafer and M. R. Kermani, "On the feasibility and suitability of mr fluid clutches in human-friendly manipulators," *Mechatronics, IEEE/ASME Transactions on*, vol. 16, no. 6, pp. 1073–1082, 2011.
- [29] A. S. Shafer and M. R. Kermani, "Design and validation of a magneto-rheological clutch for practical control applications in human-friendly manipulation," in *Robotics and Automation (ICRA), 2011 IEEE International Conference on*, pp. 4266–4271, IEEE, 2011.

- [30] P. Yadmellat, A. S. Shafer, and M. R. Kermani, “Design and development of a single-motor, two-dof, safe manipulator,”
- [31] A. S. Shafer and M. R. Kermani, “Development of high performance intrinsically safe 3-dof robot,” in *Robotics and Automation (ICRA), 2014 IEEE International Conference on*, IEEE.
- [32] A.-G. Olabi and A. Grunwald, “Design and application of magneto-rheological fluid,” *Materials & design*, vol. 28, no. 10, pp. 2658–2664, 2007.
- [33] R. W. Phillips, *Engineering applications of fluids with a variable yield stress*. PhD thesis, University of California, Berkeley, 1969.
- [34] J. Carlson, D. Catanzarite, and K. St. Clair, “Commercial magneto-rheological fluid devices,” *International Journal of Modern Physics B*, vol. 10, no. 23n24, pp. 2857–2865, 1996.
- [35] J. D. Carlson, “What makes a good mr fluid?,” *Journal of Intelligent Material Systems and Structures*, vol. 13, no. 7-8, pp. 431–435, 2002.
- [36] T. C. Halsey and W. Toor, “Structure of electrorheological fluids,” *Physical review letters*, vol. 65, no. 22, p. 2820, 1990.
- [37] P. Fauteux, M. Lauria, B. Heintz, and F. Michaud, “Dual-differential rheological actuator for high-performance physical robotic interaction,” *Robotics, IEEE Transactions on*, vol. 26, no. 4, pp. 607–618, 2010.
- [38] P. Yadmellat and M. R. Kermani, “Adaptive modeling of a magneto-rheological clutch,” in *IEEE/ASME Transactions on Mechatronics, Accepted 2nd round, under the 3rd revision*.
- [39] P. Yadmellat and M. R. Kermani, “Output torque modeling of a magneto-rheological based actuator,” in *World Congress*, vol. 18, pp. 1052–1057, 2011.

- [40] K. Gudmundsson, F. Jonsdottir, and F. Thorsteinsson, "A geometrical optimization of a magneto-rheological rotary brake in a prosthetic knee," *Smart Materials and Structures*, vol. 19, no. 3, p. 035023, 2010.
- [41] N. C. Rosenfeld and N. M. Wereley, "Volume-constrained optimization of magneto-rheological and electrorheological valves and dampers," *Smart Materials and Structures*, vol. 13, no. 6, p. 1303, 2004.
- [42] K. Karakoc, E. J. Park, and A. Suleman, "Design considerations for an automotive magnetorheological brake," *Mechatronics*, vol. 18, no. 8, pp. 434–447, 2008.
- [43] E. J. Park, L. F. da Luz, and A. Suleman, "Multidisciplinary design optimization of an automotive magnetorheological brake design," *Computers & structures*, vol. 86, no. 3, pp. 207–216, 2008.
- [44] Q. Nguyen and S. Choi, "Optimal design of an automotive magnetorheological brake considering geometric dimensions and zero-field friction heat," *Smart Materials and Structures*, vol. 19, no. 11, p. 115024, 2010.
- [45] N. Guo, H. Du, and W. Li, "Finite element analysis and simulation evaluation of a magnetorheological valve," *The international journal of advanced manufacturing technology*, vol. 21, no. 6, pp. 438–445, 2003.
- [46] Q. Nguyen and S. Choi, "Optimal design of a novel hybrid mr brake for motorcycles considering axial and radial magnetic flux," *Smart Materials and Structures*, vol. 21, no. 5, p. 055003, 2012.

## Chapter 2

# Linearized Torque Actuation using FPGA-Controlled Magneto-Rheological Actuators

*The material in this chapter is published in "IEEE/ASME Transactions on Mechatronics". A part of this work has also been published in "IEEE International Conference of Robotics and Automation (ICRA) 2014".*

This chapter presents a method to linearize the input-output of an MR actuator. Instead of modeling the hysteretic behavior of the MR actuator, a novel closed-loop control scheme is proposed to compensate the hysteresis. The feedback signal of the control scheme is the magnetic flux density acquired by the hall sensor inside the MR clutch. A novel model is able to estimate the output torque by using the magnetic field information is proposed. Compared to the other hysteretic models, the proposed model is computational efficient and easy to be applied in control scheme. Therefore, a simple PID controller can be employed to compensate the error between the desired and estimated torque. In this way, the output torque of an MR actuator can be accurately commanded without using any torque sensors. Moreover, the closed-loop control scheme is implemented on an FPGA circuit board than is embedded in the MR clutch. To this end, the MR actuator can be considered as a totally linear torque actuation. A set of experiments is performed to validate the performance and effectiveness of the proposed control scheme.

## 2.1 Introduction

During the past two decades, a wide range of compliant actuators have been proposed and developed within the context of Human-Compatible, and Human-Friendly Robots. The main idea behind introducing compliance in the actuation is to reduce the effective impedance of the actuator for leveraging the safety properties of the actuator [1, 2]. Pneumatic muscle-like actuators are perhaps among the earlier forms of compliant actuators (e.g. McKibben muscles [3]). The output impedance of pneumatic actuators is typically low due to the close-to-zero inductance of the compressible gas in the actuator. Unfortunately, the compliance of pneumatic actuators results in a reduced controllable bandwidth of these actuators.

Compliant actuators have also been realized mechanically. Series Elastic Actuator (SEA) [4] is an initial attempt to reduce the actuator's impedance using an elastic element placed between the motor and its load. Within the controllable bandwidth of the actuator, SEA has a very low output impedance, and beyond its bandwidth, SEA impedance matches the stiffness of the elastic coupling [5]. Nonetheless, similar to pneumatic actuators, SEA suffers from a limited controllable bandwidth. To address this issue, Variable Stiffness Actuator (VSA) was proposed as an alternative compliant actuation solution [6]. VSA also integrates an elastic element into its transmission path, but unlike SEA, the stiffness of the transmission coupling is variable. This allows VSA to become more compliant during high velocity tasks and stiffer during low velocity tasks to provide both improved performance and safe actuation. Instead of incorporating an elastic element, Series Damper Actuator (SDA) incorporates a rotary damper into its transmission path to increase the bandwidth [7]. This configuration allows the output force/torque of the actuator to be controlled based on the relative angular velocity between the motor and the damper. While SDA has a slightly better bandwidth than VSA, the bandwidth is still below the demand of most high performance applications. To take advantage of both VSA and SDA concepts in one unit, Variable Impedance Actuator (VIA) was proposed [8]. A combination of a variable elastic element and a variable damping element is used to connect the input and output in VIA. This configuration allows VIA to change its impedance without compromising the band-

width. Similar to VIA, Double Actuator Unit (DAU) proposed in [9] uses two actuators and a planetary gear train to immediately reduce joint impedance following the detection of a dynamic collision.

In recent years, the use of Magneto-Rheological (MR) fluids for realizing compliant actuation has received increasing attentions. In comparison to compliant actuators mentioned above, MR actuators can provide larger controllable bandwidth and safe actuation inherent in the design. To this effect, a compliant actuator using an MR clutch coupling the input and output was studied in [10]. This actuator provided a maximum torque of 5 Nm. Later, the transient response of the actuator was improved to near 30Hz by replacing Aluminum with an engineering plastic in all connecting parts of the MR clutch [11]. An MR actuator with a locking mechanism was used as an assistive knee brace in [12]. The MR device acted as a brake when the lock was on and as a clutch when the lock was off. The locking mechanism was used to interlock the shaft of the MR actuator to the brace. Dual Differential Rheological Actuator (DDRA) is another MR fluids based compliant actuator [13]. DDRA couples two different MR brakes, each of which moved at the same speed but in opposite directions. The coupled MR brakes generate an output torque with an applied magnetic field. The controllable bandwidth of DDRA is limited to 4Hz and the hysteresis of the MR brakes have not been addressed.

In our previous body of work, we developed a new actuation concept known as Distributed Active Semi-Active (DASA) Actuator using MR clutches [14]. DASA actuation and its variations are based on a novel actuation concept whose full details and advantages have been reported in [1, 15, 16]. In this actuation mechanism an electric motor (active component) can be coupled to (theoretically) unlimited number of MR clutches (semi-active component), where all clutches receive their power from the motor (distributed actuation). The electric motor provides a rather constant power and each MR clutch controls the transmission of torque to its output shaft independently. DASA actuator has high torque-to-mass and torque-to-inertia ratios and in comparison to similar actuation concepts features a more compact structure [1]. The performance of the actuator in terms of the controllable bandwidth and time response competes with servo motors within the same torque range [14]. The use of MR clutches in DASA actuation, however, presents a nonlin-

ear hysteretic relationship between the input current and output torque of the actuator. This nonlinear relationship poses a challenge in controlling the actuator. In order to overcome this shortcoming, a new hysteresis model to replicate the nonlinear relationship between the input and output of the actuator was developed [17, 18]. Moreover, it has been shown that the shear stress of MR fluids has a one-to-one relationship with the applied magnetic field [14]. In other words, the output torque of DASA actuation is almost proportional to the intensity of the applied magnetic field and the nonlinear behavior of the actuator mainly stems from hysteretic relationship between the magnetic field and the input current of the actuator. This observation provides a foundation of the novel technique presented in this chapter.

The main contribution of this chapter is to present a closed-loop control scheme that fully linearizes the behavior of DASA actuator. The feedback signal used for the closed-loop control is the magnetic field information obtained from a proprietary arrangement of embedded hall sensors in DASA actuation. Using the magnetic field information and the hysteresis model of the actuator, the controller can fully linearize the output torque of the actuator in relation to its input current. The closed-loop controller is implemented on a Field-Programmable-Gate-Array (FPGA) board which makes it possible to be fully embedded into the future generation of DASA actuator. Given the one-to-one relationship of the actuator torque with respect to its internal magnetic field, it is possible to perform high fidelity force/torque control without using any external force/torque sensor. The use of hall sensors provides a reliable, compact, and more importantly viable alternative to external force/torque sensors. This concept is validated in this chapter through a set of experiments performing on a prototyped DASA actuation with FPGA based control. The "sensor-less" torque control results (using embedded hall sensors) were also compared to those obtained using direct torque measurements (using external torque sensor). The results illustrated an accurate and competitive control performance. This technique allows DASA actuator to fully exhibit predictable and linear input-output characteristics. A block diagram of the proposed closed-loop FPGA based control scheme is shown in Fig. 2.1.

The remaining of the chapter is organized as follows. Section 2.2 reviews the structure of the MR clutch used in this chapter for validating the results. Section 2.3 discusses

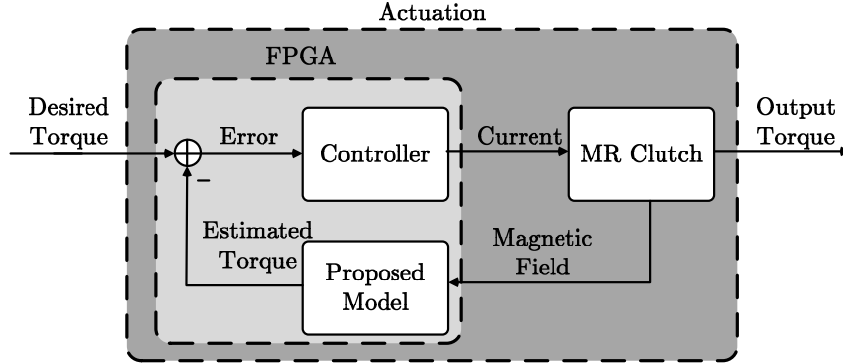


Figure 2.1: Block diagram of the proposed control scheme.

the FPGA based closed-loop scheme for controlling forces/torques using MR clutches. Section 2.4 presents experimental results for torque control using estimated torque values and compares these results with those obtained using actual torque measurements. Section 2.5 concludes the chapter.

## 2.2 MR Clutch

MR fluids, carrying micrometer-scale particles, are a kind of smart materials whose viscosity can be changed using an external magnetic field. This property of MR fluids allows to accurately control the shear stress of the fluid by controlling the intensity of an external magnetic field. A clutch-like mechanism, also known as MR clutch, is often used as means of materializing this concept through bounding the amount of transmitted torque based on the intensity of an applied magnetic field. This form of torque transmission lends itself to a new type of compliant actuator also referred to MR actuator. An MR clutch generally consists of input and output disks, the MR fluid that fills the volume between the input and output disks, and one or multiple electromagnetic coils used for generating a magnetic field. An electric motor provides the mechanical power to the clutch. The rotating speed of the motor can be constant (as in our case) or it can be adjusted based on maximum required speed, optimum operating condition, safety, and other factors. The MR clutch controls the amount of shear torques between the input and output disks by varying the input current to the electromagnetic coil that generates a magnetic field. This allows the MR clutch to trans-

mit the input power received from the motor to a load attached to the output shaft of the clutch as a function of shearing between the input and output disks. Fig.2.4 demonstrates the cross-section of a typical multi-disks style MR clutch. The input shaft breaks out into a set of input disks aligned with a set of output disks attached to the output shaft. MR fluids fill the volume between input and output disks. By energizing the electromagnetic coil, the shear stress of MR fluids can be controlled by an applied magnetic field, which leads to altering of the output torque [1].

### 2.2.1 Placement of hall sensors

While hall sensors can theoretically be placed at any position inside the magnetic circuit, the actual placement of hall sensors in practice is affected by such characteristics as size and maximum measurement range. In order to find a suitable position for hall sensors within an MR clutch, Finite Element Method (FEM) can be utilized to obtain a priori knowledge of the magnetic field distribution inside the MR clutch. The results of such an study are plotted in Fig. 2.2. As observed, in most parts of the magnetic circuit (including the shaft and hubs) the flux density is beyond the range of a typical hall sensor (i.e., less than 500 mT)<sup>1</sup>. One should also note that small hall sensors are much more desirable in order to have minimum effect on the strength of the magnetic field or the reluctance of the MR clutch. Thus, as suggested by Fig. 2.2, it seems most suitable to place the hall sensors on the disks to meet the above-mentioned requirements. At the same time, considering the magnetic field distribution along the radius of the output disk as shown in Fig. 2.3 for various input currents, is almost uniform regardless of the radius of the MR clutch and the value of the input current.

This is due to the fact that there is little variation in the reluctance along the radial axis of the MR clutch in particular in the areas where the input and output disks overlap. The reasons for this are the larger relative permeability of ferromagnetic material compared to MR fluids (by two orders of magnitude)<sup>2</sup> as well as small overlapping length of the disks

---

<sup>1</sup>Typically, the magnetic densities in these parts can be over Teslas, but regular hall sensors can only measure magnetic field around hundreds milliteslas.

<sup>2</sup>Typically, the relative permeability of ferromagnetic material used in MR clutches ranges around thou-

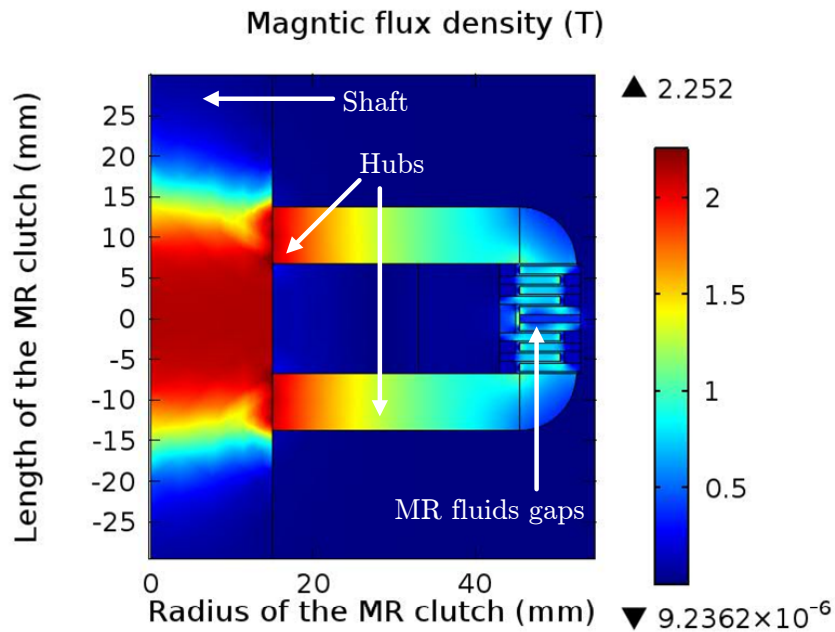


Figure 2.2: 2D MR clutch model and the magnetic field distribution.

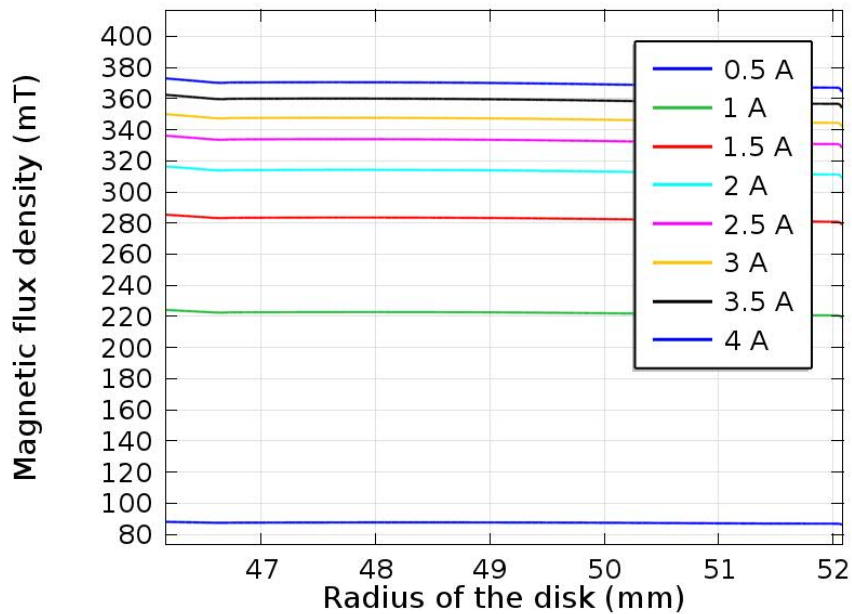


Figure 2.3: Applying different input currents, the magnetic field distribution on output disks.

sands and for MR fluids this value does not exceed one hundred.

along the radial axis of the clutch compared to the overall radius of the clutch<sup>3</sup>. Therefore, it can be concluded that hall sensors can be embedded at any radius along the output disk within MR fluid gaps (see Fig. 2.5).

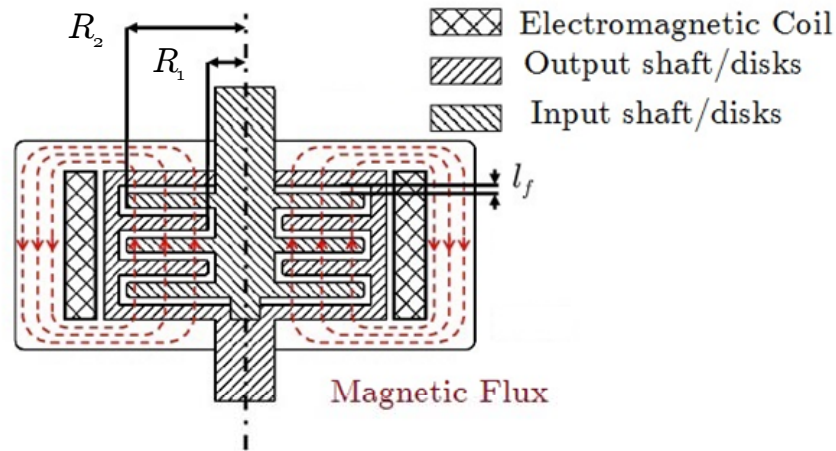


Figure 2.4: Cross-section of a multi-disk MR clutch.

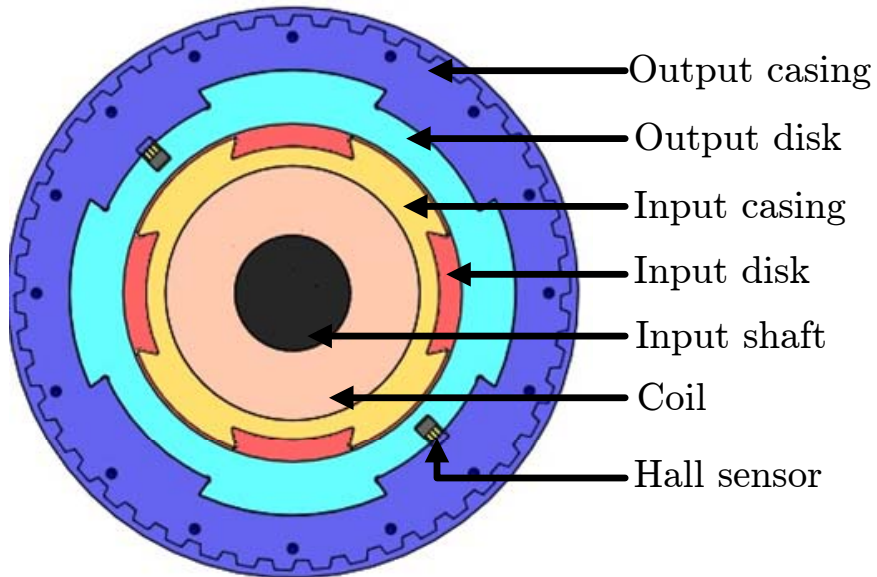


Figure 2.5: The position of hall sensors in an MR clutch.

<sup>3</sup> $\mathfrak{R} = \frac{l}{u_0 u_r A}$ , where  $\mathfrak{R}$  is magnetic reluctance,  $l$  is the length of the circuit,  $u_0$  is the permeability of vacuum, equal to  $4\pi \times 10^{-7}$  henry per meter,  $u_r$  is the relative magnetic permeability of the material and  $A$  is the cross-sectional area of the circuit.

## 2.3 Torque Control in the MR Clutch

Unlike electric motors that feature linear relationship between their input current and output torque, in an MR clutch, the input and output are nonlinearly related with hysteresis. The hysteresis phenomenon within the actuator is demonstrated in Fig. 2.6 where we have applied a sinusoidal input current with different frequencies to the MR clutch. As seen in this figure, not only is the relationship between the input current and the magnetic field hysteretic, but also the results are rate dependent. This relationship also reflects on the output torque behavior with respect to the input current. The hysteresis in the magnetic field is mainly associated with ferromagnetic components used in an MR actuator including the shaft, disks, and coil. The MR fluid exhibits a relatively linear magnetic behavior due to the soft irons used in the fluid suspension. As such little or no hysteresis is observed in the B-H curve of the fluid [19]. One way of coping with this shortcoming is to use an external torque sensor that provides the feedback signal for regulating the torque in a closed loop. Despite availability of multi-axis force/torque sensors, this technique cannot provide favorable results due to other undesired effects such as friction, backlash, cogging effects of the actuators, measurement noise, and modeling errors. Notwithstanding, the high cost of sensors and the unreliable nature of the results in particular in applications that involve interactions with humans present additional challenges. An alternative solution to deal with nonlinear behavior of an MR clutch is to compensate it, if not eliminating it, at the design level. In order to compensate the hysteretic behavior, considering the current-torque model of an MR clutch (see Fig. 2.7), compensating hysteresis is achieved using the magnetic field information within the MR clutch and then compensate it for any undesired errors. The estimation can be done accurately given the one-to-one relationship between the shear stress of MR fluids and the applied magnetic field. An analogy can be drawn between this technique and that previously used in Series Elastic actuators [4] and Hydro Elastic actuators [20] for estimating the actuator torque, in which an encoder measures the deflection of a spring. In this chapter, we discuss the use of hall sensor to measure the internal magnetic field of the MR clutch and to estimate the output torque of the clutch accurately. Since the input of the MR clutch is the electric current, the technique

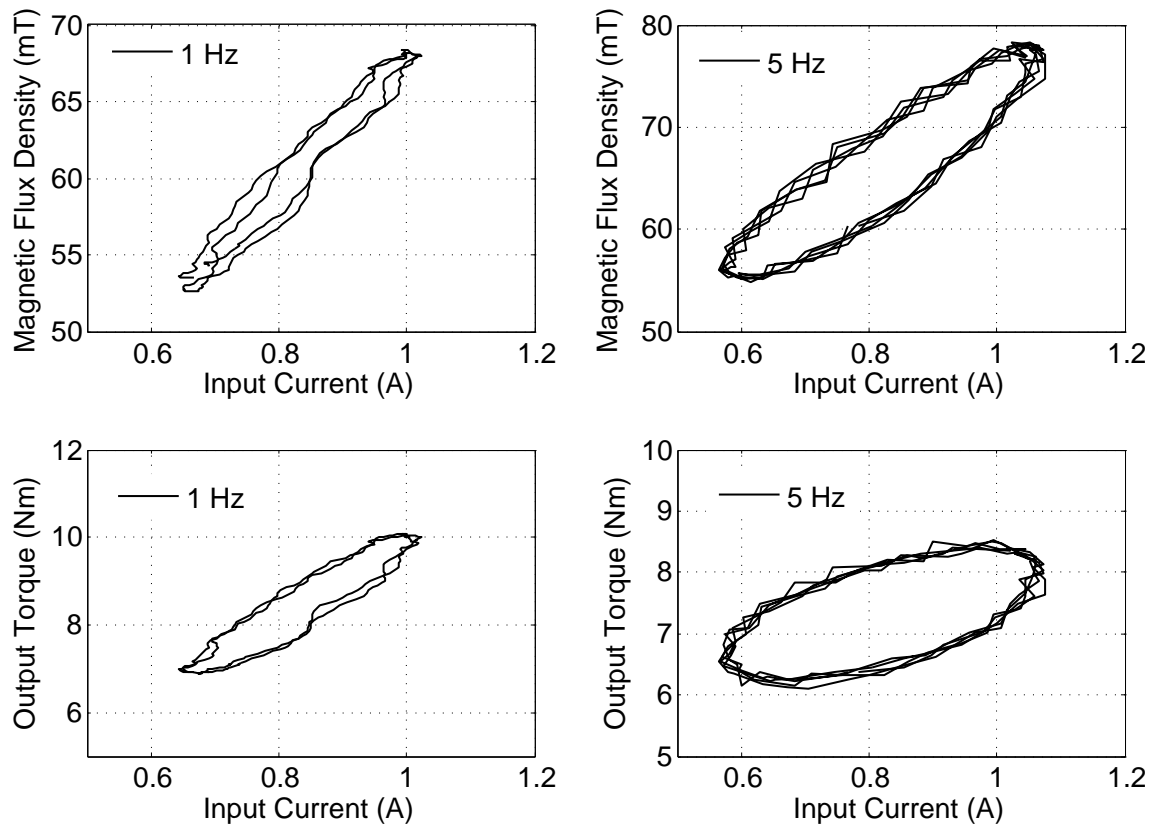


Figure 2.6: Rate-dependent hysteresis for an MR clutch.

presented here results in a linear relationship between the input current and output torque of the MR clutch. An FPGA based closed-loop control algorithm is used to implement this linearization technique. This technique results in a linear torque actuator assuming a gray-box input-output view of the MR actuator.

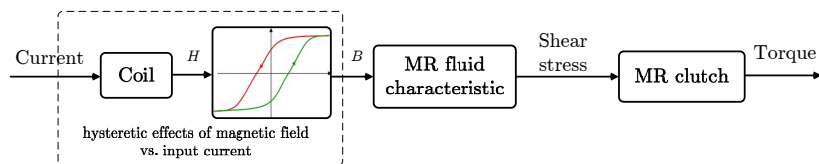


Figure 2.7: MR clutch current-torque model.

### 2.3.1 Control Scheme

As described in the previous section, the one-to-one relation between the output torque and magnetic field intensity is an explicit advantage in an MR clutch and the main notion behind the proposed model in this chapter. This relationship can be validated using a sinusoidal current applied to the MR clutch while observing the changes in output torque with respect to the magnetic field. Fig. 2.8 shows these changes due to a sinusoidal input current. As observed, despite minor lagging effect (due to the clutch dynamics), the MR clutch demonstrates a one-to-one relationship between the output torque and magnetic field. This

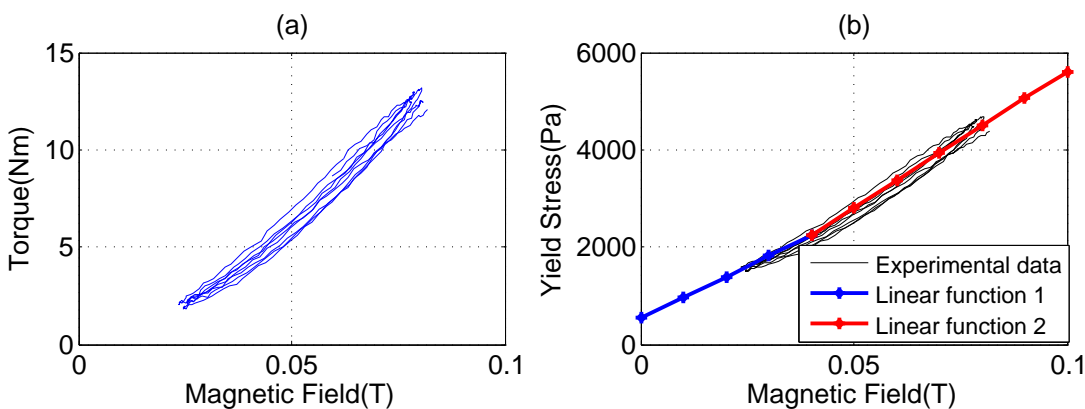


Figure 2.8: Applying a sinusoidal current to an MR clutch: (a) output torque vs. magnetic field; (b) yield stress vs. magnetic field for MR fluids and the piecewise linear function.

one-to-one relationship allows controlling the output torque of the MR clutch accurately in a configuration shown in Fig. 2.9. In this figure, a simple PID controller provides the control current for a desired torque value. The PID controller uses the error between the control current for a desired torque value. The PID controller uses the error between the estimated value of the output torque with its desired value as the input signal. The estimated value of the output torque is obtained using a model described in the following sections. This model provides an accurate estimation of the output torque given the one-to-one relation of the output torque to the applied magnetic field. The intensity of the magnetic field is measured using a proprietary arrangement of embedded hall sensors inside our MR clutch. The error between the desired output torque and its estimated values provides a reference signal for a current source that drives the electromagnetic coil inside the MR clutch. The proposed model used for estimating the output torque of the MR clutch consists

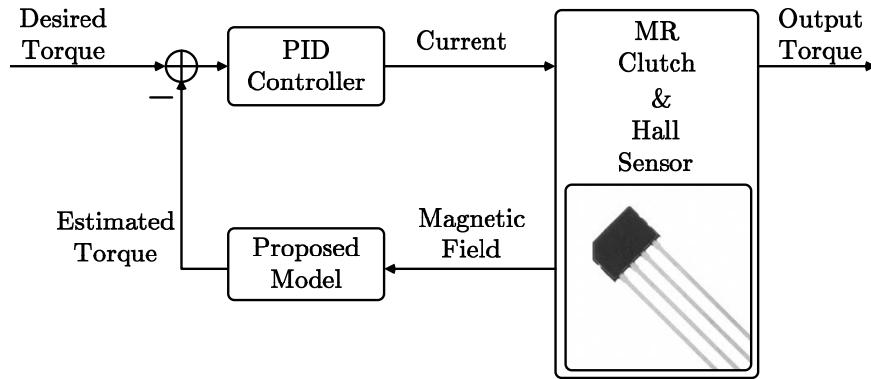


Figure 2.9: Closed-loop control configuration using embedded hall sensors.

of two parts: a static model and a dynamic model (see Fig. 2.10). Each part of the model is described in the following sections.

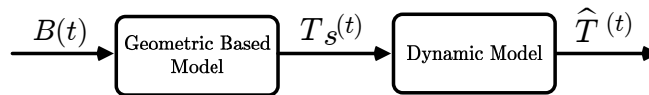


Figure 2.10: Proposed model for output torque estimation.  $B(t)$  is the magnetic field, and  $T_s(t)$  and  $\hat{T}(t)$  are static and dynamic estimations of the output torque, respectively.

### 2.3.2 Static Model

It has been shown that the visco-plastic Bingham model is a good candidate for representing the static behavior of the output torque in an MR clutch [21, 22, 23, 24, 19]. The Bingham model is a geometrical based model, which relates the shear stress of MR fluids to the yield stress and the shear rate in an MR clutch. The static output torque of an MR clutch can be obtained by integrating the shear stress over the effective area. A model based on the Bingham model for our MR clutch was developed in [1, 17] to predict the rheological properties of the actuator. We briefly review this model for the continuity of our discussion. According to Bingham model, the shear stress can be presented as ,

$$\tau = \tau_y(B) + \eta \frac{dv}{dz}, \tau > \tau_y \quad (2.1)$$

where  $\tau$  is the shear stress,  $\tau_y$  is the field dependent yield stress,  $B$  is the magnetic field,  $\eta$  is the Newtonian viscosity, and  $\frac{dv}{dz}$  is the velocity gradient in the direction of the field. The viscosity  $\eta$  of the carrier fluid is typically within the range of 0.1 to 0.3 Pa. The second term in (2.1) can be ignored due to its negligible effect on the estimated values of the output torque. In fact, the contribution of the first term in (2.1) for typical MR fluids is in the range of kPa torque, whereas for the second term this value does not exceed a few Pa-s.

Assuming the configuration depicted in Fig. 2.4 for an MR clutch, the torque produced by a circumferential element at a radius  $r$  is given by,

$$dT = 2\pi r^2 \tau dr. \quad (2.2)$$

Integrating (2.2) across the output disks and substituting  $\tau$  from (2.1) yields the static output torque of the MR clutch as follows,

$$T_s \simeq \frac{4}{3} N \pi \tau_y(B) (R_2^3 - R_1^3). \quad (2.3)$$

where  $N$  is the number of output disks, and  $R_1$  and  $R_2$  are the inner and outer radius of the disks, respectively. Moreover, considering the one-to-one relationship between yield stress and magnetic field, we can use a piecewise linear function to define this relation which is assumed as,

$$\tau_y(B) = \begin{cases} = C_1 B + d, & B < 0.04T \\ = C_2 B, & B \geq 0.04T \end{cases} \quad (2.4)$$

where  $C_1 = 42.59 \text{ kPa}/T$ ,  $d = 0.5413 \text{ kPa}$  and  $C_2 = 56.136 \text{ kPa}/T$  are constant values. This piecewise linear function is plot in Fig. 2.8 where the yield stress for applying a sinusoidal current to an MR clutch is calculated using 2.3. As observed, this piecewise linear function can model the yield stress-magnetic field relationship accurately. Substituting (2.4) into (2.3) yields the output torque of the MR clutch as a static function of the magnetic field  $B$ , i.e.,

$$T_s \simeq \begin{cases} k(C_1 B + d), & B < 0.04T \\ k(C_2 B), & B \geq 0.04T \end{cases} \quad (2.5)$$

where  $k = 4N\pi(R_2^3 - R_1^3)/3$  is a constant that depends on the geometrical parameters of the clutch.

In order to examine the accuracy of the static model, a constant current was applied to our MR clutch prototype. Fig. 2.11 presents the measurement and the estimation of the output torque for the applied step constant current. One can note that the estimated torque closely matches its measured value and the error between the two signals is insignificant, which validates the use of an static model for output torque estimation of an MR clutch. On the other hand, it should be noted that the estimated and measured torque values in this test are for a constant magnetic field generated using a constant current. Hence, the results here do not include the effects of dynamic characteristics of the MR clutch.

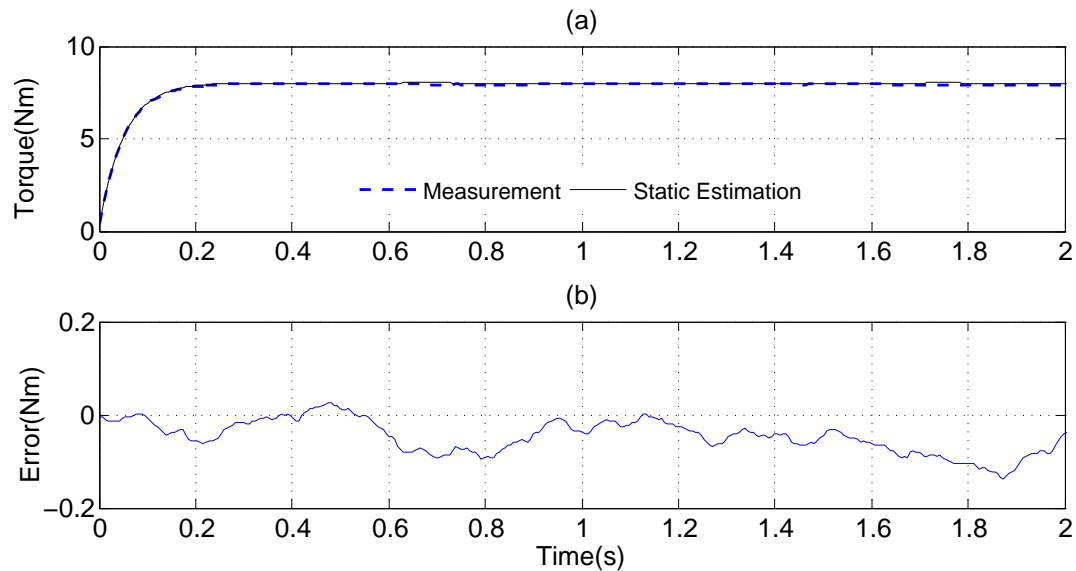


Figure 2.11: Output torque of the MR clutch in response to a step input current; (a) measured and estimated torques, (b) error between the measured and estimated torques.

### 2.3.3 Dynamic Model

While the Bingham model can accurately estimate the output torque of an MR clutch statically, there can be significant discrepancies between the estimated values of the torque and its actual values in a dynamic mode. It has been studied that there is no hysteresis for MR fluids and the response time for MR fluids is smaller than milliseconds [25]. Therefore, comparing with MR fluids, the presence of the mechanical components within an MR clutch is perhaps the main factor that differentiates the dynamic behavior of an MR clutch

from its static model. Not unlike other mechanical systems, the disk's inertia in an MR clutch, fluidic frictions, and gravity can affect the dynamic behavior of the clutch. Another factor that is specific to MR clutches is the various response time of MR fluids in different parts of the clutch. Using finite element analyses, it has been shown that the magnetic field can be much stronger near the coil than elsewhere within the clutch (e.g. in [26, 27]). As a consequence, the MR fluid reacts with different time responses in different locations of an MR clutch. Taking all these issues into consideration, it is very difficult, if not impossible, to develop an accurate physic-based dynamic model for an MR clutch and it would be outside the scope of the current study. However, to include the dynamic behavior of an MR clutch in the modeling, we use a well-known Auto Regressive technique with eXternal input (ARX) [28, ch. 10]. An ARX model is essentially a linear difference equation between the input and output of the model, relating the next output sample of the model to its previous observations, i.e.,

$$\begin{aligned} y(t) = & -a_1y(t-1) - \dots - a_ny(t-n) \\ & + b_1u(t-1) + \dots + b_mu(t-m), \end{aligned} \quad (2.6)$$

where  $y(t-i)$  and  $u(t-i)$ ,  $i = 1, 2, \dots$ , are the previous observations of the input and output, respectively, and  $a_i$  and  $b_i$ ,  $i = 1, 2, \dots$ , are the model parameters to be identified using experimental data.

Using (2.6), a dynamic model for estimating the output torque of the MR clutch can be constructed. The input to this model is the static torque obtained in (2.5) and the output is the estimated dynamic torque. The resulting model is given by,

$$\begin{aligned} \hat{T}(t) = & -a_1\hat{T}(t-1) - \dots - a_n\hat{T}(t-n) \\ & + b_1T_s(t-1) + \dots + b_mT_s(t-m), \end{aligned} \quad (2.7)$$

where  $\hat{T}$  is the estimated values of the output torque and  $T_s$  is the static torque obtained in (2.5).

### 2.3.4 Implementation on an FPGA Board

In order to implement the PID controller and the model proposed previously for linearizing the MR clutch, a Field-Programmable-Gate-Array (FPGA) board is employed in a closed-loop feedback configuration. The PID controller and the proposed model are both implemented on the FPGA board using Verilog Hardware Description Language (HDL). The FPGA board receives the desired torque value, and the magnetic field intensity obtained from the hall sensors and generates a reference current signal for a current source that drives the MR clutch. These signals are all analog and are descritized/reconstruced as they enter/leave the FPGA board.

An FPGA-based controller provides a fast and flexible platform for linearizing MR clutches using various functions and configurations. More importantly, the use of FPGA technology facilitates its future integration within the structure of MR clutch and DASA actuator as a fully embedded component. The Serial Peripheral Interface (SPI) Bus is employed to connect different functional components of the system, among which the FPGA acts as the SPI MASTER while others are SPI SLAVE. The SPI bus only takes 4 pins and routes on a circuit board to save the space on the board. Our objective is to integrate a small-size FPGA board inside the future generation of our MR clutch.

## 2.4 Experimental Results

A set of experiments to validate the proposed model and the effectiveness of the overall control scheme is presented in this section. Fig. 2.12 shows the schematic architecture of the experimental setup, in which the MR clutch prototype is driven by a servo amplifier (Maxon 4-Q-DC Servo-amplifier ADS 50/5) configured in torque mode for providing the command current. A static load cell (Transducer Techniques SBO-1K) is mounted on the output shaft for torque measurements and a hall sensor (TLE 4990 Infineon Technologies) is integrated inside the MR clutch for magnetic field measurements. In this MR clutch, only one hall sensor was employed on an aluminium disk to measure the magnetic field strength. A servo motor (Maxon EC 60) provides the rotational input to the MR clutch. A National Instruments (NI USB-6229) multifunction I/O device is employed to provide reference

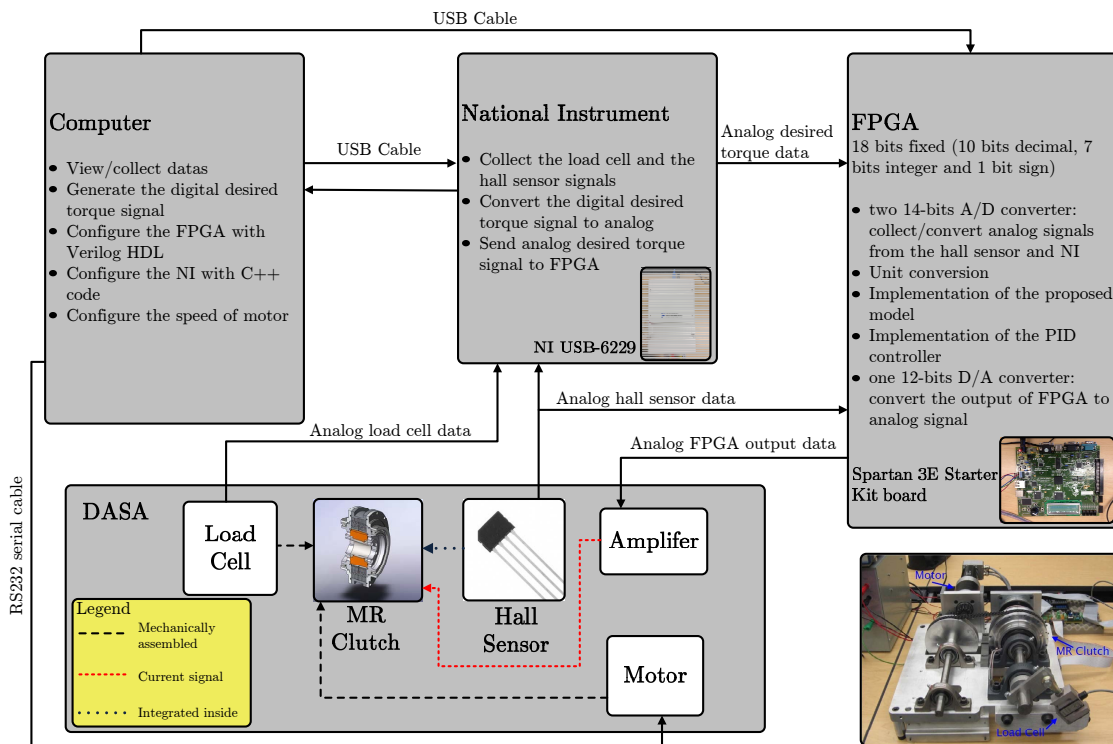


Figure 2.12: Schematic architecture of the experimental setup.

torque values for the actuator and to acquire the output signals from the load cell. The proposed model and the PID controller are implemented on a spartan-3E starter kit board from Xilinx. The Xilinx FPGA board features two analog-to-digital (A/D) converters and a digital-to-analog (D/A) converter. One of the A/D converters is used to receive the readings of the hall sensors, while the other one is used to acquire the reference torque value. The D/A converter converts the digital output value of the PID controller to an analog reference signal for the Maxon servo amplifier.

### 2.4.1 Validation of the Proposed Model

The proposed model consists of two parts: a static model and a dynamic model. The static model is based on the geometrical structure of the MR clutch and is obtained as described in Section III. The dynamic model whose input and output are static and dynamic torque values, respectively, is obtained using System Identification toolbox of MATLAB with a set of experimental data. In order to have as much information in the experimental

data as possible, we used Multi-Sine<sup>4</sup> and Swept-Sine<sup>5</sup> signals within a certain range of frequencies as the input currents of the MR clutch. These two signals are often used to validate (or invalidate) the accuracy of a model, given their richness in exciting all possible modes of a dynamic system [28, ch. 13]. The Multi-Sine current signal used in our study was an average of 10 sinusoids with different frequencies selected uniformly within the range of 0.5Hz to 15Hz. The same frequency range for the Swept-Sine current signal was selected. Fig. 2.13 and 2.14 represents the actual output torques and their estimated values for the Multi-Sine and Swept-Sine current signals. Despite the low frequency of the input signals for avoiding any dynamics introduced by load cell or hall sensor<sup>6</sup>, there is still some discrepancies between the static estimation and the measurements. These discrepancies are an indication of dynamics within the MR clutch that should be considered for a true description of the MR actuator behavior. To this end, we use an ARX model from System Identification Toolbox in MATLAB along with two data sets obtained using the Multi-Sine and Swept-Sine current inputs. Each set contained the estimated and measured torques for the corresponding excitations. With these two sets of data, two ARX models, namely Model I and Model II for Multi-Sine data and Swept-Sine data, respectively, were obtained. Table. 2.1 lists the Root Mean Square Errors (RMSEs) between the dynamic estimation and the actual measurement for each ARX model and each validating signal.

Inspecting the results of Table. 2.1, shows that the RMSE values are within an acceptable range, allowing both models to be effectively used for general control purposes. However, each model can outperform the other depending on a specific application. Since the objective of our study is to develop a general purpose torque actuator, we adopted Model II which seem to perform better across the selected frequency range.

In order to initially evaluate the accuracy of the adopted dynamic model, the same Multi-Sine and Swept-Sine current signals were applied to MR clutch prototype for a im-

---

<sup>4</sup> $i(t) = \sum_{k=1}^n \mu_k \cos(\omega_k)$ , where  $\mu_k$  and  $\omega_k$ ,  $k = 1, \dots, n$  are amplitudes and frequencies of sinusoids, respectively.

<sup>5</sup> $i(t) = A \sin(\frac{1}{2}(\frac{2\pi(f_2-f_1)}{n})^2 + 4\pi f_1)$ , where  $A$ ,  $f_1$ ,  $f_2$  and  $n$  are amplitude, normalized start frequency, normalized stop frequency and number of samples of Swept-Sine signal, respectively.

<sup>6</sup>The bandwidth of the load cell and hall sensor used in this chapter are 220Hz and 1.6 kHz which are much higher than the selected frequency range.

Table 2.1: RMSE of Dynamic Model

Dynamic Model	Validating signals	
	Multi-Sine	Swept-Sine
Model I (using Multi-Sine data)	0.2733Nm	0.7370Nm
Model II (using Swept-Sine data)	0.3164Nm	0.3644Nm

mediate comparison. Figs. 2.13 and 2.14 depict predicted output torques versus their corresponding measured values for Multi-Sine and Swept-Sine signals, respectively. The results show that the prediction results follow closely the actual measurements. The Root Mean Square Errors (RMSEs) between the estimated and the actual torque values are 0.1732 Nm and 0.2877 Nm for the Multi-Sine and Swept-Sine signals, respectively. Moderate errors at the beginning of the results are associated with the low frequency components of the input signals, where the proposed dynamic model shows the least accuracy. Nonetheless, the results show a very accurate estimation for high frequency which is usually more desirable for control purposes.

## 2.4.2 Torque Control Experiments

The performance of the proposed FPGA based closed-loop controller is further evaluated in this section. The results presented in this section are of particular importance as they introduce a new and cost effective approach to an old and sought after problem, i.e. force/torque control. The novelty aspect of this approach is in performing force/torque control without the use of external force/torque sensor which is a significant improvement in the state of the art. While our proposed technique does not outperform conventional force/torque control schemes (at least by a significant margin) in terms of the accuracy of the delivered torque, it provides a much more viable alternative to these schemes. Moreover, in certain applications where the collocation of the actuators and sensors is an issue, e.g., surgical laparoscopic tools, eliminating the need for an external sensor becomes a major advantage.

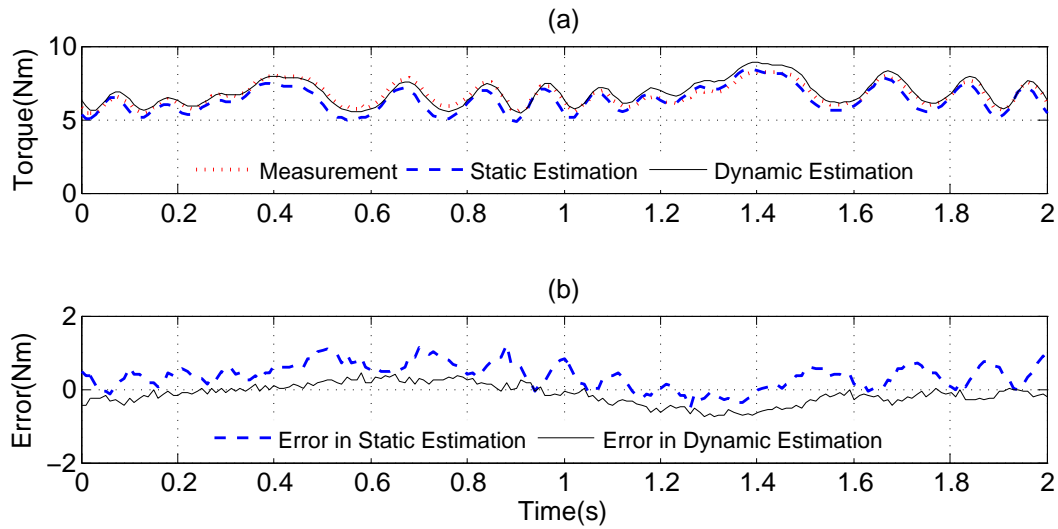


Figure 2.13: Multi-Sine input current, (a) estimated and measured torques, (b) error between measured and estimated torques

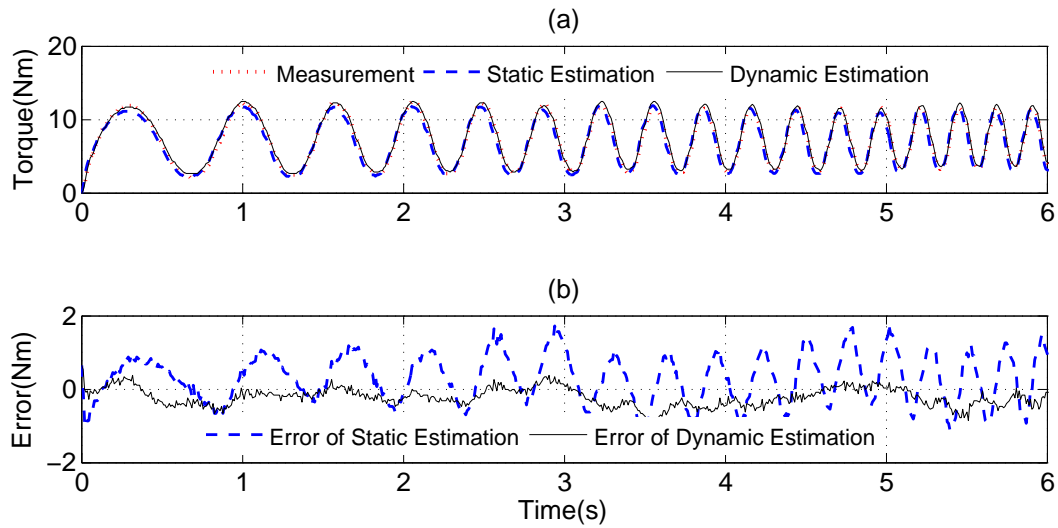


Figure 2.14: Swept-Sine input current, (a) estimated and measured torques, (b) error between measured and estimated torques

To compare/demonstrate closed-loop torque control using MR clutches, we have considered two configurations. Fig. 2.15 presents the control schemes for both configurations. In the first configuration, the proposed FPGA based method uses the magnetic field mea-

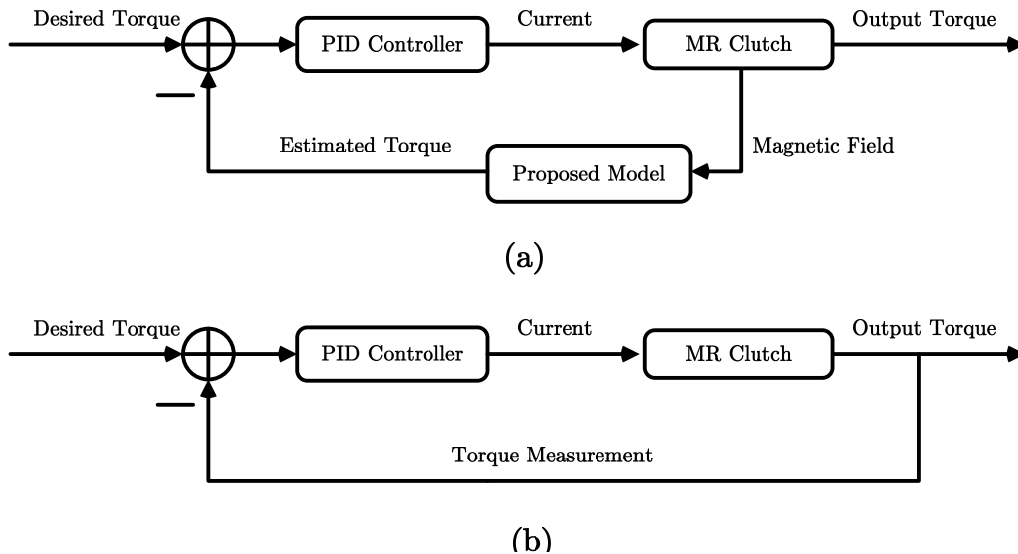


Figure 2.15: Closed-loop control scheme for: (a) 1st configuration, (b) 2nd configuration.

measurements from hall sensors for estimating the output torque and performing closed-loop torque control. In the second configuration, the actual torque measurements are used in the closed-loop control as the required feedback signal. Both configurations use a PID controller in their control loop. The error signal in the first configuration is computed as the difference between the estimated and the desired torque values, while the actual torque measurements are used for error calculations in the second configuration. Several desired torque signals were considered. In each case, the PID controllers were tuned for obtaining the best possible control results. Fig. 2.16, Fig. 2.17, Fig. 2.18, Fig. 2.19 and Fig. 2.20 show the results for a square, 1, 5 and 10 Hz sinusoids, and a Multi-Sine desired torque signals, respectively. In these figures, there are two measurements of load cell corresponding to the first and second configurations. We also show the errors, currents and magnetic field intensities of both configurations as well. These results clearly validate the efficacy of our proposed model for tracking a desired torque using an MR clutch, where no external torque measurements are used in the control loop. The results closely match those are obtained using actual torque measurements and the errors in these two configurations are comparable.

The RMSE values of the errors associated with each desired torque signal are listed in

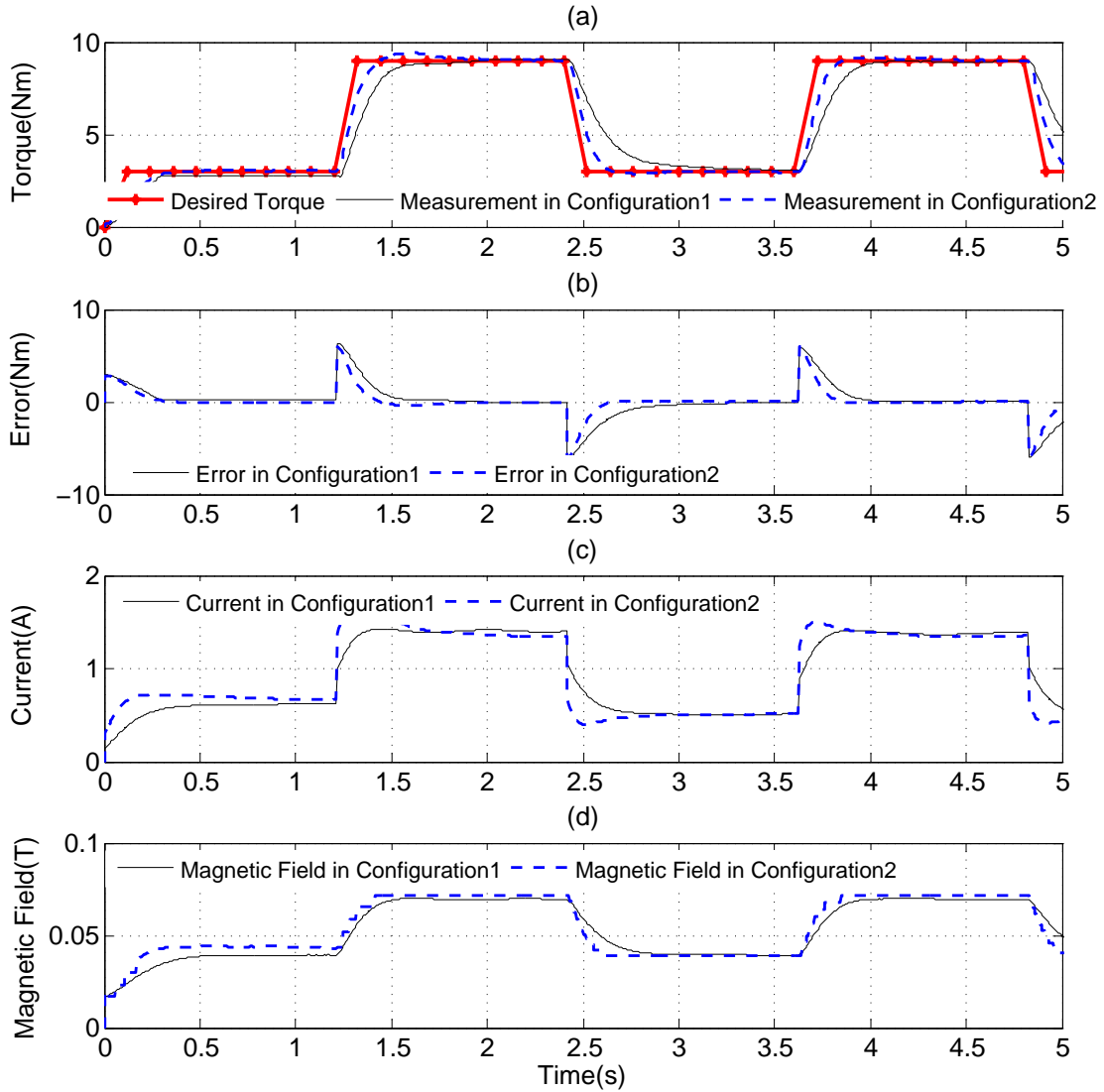


Figure 2.16: Closed-loop tracking of a square reference torque using hall sensor vs external force/ torque sensor; (a) generated torques, (b) error signal, (c) input current, and (d) magnetic field inside MR clutch.

Table 2.2. To eliminate the error resulted from a limited MR clutch bandwidth, the RMSE for the square command is calculated twice; once using the entire error signal, and another time using the steady state error signal following the transitional period. While there is a slight difference between the results of the two configurations, it can be clearly seen that accurate torque control is achieved in both configurations. One should however, note that the first configuration requires no additional torque sensor which is the main significance and contribution of the current work. Typically, hall sensors feature 20-60  $\mu\text{T}$  resolution,

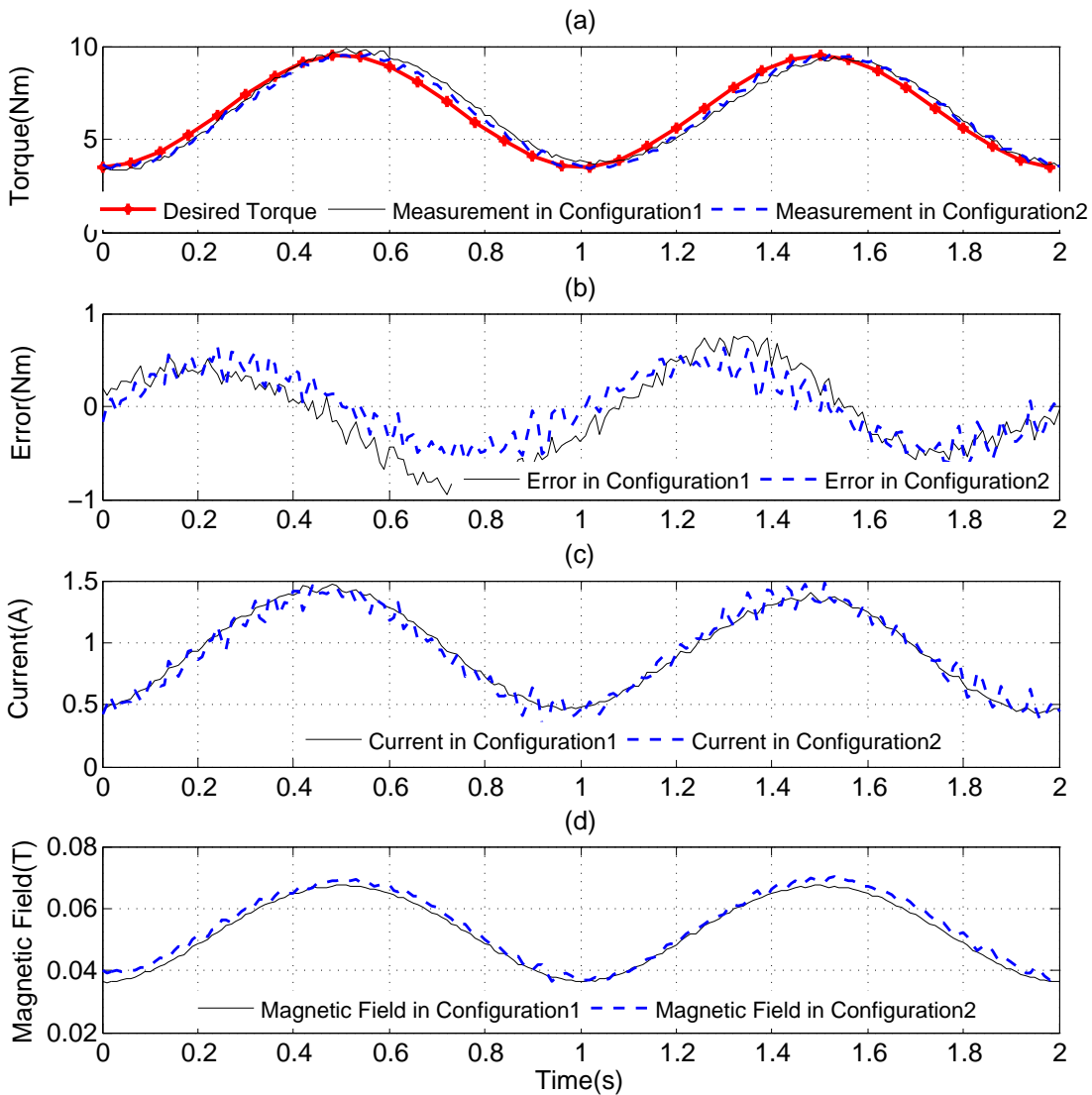


Figure 2.17: Closed-loop tracking of a 1 Hz sinusoid reference torque using hall sensor vs external force/ torque sensor; (a) generated torques, (b) error signal, (c) input current, and (d) magnetic field inside MR clutch.

that corresponding to a high resolution of 4 mNm torque estimation for the MR actuator considered in this chapter. The bandwidth and output delay in hall sensors are in the range of 1.6 kHz and 0.1 ms, respectively, which are comparable with what force sensors typically offer<sup>7</sup>. Moreover, it is reasonable to assume that improving the accuracy of the dynamic model can lead to a more accurate torque control.

<sup>7</sup>For instance, ATI sensors with F/T controller have a latency of 0.8-2.6 ms at 0.56-2.5 kHz bandwidth.

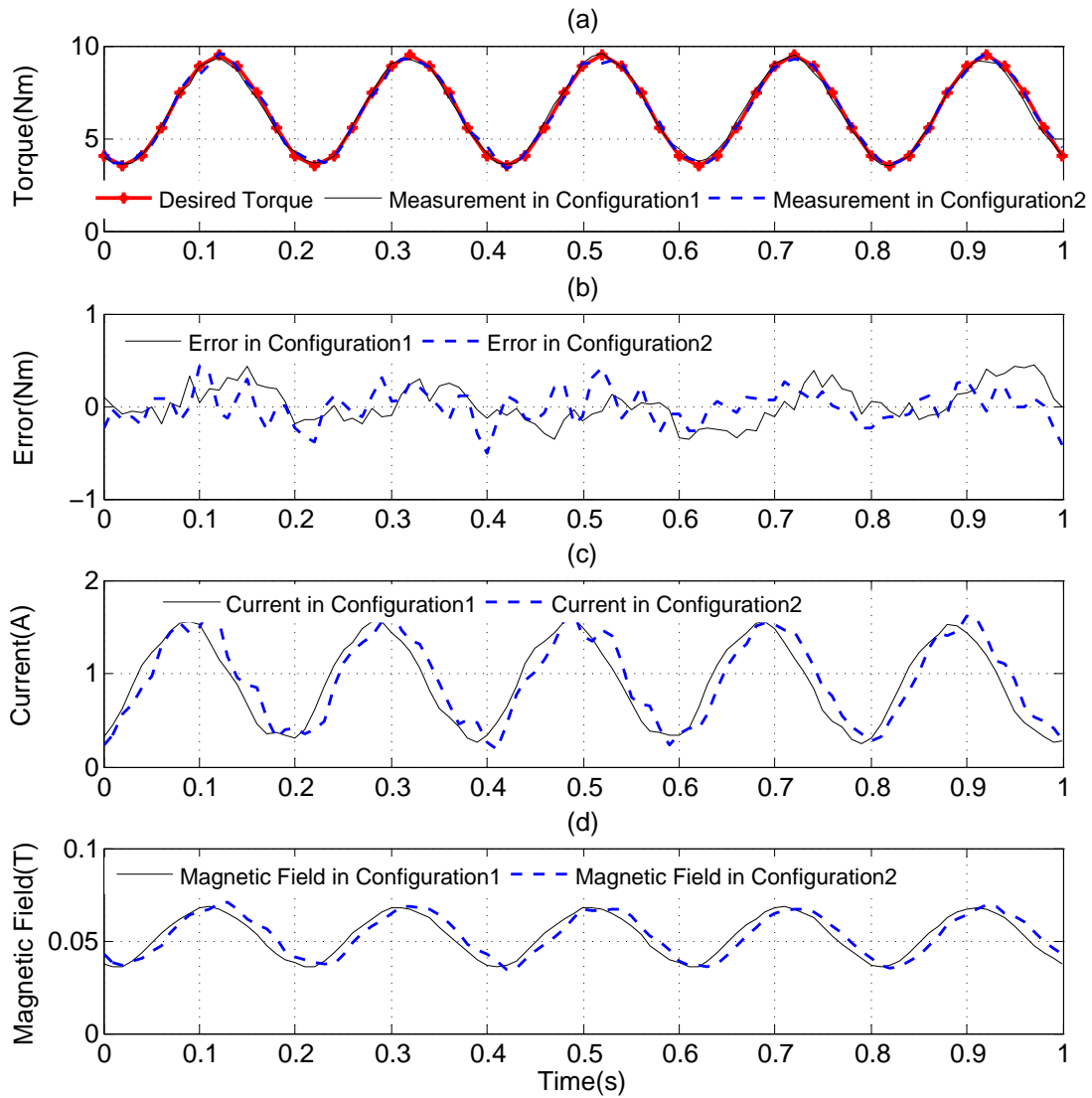


Figure 2.18: Closed-loop tracking of a 5 Hz sinusoid reference torque using hall sensor vs external force/ torque sensor; (a) generated torques, (b) error signal, (c) input current, and (d) magnetic field inside MR clutch.

Moreover, another comparison is studied to inspect the performance of the proposed models that are obtained by using input signals with different ranges of frequency. The proposed model employed above is modeled from MATLAB with Swept-Sine input current whose frequency ranges from 0.5 Hz to 15 Hz. In order to improve the performance of the control scheme, there are two models which are acquired in the same way from MATLAB, but the Swept-Sine input currents are 0.5-5 Hz and 0.5-10 Hz respectively. Then the

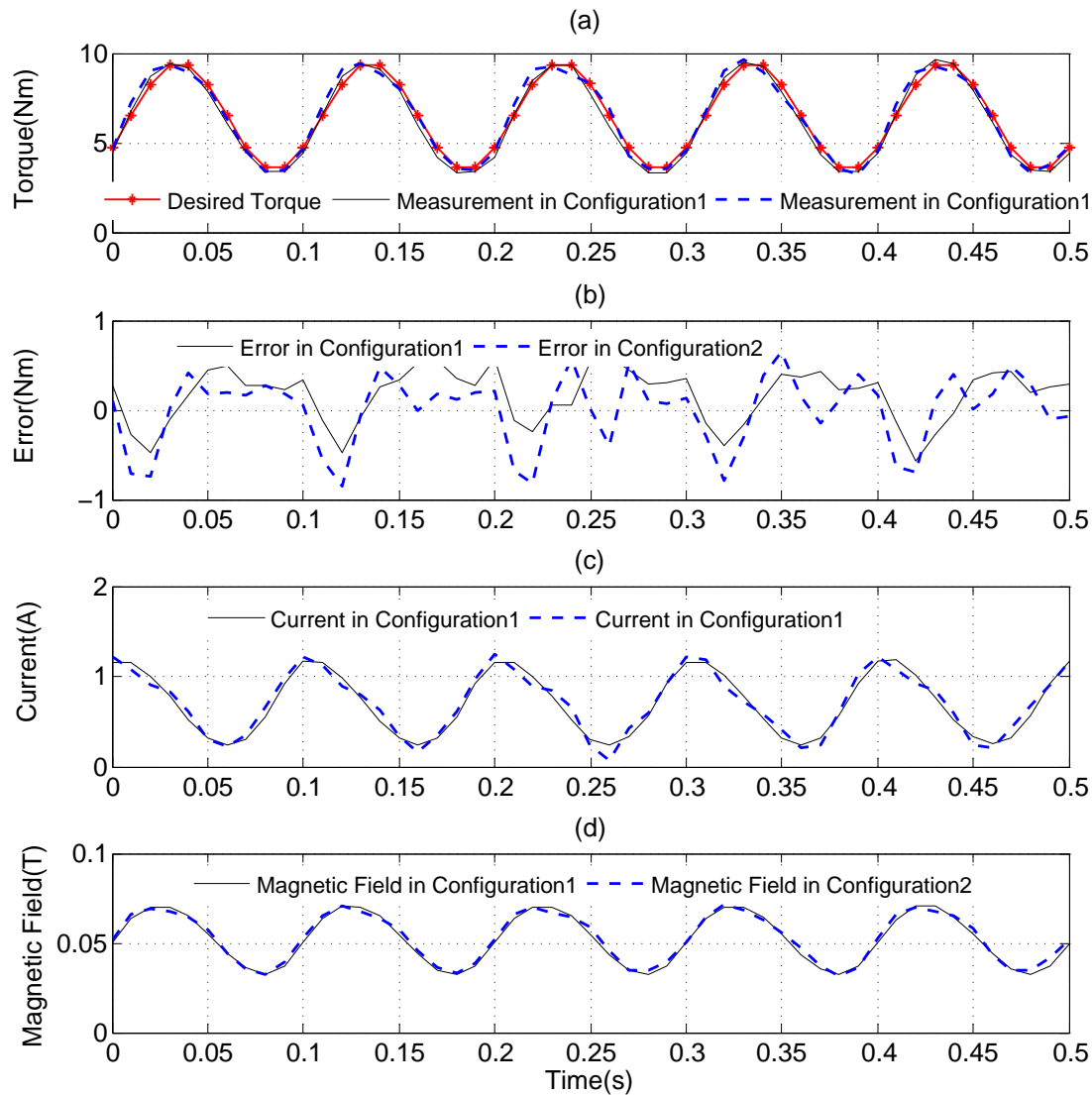


Figure 2.19: Closed-loop tracking of a 10 Hz sinusoid reference torque using hall sensor vs external force/ torque sensor; (a) generated torques, (b) error signal, (c) input current, and (d) magnetic field inside MR clutch.

proposed close-loop control scheme hires all models to command the same desired torque. While all the models are able to get accurate output, the effectiveness of different models still exists difference in terms of RMSE which is shown in Table 2.3. As observed, the model whose frequency range includes the frequency of the desired torque always features better performance than the model whose frequency range is below the frequency of the desired torque. On the other hand, if the frequency range of a model is too wider than that

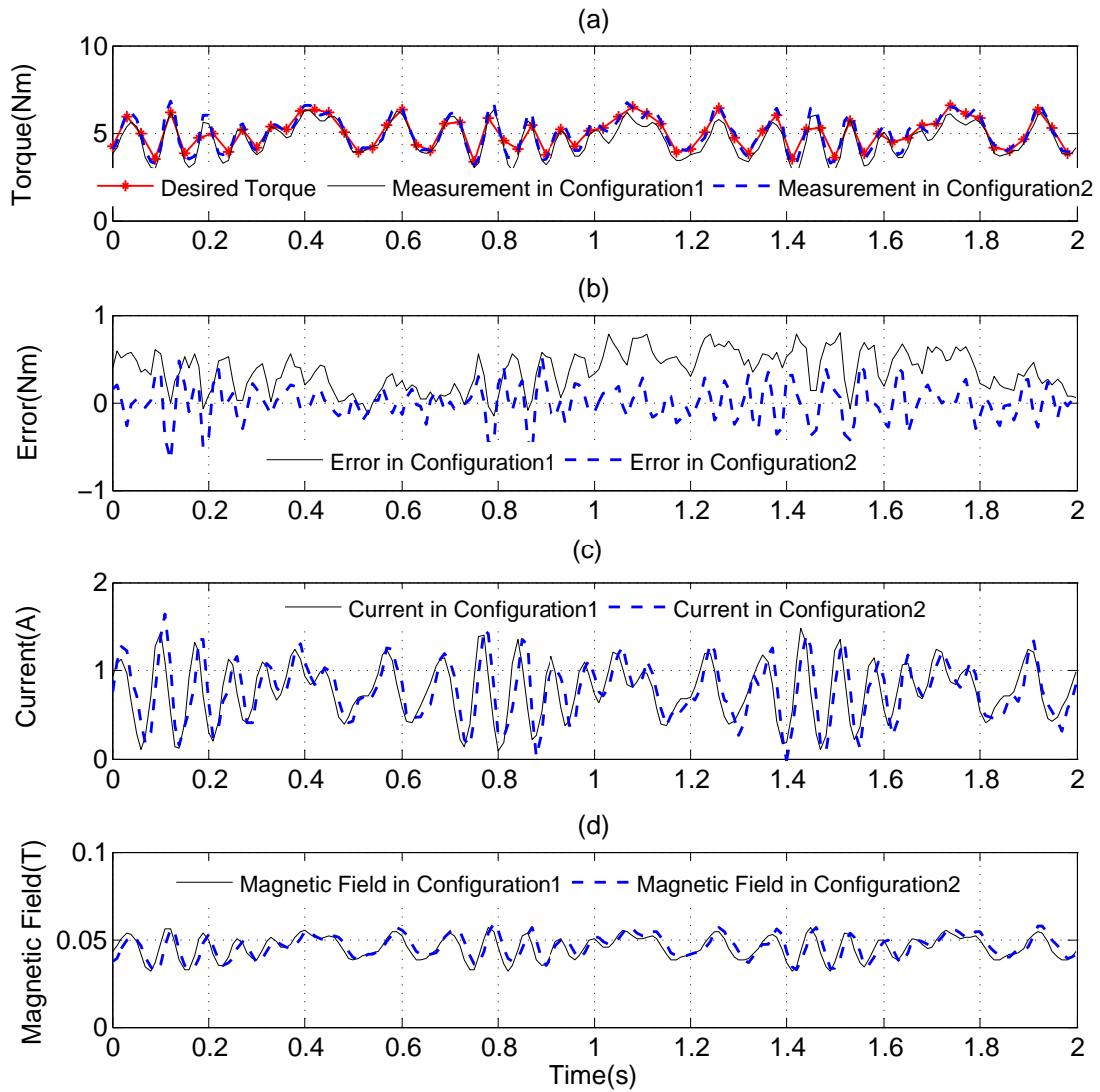


Figure 2.20: Closed-loop tracking of a Multi-Sine reference torque using hall sensor vs external force/ torque sensor; (a) generated torques, (b) error signal, (c) input current, and (d) magnetic field inside MR clutch.

of the desired torque, the result of control is not so good as the result that achieved by using a model whose frequency is narrower but covers the frequency of desired torque. To this end, the proposed model can be developed by using input signals based on the frequency of the desired torque. However, the control results for all models are comparable with the results obtained by using torque sensor.

Table 2.2: RMSE for torque control experiments

Tracking Experiments	RMSE (Nm)	
	1st Configuration using estimated torque	2nd Configuration using actual torque
Square	1.3271	1.3170
Square after transition	0.1648	0.1946
1Hz Sinusoidal	0.4609	0.3495
5Hz Sinusoidal	0.1998	0.1818
10Hz Sinusoidal	1.1930	1.1955
Multi-Sine	0.4954	0.6164

Table 2.3: RMSE for torque control experiments with different models

Tracking Experiments	RMSE (Nm)			
	1st Model	2nd Model	3rd Model <sup>8</sup>	Sensor <sup>9</sup>
5Hz Sinusoidal	<b>0.1864</b>	0.1900	0.1998	0.1818
10Hz Sinusoidal	1.3200	1.2030	<b>1.1930</b>	1.1955
Multi-Sine (5Hz)	<b>0.3019</b>	0.4000	0.3800	0.3000
Multi-Sine (10Hz)	0.5273	<b>0.3604</b>	0.4186	0.3806
Multi-Sine (15Hz)	0.7200	0.7188	<b>0.4954</b>	0.6164

## 2.5 Conclusion

In this chapter, a novel FPGA based closed-loop control scheme was proposed for linearizing the output torque of an MR clutch as a function of its input current. In the proposed scheme, the FPGA board regulates the output torque of the MR clutch using its magnetic field measurements acquired by a set of embedded hall sensors. Using this information, the output torque of the clutch is first estimated and is then used to provide the required feedback for adjusting the input current of the clutch accordingly. To this effect, the FP-

<sup>8</sup>The frequency range of models: 1st 0.5-5Hz, 2nd 0.5-10Hz, 3rd 0.5-15Hz.

<sup>9</sup>The results are acquired by using the load cell.

GA board implements a PID controller to eliminate the error between the estimated and desired torque values. A set of experiments were conducted to validate the efficacy of this technique. The results clearly demonstrated that an MR clutch could act as a linear torque actuator to follow any reference torque signal. More importantly, this technique provides a very low-cost alternative to traditional force/torque control by eliminating the need for external sensors. This presents a significant advantage and contribution in force/torque control applications. Our future attention will be on the integration of the FPGA boards into the structure of MR actuators as shown in Fig. 2.21. More results in this regard will be reported in our future publications.



Figure 2.21: Embedded FPGA board inside MR clutches.

## Bibliography

- [1] A. S. Shafer and M. R. Kermani, “On the feasibility and suitability of mr fluid clutches in human-friendly manipulators,” *Mechatronics, IEEE/ASME Transactions on*, no. 99, pp. 1–10, 2011.
- [2] P. Yadmellat, A. S. Shafer, and M. R. Kermani, “Design and development of a single-motor,two-dof, safe manipulator,” in *Mechatronics, IEEE/ASME Transactions on In press*,doi:10.1109/TMECH.2013.2281598.
- [3] B. Tondu and P. Lopez, “The mckibben muscle and its use in actuating robot-arms showing similarities with human arm behaviour,” *Industrial Robot: An International Journal*, vol. 24, no. 6, pp. 432–439, 1997.
- [4] G. Pratt and M. Williamson, “Series elastic actuators,” in *Intelligent Robots and Systems 95.'Human Robot Interaction and Cooperative Robots', Proceedings. 1995 IEEE/RSJ International Conference on*, vol. 1, pp. 399–406, IEEE, 1995.
- [5] M. Zinn, B. Roth, O. Khatib, and J. Salisbury, “A new actuation approach for human friendly robot design,” *The international journal of robotics research*, vol. 23, no. 4-5, pp. 379–398, 2004.
- [6] A. Bicchi and G. Tonietti, “Fast and soft-arm tactics [robot arm design],” *Robotics & Automation Magazine, IEEE*, vol. 11, no. 2, pp. 22–33, 2004.
- [7] C. Chew, G. Hong, and W. Zhou, “Series damper actuator: a novel force/torque control actuator,” in *Humanoid Robots, 2004 4th IEEE/RAS International Conference on*, vol. 2, pp. 533–546, IEEE, 2004.
- [8] A. Bicchi, G. Tonietti, and R. Schiavi, “Safe and fast actuators for machines interacting with humans,” in *Robotics and Automation, 2004. TExCRA'04. First IEEE Technical Exhibition Based Conference on*, pp. 17–18, IEEE, 2004.
- [9] B. Kim, J. Park, and J. Song, “Double actuator unit with planetary gear train for a safe

- manipulator,” in *Robotics and Automation, 2007 IEEE International Conference on*, pp. 1146–1151, IEEE, 2007.
- [10] N. Takesue, H. Asaoka, J. Lin, M. Sakaguchi, G. Zhang, and J. Furusho, “Development and experiments of actuator using mr fluid,” in *Industrial Electronics Society, 2000. IECON 2000. 26th Annual Conference of the IEEE*, vol. 3, pp. 1838–1843, IEEE, 2000.
- [11] N. Takesue, J. Furusho, and Y. Kiyota, “Fast response mr-fluid actuator,” *JSME International Journal Series C*, vol. 47, no. 3, pp. 783–791, 2004.
- [12] J. Chen and W. Liao, “Design, testing and control of a magnetorheological actuator for assistive knee braces,” *Smart Materials and Structures*, vol. 19, no. 3, p. 035029, 2010.
- [13] P. Fauteux, M. Lauria, B. Heintz, and F. Michaud, “Dual-differential rheological actuator for high-performance physical robotic interaction,” *Robotics, IEEE Transactions on*, vol. 26, no. 4, pp. 607–618, 2010.
- [14] A. S. Shafer and M. R. Kermani, “Design and validation of a magneto-rheological clutch for practical control applications in human-friendly manipulation,” in *Robotics and Automation (ICRA), 2011 IEEE International Conference on*, pp. 4266–4271, IEEE, 2011.
- [15] A. S. Shafer and M. R. Kermani, “Magneto-rheological clutch with sensors measuring electromagnetic field strength,” Apr. 14 2011. WO Patent/2011/041890.
- [16] A. S. Shafer and M. R. Kermani, “Magneto- and electro- rheological based actuators for human friendly manipulators,” Nov. 1 2009. United States Patent U.S. Provisional Patent, Serial No. 61/272,597. 2009.
- [17] P. Yadmellat and M. R. Kermani, “Adaptive modeling of a magneto-rheological clutch,” in *IEEE/ASME Transactions on Mechatronics, Accepted 2nd round, under the 3rd revision*.

- [18] P. Yadmellat and M. R. Kermani, "Output torque modeling of a magneto-rheological based actuator," in *World Congress*, vol. 18, pp. 1052–1057, 2011.
- [19] M. Jolly, J. Bender, and J. Carlson, "Properties and applications of commercial magnetorheological fluids," *Journal of Intelligent Material Systems and Structures*, vol. 10, no. 1, pp. 5–13, 1999.
- [20] G. Pratt and D. Robinson, "Force-controlled hydro-elastic actuator," Dec. 17 2002. US Patent 6,494,039.
- [21] P. Yadmellat and M. R. Kermani, "Adaptive modeling of a fully hysteretic magneto-rheological clutch," in *Robotics and Automation (ICRA), 2012 IEEE International Conference on*, pp. 2698–2703, IEEE, 2012.
- [22] D. Wang and W. Liao, "Magnetorheological fluid dampers: a review of parametric modelling," *Smart Materials and Structures*, vol. 20, p. 023001, 2011.
- [23] R. Phillips, "Engineering applications of fluids with a variable yield stress," 1969.
- [24] J. Carlson, "What makes a good mr fluid?," *Journal of intelligent material systems and structures*, vol. 13, no. 7-8, pp. 431–435, 2002.
- [25] J. D. Carlson and M. R. Jolly, "Mr fluid, foam and elastomer devices," *Mechatronics*, vol. 10, no. 4, pp. 555–569, 2000.
- [26] M. Avraam, *MR-fluid brake design and its application to a portable muscular rehabilitation device*. PhD thesis, Ph. D. thesis, Université Libre de Bruxelles, Bruxelles, Belgium, 2009.
- [27] P. Kielan, P. Kowol, and Z. Pilch, "Conception of the electronic controlled magnetorheological clutch," *Przegląd Elektrotechniczny*, vol. 3, pp. 93–95, 2011.
- [28] L. Lennart, "System identification: theory for the user," *PTR Prentice Hall, Upper Saddle River, NJ*, 1999.

## Chapter 3

# Design Optimization and Comparison of Magneto-Rheological Actuators

*A part of this work has also been published in "IEEE International Conference of Robotics and Automation (ICRA) 2014".*

In this chapter, an optimization method for designing MR clutches is studied. The proposed method optimizes the geometrical dimensions of an MR clutch, hence its mass, for given output torque and electrical input power. The main idea behind this optimization is that the input power and output torque are two parameters that are normally known to the designer prior to the design of an MR clutch and considering these parameters in the optimization as fixed values has a practical significance. Having presented the optimization method, we compare the characteristics of three different MR clutch configurations in order to demonstrate the effectiveness of the proposed method. A comparison between the drum, single-disk and multi-disk configurations of MR clutches is performed. Using the proposed method one can select a suitable configuration as well as the geometrical dimensions for an MR clutch that best suits the requirements of each individual design.

## 3.1 Introduction

Magneto-Rheological (MR) fluids, carrying micrometer-scale particles, are a kind of smart material whose viscosity can be changed fast and reversibly using an external magnetic field. This property of MR fluids allows to accurately control the shear stress of the fluid by controlling the intensity of an external magnetic field [1]. As a result, MR fluids devices such as dampers, brakes and clutches have increasingly attracted attentions for various applications in recent years. Regardless of their applications, MR fluid devices hold great potentials in commercial field.

To this effect, a wide range of studies have been proposed within the context of designing good MR devices. The response time of an MR damper is discussed in [2] and the study shows that the response time decreases as the applied current or piston velocity increases. Using the results in [3], the geometrical parameters of a drum-type MR brake including the thickness of MR fluids can be calculated theoretically. After studying the influence of the material and the air gap in an MR clutch, Xu and Zeng proposed a design of an MR clutch for controlling the fan speed of an engine in a cooling system [4]. In order to achieve large output torque, Kwan, et al., proposed a new approach to build an MR brake by using small steel rollers as over-sized magnetic particles [5]. Recently, Finite Element Analysis (FEA) and optimization have been increasingly employed to design MR devices. A rotary MR brake was designed in [6] for a prosthetic knee optimized for maximum output torque and minimum off-state torque. The number of turns for a electromagnetic coil inside an MR brake was optimized in [7]. Multi objectives optimization techniques were employed in [8, 9], in order to design an MR brake with large output torque and small weight. The geometrical parameters of a disk-type MR brake were optimized in [10]. The objective of the optimization was to maximize the output torque of an MR brake which was constrained with a certain space. Achieving maximum magnetic flux density on MR fluids was selected as the objective of the optimization in [11]. A T-shape MR brake that used magnetic field in the axis and radius directions was proposed in [12]. The geometrical parameters of this brake were optimized considering the output torque, the mass of the brake, and the temperature caused by friction.

In our previous body of work, we developed a new actuation mechanism known as Distributed Active Semi-active Actuator (DASA) using MR clutches [13]. DASA is a novel actuation concept that emphasizes safe actuation without compromising the performance for Human-Compatible and Human-Friendly robots. The details and advantages of DASA have been reported in [14, 15, 16]. Unlike the design of MR devices mentioned above, achieving as large output torque as possible in designing MR clutches is not the primary concern. A larger output torque in an MR clutch may lead to more power consumption or lower control resolution which are not desired for human-safe robots. Thus, employing the optimization methods discussed in the aforementioned papers do not provide the most suitable solution in the case of designing an MR clutch. The concept of using an MR clutch in an actuator is presented in Fig. 3.1. As shown, the output torque of an MR clutch can be controlled using two inputs, namely the input current and the input mechanical power. In practice, the input mechanical power is often kept as a constant and an MR clutch is mainly controlled using the input current. The value of the input current is determined by the resistance of the coil inside the MR clutch and the electrical components outside the MR clutch. The resistance of the coil is dependent on the dimensions of the coil which can be optimized. Yet, the electrical components are normally determined prior to designing the MR clutch.

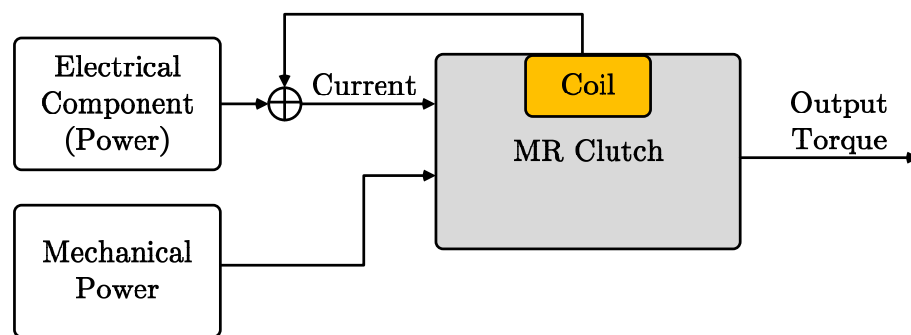


Figure 3.1: Use of MR clutch to an actuator.

The main contribution of this chapter is to propose an optimization method for designing MR clutches. In this optimization, the input electrical power of the MR clutch is considered as a fixed value and the geometrical dimensions of the clutch are optimized so as to make the MR clutch generate a certain output torque with the least possible mass. As men-

tioned above, the input electrical power and the output torque are commonly known before designing an MR clutch, hence considering them as fixed values during the optimization is a practical approach. This allows to change the values of the input power and the output torque based on the requirements of the problem so as to obtain the best configurations and geometrical dimensions.

In this chapter, we first compare three different MR clutch configurations, i.e., drum, single-disk, and multi-disk clutches with no constraints on the input current and output torque. While similar comparisons for MR brakes have been discussed in [17, 18], such comparisons are not directly applicable to MR clutches as explained previously. To the best of our knowledge, there is no reported study that draw a comparison between the characteristics of different MR clutch configurations. Having discussed the optimization method, we compare the characteristics of different MR clutch configurations for the case of constant input power and output torque. Using this method allows for the selection of a suitable configuration as well as geometrical dimensions for an MR clutch that best suits the requirements of each individual design.

The remaining of the chapter is organized as follows. Section 3.2 reviews three configurations of MR clutches and employs Bingham model to calculate the output torques for each of them. Section 3.3 presents the optimization process for the three configurations. Section 3.4 draws a comparison among the configurations considered and discusses the characteristics of each configuration. Finally, Section 3.5 concludes the chapter.

## 3.2 MR clutch

As known, with the effect of an external magnetic field, the particles within MR fluids join into columns aligned in the direction of the field. These columns can resist the shearing of the fluid perpendicular to the field. MR clutches are employed as a means of materializing this concept through bounding the amount of transmitted torque based on the intensity of an applied magnetic field. An MR clutch generally consists of input and output mechanical components, the MR fluids which fill the volume between the input and output components, and one or multiple electromagnetic coils used for generating a magnetic field. An

MR clutch provides two inputs for control the out of the clutch. One input is a rather constant mechanical power provided, for example, by an electric motor. This input introduces shearing between input and output mechanisms. The other input is the current into the electromagnetic coils to generate a magnetic field. With this magnetic field, the shear stress of the MR fluids would be altered, which allows the MR clutch to transmit the input power to the output as a function of shearing between input and output components.

### 3.2.1 Drum MR clutch

A drum-type MR clutch is one of the earliest proposed configurations. This configuration is often used to demonstrate the design of MR devices [19]. Fig. 3.2 demonstrates the cross section of a typical drum-type MR clutch. The output part includes an output shaft and an electromagnetic coil. The input part is a hollow cylindrical casing which surrounds the output part. The volume between the input and output parts is filled with MR fluids. Both output shaft and input parts are made of ferromagnetic materials in order to form a magnetic circuit path inside the MR clutch.

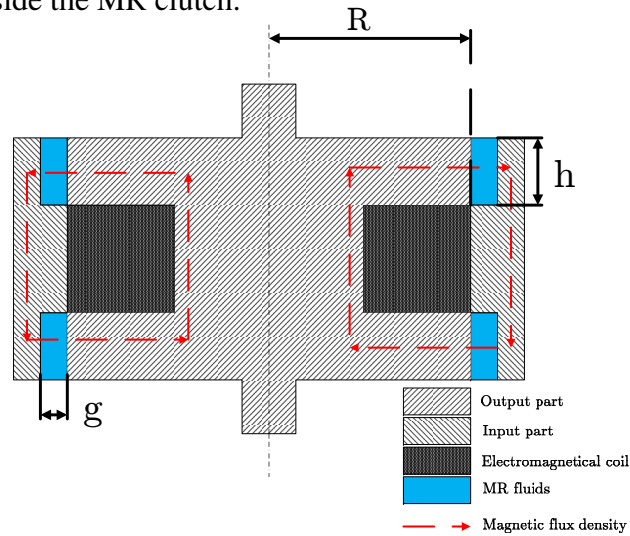


Figure 3.2: Cross section of the drum-type MR clutch.

The Bingham visco-plastic model is a good candidate to represent the shear stress of the MR fluids as a function of the applied field and shear rate [20, 21, 22, 23, 24]. According to the Bingham model, the shear stress can be presented as:

$$\tau = \tau_y(H) + \eta \frac{dv}{dz}, \quad \tau > \tau_y \quad (3.1)$$

where  $\tau$  is the shear stress,  $\tau_y$  is the field dependent yield stress,  $H$  is the applied magnetic field intensity,  $\eta$  is the Newtonian viscosity, and  $\frac{dv}{dz}$  is the velocity gradient in the direction of the field. Applying the Bingham model to the MR clutch in Fig. 3.2, results in the following new model:

$$\tau = \tau_y(H) + \eta\dot{\gamma}(\omega, r, g), \quad \tau > \tau_y \quad (3.2)$$

where the shear rate  $\dot{\gamma}$  is defined as

$$\dot{\gamma} = \frac{\omega r}{g} \quad (3.3)$$

in that  $\omega$  is the angular velocity between input and output parts,  $r$  is the radius from the rotational axis, and  $g$  is the thickness of fluid-filled gap between input and output parts. It is interesting to note that the first term on the right-hand side of (3.2) is only related to the electrical input while the second term is only related to the mechanical input to the MR clutch. In other words, the input current can only affect the output torque via the field dependent yield stress, i.e.,  $\tau_y$ .

In an MR clutch, the output torque can be presented as

$$dT = r\tau dA \quad (3.4)$$

where  $r$  is the radius from the rotational axis,  $\tau$  is the shear stress of the MR fluids, and  $A$  is the area of active MR fluids inside the clutch. Substituting (3.2) into (3.4) and integrating across the MR fluids area for a drum-type clutch (shown the Fig. 3.2), we can obtain the output torque of the clutch as,

$$T_{Drum} = 4\pi\tau_y(H)R^2h + 4\pi\eta\frac{\omega R^3}{g}. \quad (3.5)$$

It should be noted that in this output torque, the viscosity of the carrier fluid  $\eta$  is typically within a range of 0.1 to 0.3 Pa-s and  $\omega$  approaches zero as the MR fluids become more solidified. On the other hand, the contribution of  $\tau_y(H)$  to the output torque is within a range of kPa-s torque for typical MR fluids. Thus, it is reasonable to ignore the second term in (3.5) due to its negligible effect on the estimated value of the output torque. As a result, the output torque of a drum-type MR clutch can be approximately rewritten as,

$$T_{Drum} \approx 4\pi\tau_y(H)R^2h. \quad (3.6)$$

As mentioned earlier, the only parameter affecting  $\tau_y(H)$  is the electrical current input. Given that the mechanical input to an MR clutch is often a constant value, one can define the dynamic range of an MR clutch  $DR$  with respect to its input current as,

$$DR = \frac{\int_A r\tau_{y_{max}}dA}{\int_A r\eta\dot{\gamma}dA} \quad (3.7)$$

where  $\tau_{y_{max}}$  is the maximum attainable shear stress with the MR fluids for a given input current and configuration of an MR clutch. The nominator of (3.7) represents the maximum output torque that the MR clutch can generate while the dominator is the output torque that the MR clutch can generate with zero input current applied. According to (3.7), the dynamic range of a drum-type MR clutch can be obtained as,

$$DR_{Drum} = \frac{\tau_{y_{max}}g}{\eta\omega R} \quad (3.8)$$

### 3.2.2 Single-Disk MR clutch

The disk-type, including single-disk and multi-disk MR clutch is the most common configuration due to its good performance. This configuration has been employed for commercial purposes. A number of studies on disk-type MR devices, including MR clutches, can be found in the literature where incremental modifications on this configuration have been proposed and exercised. In this chapter, we consider a typical disk-type MR clutch only, for the purpose of our study.

Fig. 3.3 shows the cross-section of a single-disk MR clutch. Similar to a drum-type MR clutch, the output part of a single-disk MR clutch also serves as the output shaft. An electromagnetic coil is mounted on the shaft. Additionally, there is a single thin output disk mounted on the output shaft. The input part encloses the output parts, and the volume between the input and the output parts is filled with MR fluids. In this configuration, the magnetic field generated by the coil along the output shaft axis crosses the MR fluids perpendicularly. Providing the mechanical input to rotate the input part of a signal-disk MR clutch introduces shearing on both sides of the output disk when the coil is activated, thereby resulting in an output torque on the shaft. Using to (3.2) and (3.4), the output torque of

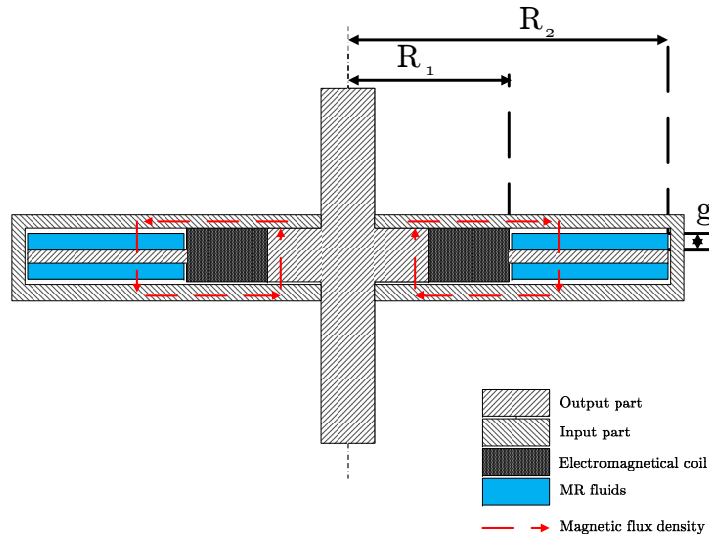


Figure 3.3: Cross section of a single-disk-type MR clutch.

a single-disk MR clutch can be obtained in a similar way as before as,

$$\begin{aligned}
 T_{SingleDisk} &= 2 \int_{R_1}^{R_2} 2\pi \left( \tau_y(H)r^2 + \eta \frac{\omega r^3}{g} \right) dr \\
 &= 4\pi \left( \frac{\tau_y(H)(R_2^3 - R_1^3)}{3} + \frac{\eta\omega(R_2^4 - R_1^4)}{4g} \right)
 \end{aligned} \quad (3.9)$$

where  $R_1$  and  $R_2$  are the inner and outer radius of the disk as shown in Fig. 3.3 and other parameters are as defined previously. Under the same assumptions made in the case of a drum-type clutch, the major contribution to the output torque is made by the first term in (3.9). In this way, the output torque of a single-disk MR clutch can be rewritten as,

$$T_{SingleDisk} \approx \frac{4\pi\tau(H)(R_2^3 - R_1^3)}{3} \quad (3.10)$$

Following the same definitions given in (3.7), the dynamic range of the single-disk MR clutch is obtained as,

$$DR_{SingleDisk} = \frac{4\tau_{y\max}g(R_2^3 - R_1^3)}{3\eta\omega(R_2^4 - R_1^4)}. \quad (3.11)$$

where  $\tau_{y\max}$  is the maximum shear stress that the MR fluids can achieve in a single-disk MR clutch.

### 3.2.3 Multi-Disk MR clutch

In order to achieve a considerable torque capacity, multi-disk MR clutches can be used to increase the active areas of the MR fluids. Each individual disk inside a multi-disk MR

clutch can provide two sides of the disk as the active areas and with  $N$  output disks, the active areas inside a multi-disk MR clutch can be expanded up to  $2N$  times larger than the active area of a single-disk MR clutch. Fig. 3.4 demonstrates the cross section of a typical multi-disk MR clutch. Assuming  $N$  output disks, the output torque and the dynamic range of a multi-disk clutch can be derived from those for a single-disk MR clutch as,

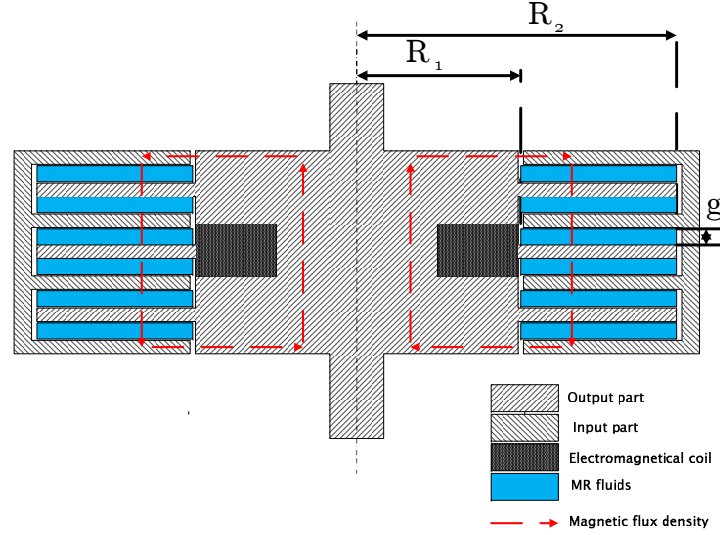


Figure 3.4: Cross section of the multi-disk-type MR clutch.

$$T_{MultiDisk} \approx \frac{4N\pi\tau(H)(R_2^3 - R_1^3)}{3} \quad (3.12)$$

$$DR_{MultiDisk} = \frac{4\tau_{ymax}g(R_2^3 - R_1^3)}{3\eta\omega(R_2^4 - R_1^4)}. \quad (3.13)$$

in that all parameters are as defined previously. As expected, the output torque of an  $N$ -disk MR clutch is  $N$  times larger than the output torque of a single-disk MR clutch with similar dimensions. However, given that the zero-current output torque of an  $N$ -disk MR clutch is also increased by a factor of  $N$ , an  $N$ -disk MR clutch enjoys the same dynamic range as a single-disk MR clutch.

In this section, the output torque of drum, single-disk, and multi-disk type MR clutches were obtained using Bingham model. The dynamic range of each configuration were also obtained and compared. While using these results it is possible to directly compare different configurations for their achievable torques, to draw a more inclusive comparison, other parameters such as mass, volume, coil size, etc. need to be considered. This will be the subject of the following sections.

### 3.3 Design Optimization

The three mentioned configurations are optimized in this section, so as to accommodate a fair comparison between different MR clutch configurations. To be able of comparing different configurations, it is required to calculate the characteristics of each configuration. The characteristics considered in this body of work include weight, current capacity, torque-mass ratio, and moment of inertia, all of which are functions of the geometrical parameters for a given configuration. The magnetic field estimation is required to optimize these characteristics. The well-known Finite Element Method (FEM) was hired to estimate the magnetic field and calculate the characteristics for each configuration, using COMSOL Multiphysics software.

#### 3.3.1 Material Selection

For the sake of achieving acceptable distribution of magnetic field inside MR clutches, different parts of an MR clutch are designed to use specific materials. These materials affect the performance of an MR clutch significantly. During the process of FEM and optimization, properties of all materials are required in COMSOL Multiphysics. To build an MR clutch, basically, there are four kinds of materials should be confirmed. They are the materials of coil and MR fluids, ferromagnetic material and nonmagnetic material. In this chapter, each of the above four materials is selected identical for different configurations. To this end, there is no difference caused by materials in comparison among all configurations.

For drum, single-disk and multi-disk MR clutches in this chapter, we employ copper as the material of their coils. In order to achieve magnetic field whose direction is perpendicular to disks, the materials of outer casings in single-disk and multi-disk configurations must be nonmagnetic. Aluminum is a good candidate for this material as its relative small mass density. MRF-140CG fluids, selected as MR fluids, are a kind of high yield stress MR fluid whose mass density is  $3540\text{--}3740\text{ kg/m}^3$ , and viscosity is  $0.280\pm 0.07\text{ Pa}\cdot\text{s}$  at  $40^\circ\text{C}$ . Fig. 3.5 demonstrates the relationship between shear stress and magnetic field intensity for MRF-140CG. According to this relationship and the Bingham model, once we obtain magnetic field information through using FEM, the output torque of an MR clutch can be

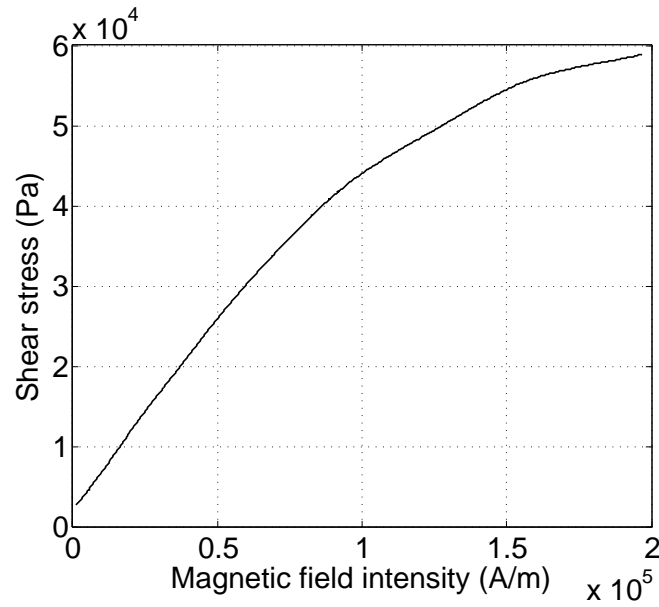


Figure 3.5: Shear stress versus magnetic field intensity for MRF-140CG.

calculated easily. To form magnetic circuits inside MR clutches, ferromagnetic material is used to make some particular parts of MR clutches, including shafts and inter casings in all configurations, disks in disk-type configurations and the outer casing in drum configuration. AISI steel 1018 is employed as ferromagnetic material in this chapter. However, both MRF-140CG fluids and AISI steel 1018 feature nonlinearity in magnetic property. Their relationships between magnetic intensity ( $H$ ) and magnetic flux density ( $B$ ) is presented as:

$$B = \mu_0 \mu_r H \quad (3.14)$$

where  $\mu_0 = 4\pi \times 10^{-7}$ , is vacuum permeability and  $\mu_r$  is relative permeability whose value is dependent on magnetic field. Fig. 3.6 and Fig. 3.7 report relative permeabilities of MRF-140CG fluids and AISI steel 1018 whose values are changing with magnetic flux densities

Using equation (3.14) and information from Fig. 3.6 and 3.7, magnetic properties of MRF-140CG fluids and AISI steel 1018 can be imported into COMSOL Multiphysics through employing B-H curves respectively.

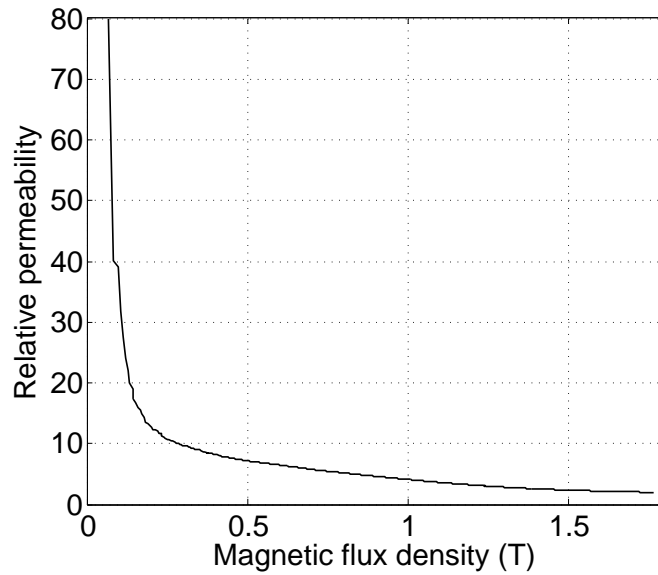


Figure 3.6: Relative permeability versus magnetic flux density for MRF-140CG.

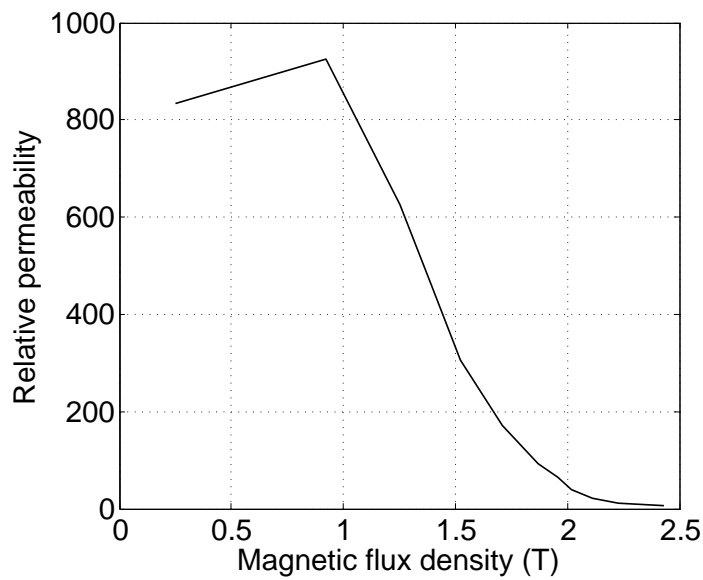


Figure 3.7: Relative permeability versus magnetic flux density for AISI steel 1018.

### 3.3.2 Optimal design of MR clutches

In order to obtain optimal designs for MR clutches the following objective function is proposed,

$$\text{Obj} = \min(W_1|T_r - T_d| + W_2M) \quad (3.15)$$

subject to  $J_D \leq 2.5A/mm^2$

where  $W_1$  and  $W_2$  are weighting coefficients such that  $W_1 + W_2 = 1$ ,  $T_r$  is the desired torque,  $T_a$  is the predicted output torque of the clutch,  $M$  is the mass, and  $J_D$  is the current density applied to the coil. The rationale behind selecting this objective function is to minimize the clutch weight, yet being capable of providing the desired torque. Optimizing MR clutches weights are important in employment of them as part of robots actuators. Obviously, the objective function results in the maximum torque-to-mass ratio, for a given desired torque. A practical limitation, the temperature tolerance of copper wires for coil, is considered in the proposed objective function. The maximum allowable current density for copper wires is  $2.5A/mm^2$  pertinent to their temperature tolerances[25].

In order to find solutions for the optimization problem defined in (3.15), the coil current density is required. The cross section of a coil in MR clutches is depicted in Fig. 3.8. To obtain  $J_D$ , the coil resistance produced by a circumferential element at radius  $r$  is given by

$$dR = \rho_c \frac{2\pi r}{H_c dr}, \quad (3.16)$$

where  $\rho_c$  is the resistivity of the coil wire,  $H_c$  is the length of the coil. Then the power required at radius  $r$  is given by  $dP = (dI)^2 dR$ , where  $dI = J_D H_c dr$  is the current at radius  $r$ . Hence,

$$dP = (J_D H_c dr)^2 \rho_c \frac{2\pi r}{H_c dr}. \quad (3.17)$$

Integrating across the whole cross section gives the required power for a given  $J_D$  as follows,

$$P = J_D^2 H_c \rho_c 2\pi \int_{r_1}^{r_2} r dr. \quad (3.18)$$

Given the fact that the available electrical power is limited for a specific application, we define  $P_r$  as the available electrical power as an added consideration for the design of an MR clutch. According to (3.18), an added condition for the current density  $J_D$  can be given as

$$J_D \leq \left( \frac{P_r}{2\pi H_c \rho_c \int_{r_1}^{r_2} r dr} \right)^{\frac{1}{2}}. \quad (3.19)$$

Note that the application of the optimization results may become controversial without considering the power limitation as well as the temperature tolerance.

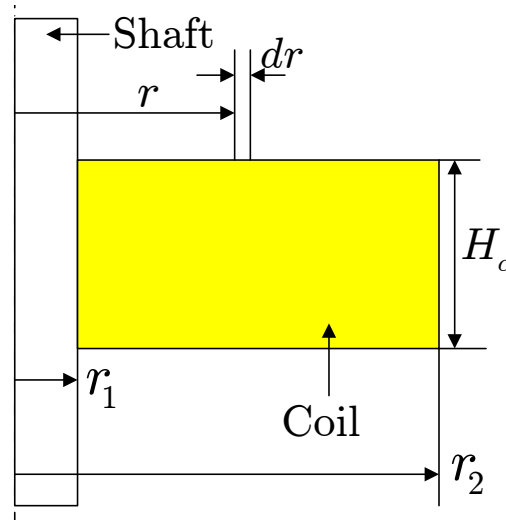


Figure 3.8: Cross section of the coil.

### 3.4 Results and Discussions

Optimal designs of single-disk, multi-disk, and drum based MR clutch configurations are presented in this section. To obtain optimal design for each configuration, the objective function given in (3.15) is considered. To make different configurations comparable, we considered the situation when the desired output torque and the available electrical power for all configurations are identical. Accordingly,  $P_r$  was set as  $2W$  and the desired torque  $T_r$  was considered as  $20Nm$ . Further, the weighting coefficients  $W_1$  and  $W_2$  in (3.15) were set as 0.7 and 0.3, respectively. Since our primary goal is to obtain clutch parameters under which the clutch can provide the desired torque, more weight was put on the torque term in the objective function compared to the clutch mass.

Due to the fact that drum and disk-based configurations differ topologically, different optimization variables should be considered. Table 3.1 lists the optimization variables for drum configuration, while the optimization variables for disk-type configurations are listed in Table 3.2. Due to manufacturing and implementation considerations, the thickness of disk and the size of MR fluids gaps were fixed to  $1\text{ mm}$  and  $0.5\text{ mm}$  in both disk-type configurations. Figs. 3.9 and 3.10 display the magnetic flux density, respectively, in drum and single-disk configurations.

Similar to single-disk MR clutch, the thickness of output disks and the MR fluids gaps

Table 3.1: Optimized dimensional variables in Drum configuration

Variables to be optimized	Corresponding position in Fig. 3.9
radius of shaft	A
width and height of inner casing	B
width and height of coil	C
width of outer casing	D
height of MR fluids	E

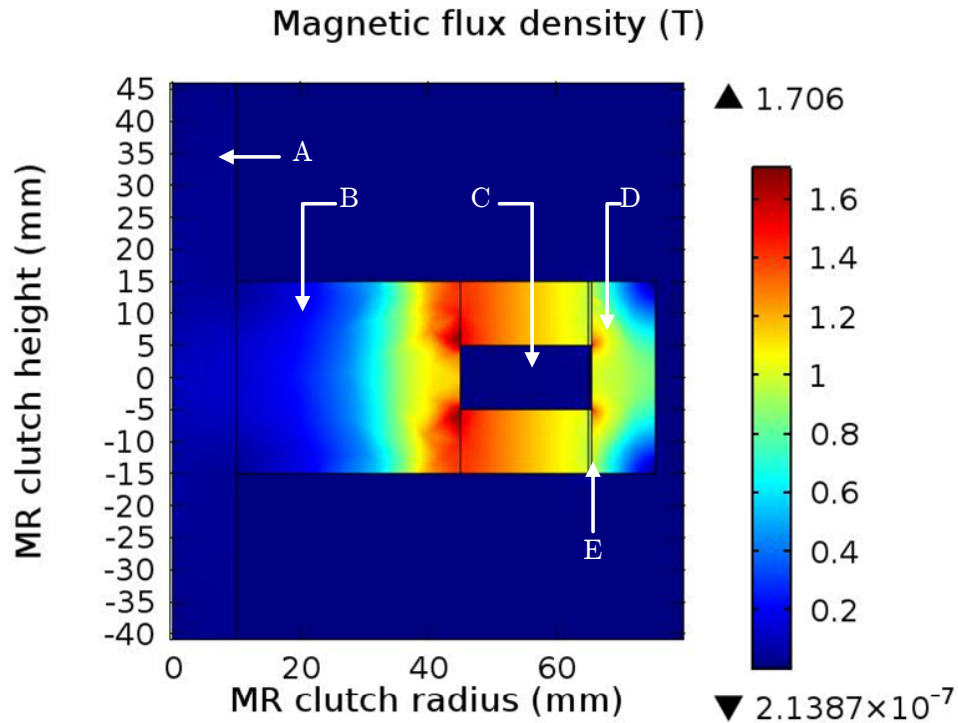


Figure 3.9: Magnetic flux density contour map in drum configuration with 2 W input power.

of the multi-disk MR clutch are set to be 1 mm and 0.5 mm. In this study, a 3-output-disk MR clutch is selected as an example of multi-disk configuration. Dimension variables that should be optimized and magnetic flux density in this configuration are shown in Table 3.3 and Fig. 3.11.

Table 3.2: Optimized dimensional variables in Single-Disk configuration

Variables to be optimized	Corresponding position in Fig. 3.10
radius of shaft	A
width and height of inner casing	B
width and height of coil	C
width of outer casing	D
radiuses of output disk	$R_1, R_2$

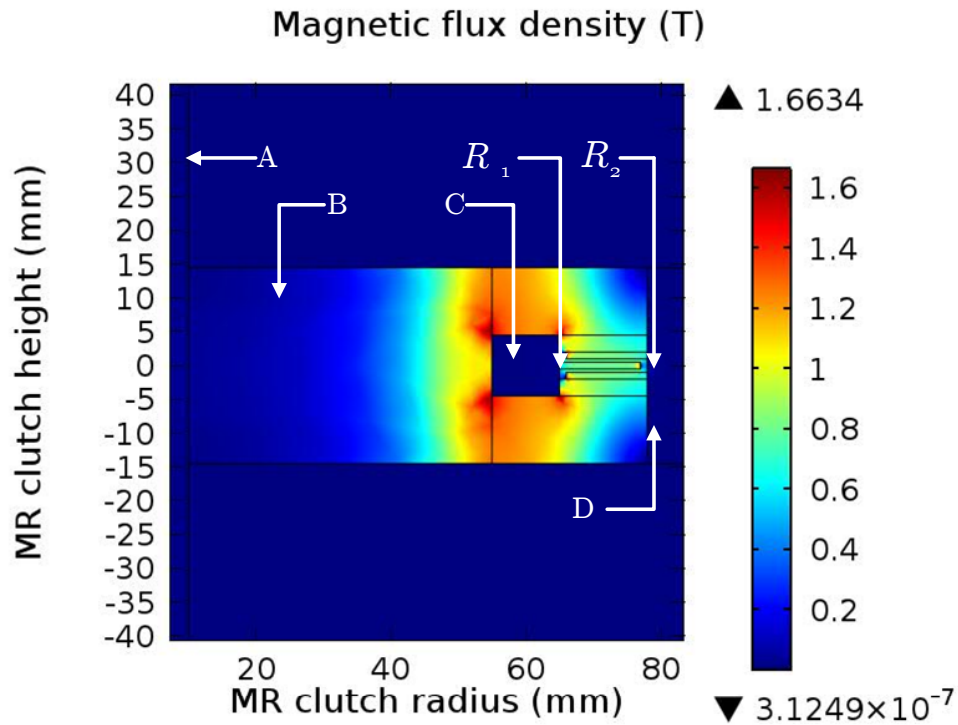


Figure 3.10: Magnetic flux density contour map in single-disk configuration with 2 W input power.

### 3.4.1 Validation of the model in COMSOL Multiphysics

Since the optimization results provided in this work were obtained using COMSOL Multiphysics, it is necessary to validate the model considered in the software. To this end, the results of the COMSOL model is compared with an experimental results obtained from a developed MR clutch. The MR clutch considered for this comparison was implemented for actuation of a 2-DOF manipulator, detailed in [26]. Table 3.4 lists the specification-

Table 3.3: Optimized dimensional variables in Multi-Disk configuration

Variables to be optimized	Corresponding position in Fig. 3.11
radius of shaft	A
width and height of inner casing	B
width and height of coil	C
width of outer casing	D
radiuses of output disk	$R_1, R_2$

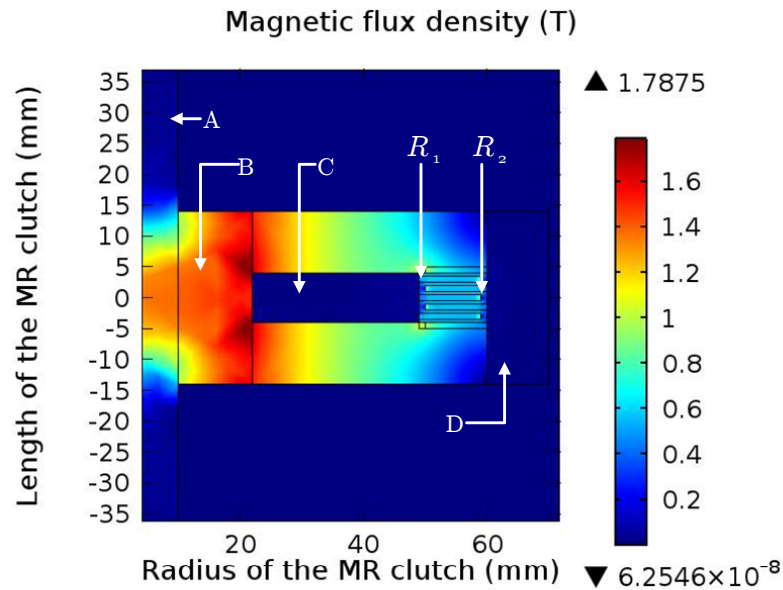


Figure 3.11: Magnetic flux density contour map in 3-disk configuration with 2 W input power.

s of the developed clutch for the 2-DOF manipulator. The materials used in this clutch were selected as the same as materials considered in this study. A couple of linear hall sensors were embedded inside the clutch, accommodating magnetic field measurements. A force/torque sensor (ATI Gamma US-15-50) was employed for torque measurements. Fig. 3.12 shows the results obtained in COMSOL Multiphysics corresponding to this MR clutch simulated for 1 A input current. To validate the COMSOL model, the output torque and magnetic field were simulated in COMSOL for two different amount of input currents. Same input currents were applied to the developed MR clutch, and the magnetic field and

Table 3.4: Specifications of the developed MR clutch for the 2-DOF manipulator

Number of disks	2
Disk thickness [mm]	1
MR fluid gap thickness [mm]	0.5
Inner radius of the disks [mm]	44.9
Outer radius of the disks [mm]	50.4

the output torque were experimentally measured. Table 3.5 compares the results simulated in COMSOL with those measured experimentally. The comparison results confirm that the simulation are very close to the measurements, verifying the model considered in COMSOL Multiphysics can effectively estimate characteristics of actual MR clutches.

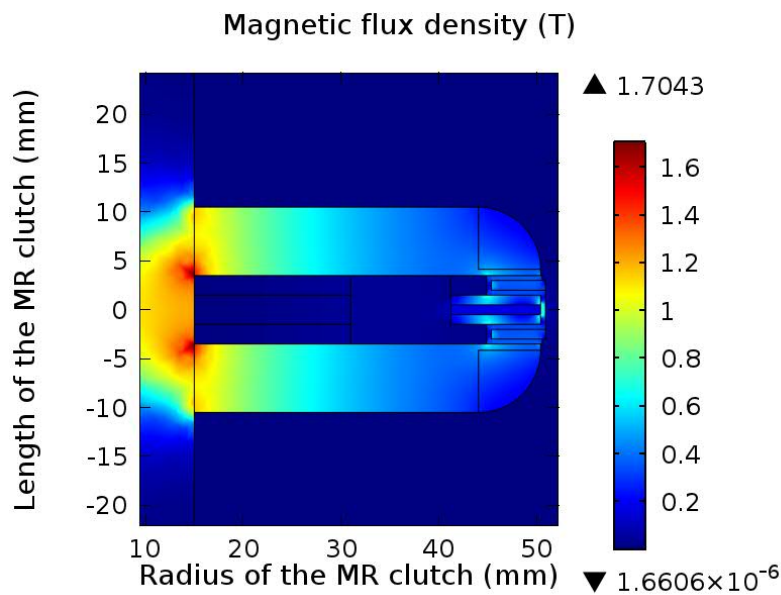


Figure 3.12: Magnetic flux density contour map in corresponding model of MR clutch with 1 A input current.

### 3.4.2 Analysis Results

The optimization results for drum, single-disk and 3-disk MR clutch configurations are given in Table 3.6. The output torques reported in Table 3.6 were calculated based on the

Table 3.5: Comparison between measured results and simulation

	Measured results	Simulation results
<b>with 1.12 A input current</b>		
Output torque [Nm]	1	1.12
Magnetic flux density [mT]	61.5	67
<b>with 2.12 A input current</b>		
Output torque [Nm]	2	2.07
Magnetic flux density [mT]	118.5	123.9

Bingham model. As observed, the output torque estimated for all configurations are close to the desired torque, i.e.  $T_r = 20 \text{ Nm}$ . Moreover, considering the optimized volume and mass of each configuration, disk-type MR clutches offers smaller volume and mass comparing with the drum configuration. The maximum current density is obtained for single-disk configuration, indicating that this configuration requires electrical components with higher current capacity compared to the other configurations. As an important result, the 3-disk MR clutch features the lowest moment of inertia, while the moment of inertia is significantly higher in drum and single-disk configurations. This is because the optimization for drum and single-disk configurations resulted in heavier components for drum-type and larger radius components for single-disk. Furthermore, assuming the relative velocity between input and output shafts is  $1 \text{ rad/s}$ , zero-current-applied output torques were calculated. As can be seen, the calculated torques are insignificant for all configurations, while the drum configuration gives the smallest value. As an additional design consideration, H-R ratio is defined, where H and R stand for the height and radius of the resultant MR clutches. In this respect, the drum configuration features relatively large H-R value, which makes it more suitable for applications requiring small radius clutch, while the height might not be an issue.

The last row of Table 3.6 reports the time constant of coil circuit which is estimated by using mathematic method. The coil circuit inside an MR clutch is actually a resistor-inductor (R-L) circuit. Once the geometrical dimensions of coil are determined (see the

Table 3.6: Comparison among MR clutches in different configurations

	Drum	1-disk	3-disk
Output torque			
[Nm]	19.97	19.91	19.78
Volume			
[ $mm^3$ ]	556.24	391.18	<b>337.06</b>
Mass			
[kg]	4.15	2.81	<b>2.36</b>
Current density			
[ $A/mm^2$ ]	<b>1.32</b>	1.88	1.58
Output moment inertia			
[ $gm^2$ ]	6.81	4.66	<b>3.84</b>
Zero-current-applied torque			
$\omega = 1rad/s$ , [Nm]	<b>0.0138</b>	0.02174	0.02395
H-R ratio	<b>0.55</b>	0.38	0.47
Time constant			
( $ms$ )	5	<b>3</b>	13

Fig. 3.13), the value of electrical resistance can be calculated as:

$$\mathfrak{R} = \frac{2\pi NR_a}{S\pi r_c^2} \quad (3.20)$$

$$R_a = R_s + W_i + \frac{1}{2}W_c$$

where  $N$  is number of turns,  $R_a$  is average radius of coil,  $S$  is electrical conductivity of copper,  $r_c$  is radius of a copper wire. The average radius of coil is the sum of shaft radius, width of inner casing and half width of coil. Based on the formula in [27], the inductance

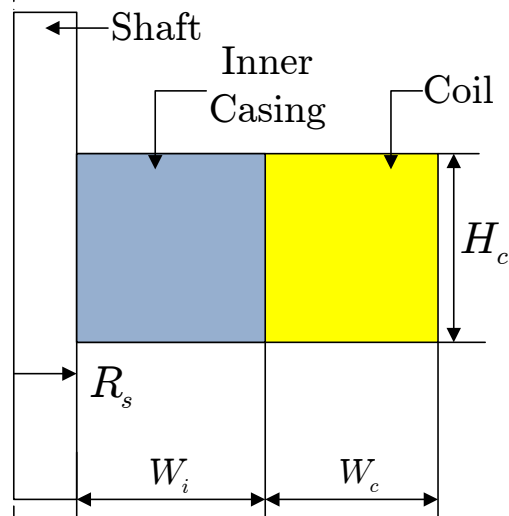


Figure 3.13: Cross section of the coil circuit.

of coil can be presented as:

$$\begin{aligned} \ell &= \frac{0.8a^2N^2}{6a + 9b + 10c} \\ a &= R_s + W_i + \frac{1}{2}W_c \\ b &= H_c \\ c &= W_c \end{aligned} \quad (3.21)$$

Considering the cross area of coil and the radius of a copper wire, the number of turns is:

$$N = \frac{W_c H_c}{2r} \quad (3.22)$$

Therefore, the time constant  $\tau$  for R-L circuit in an MR clutch is calculated as:

$$\begin{aligned} \tau &= \frac{\ell}{\mathfrak{R}} \\ &= \frac{0.1aH_cW_cS}{6a + 9b + 10c} \end{aligned} \quad (3.23)$$

it is interesting to note that the value of time constant is only related to the geometrical dimensions. No matter what kind of copper wires are selected or how we wind coil, the time constant keeps the same. From results in the last row, single-disk configuration features the smallest time constant of coil circuit.

Torque-to-mass ratio is widely recognized as an important criterion for human-safety actuation. Fig. 3.14 presents the torque-to-mass ratio for drum, single-disk and multi-disk configurations. Among them, the multi-disk configuration offers higher torque-to-mass ratio compared to the drum and single-disk configurations.

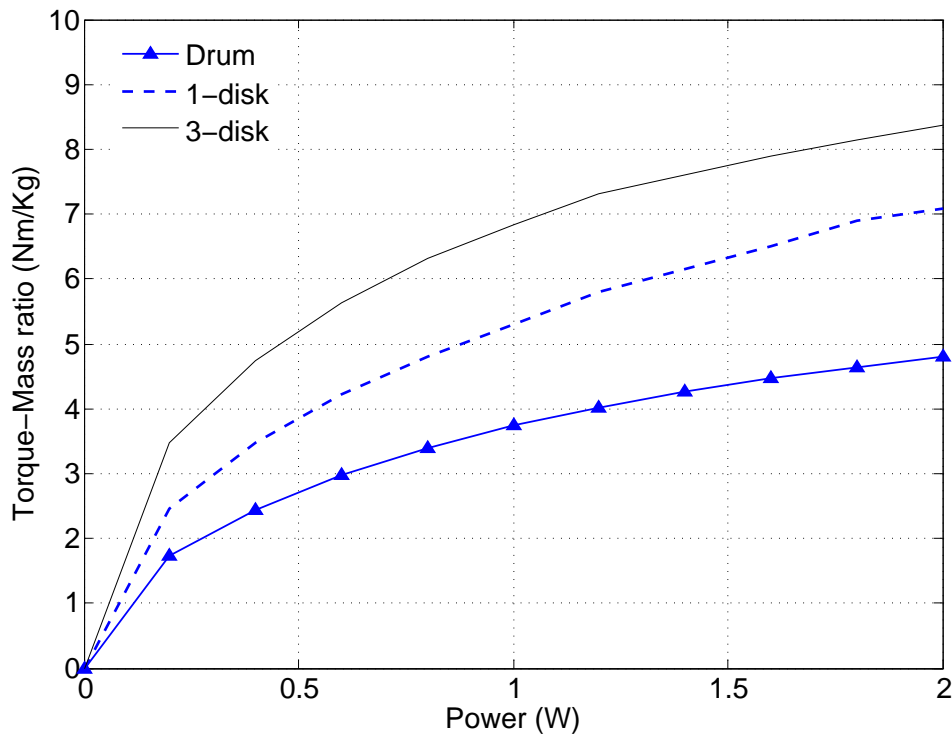


Figure 3.14: Torque-mass ratio versus input power for three configurations.

Characteristics of multi-disk MR clutches change by varying the number of output disks. To inspect this effect, the 5-disk MR clutch was optimized to compare its characteristics with 3- and single-disk clutches. The comparison results are given in Table 3.7. The 5-disk features the lightest and most compact design among other clutches.

Fig. 3.15 demonstrates the torque-to-mass ratios for 1-, 3- and 5-disk MR clutches when input power increases from 0 to 2 W. The 5-disk MR clutch features the highest torque-to-mass ratio optimized for input power within 0 to 2 W range, suggesting that increasing number of disk can be resulted in higher torque-to-mass ratio irrespective to the considered input electrical power. However, the torque-mass ratio would not increase all the time by adding more disks. A 9-disk MR clutch was optimized using the same method and its torque-to-mass ratio is shown in Fig. 3.15 as well. It can be seen that the torque-to-

Table 3.7: Comparison among disk-type MR clutches with different number of output disks

	1-disk	3-disk	5-disk
Output torque			
[Nm]	19.91	19.78	19.23
Volume			
[ $mm^3$ ]	391.18	337.06	<b>234.12</b>
Mass			
[kg]	2.81	2.36	<b>1.50</b>
Current density			
[ $A/mm^2$ ]	1.88	1.58	<b>1.35</b>

mass ratio can drop significantly exceeding a certain number of disks. In our analysis, the torque-to-mass ratio for the 9-disk was obtained even less than that of 1-disk. Intuitively, adding more disks result in a heavier MR clutch, while the output torque may decrease due to more fluid gaps. Note that the magnetic field within MR clutches depend on the number of fluid gaps, and increasing the number of fluid gaps can significantly reduce the magnetic field. This is because of high reluctance of MR fluids.

MR fluid gap sizes can be considered as another design consideration specifically for multi-disk configuration. Theoretically, increasing/decreasing the gap sizes of MR fluids results in dramatically increasing/decreasing of total reluctance of the magnetic circuit, which significantly effects on the MR clutches characteristics. To observe this effect, the geometrical dimensions of 3-disk MR clutch were optimized considering different fluid gap sizes. The MR fluids gaps for this purpose were chosen as 0.1 mm, 0.5 mm and 0.9 mm respectively. The resultant characteristics for each case are given in Table 3.8

As observed, smaller fluid gap size offers lighter and more compact clutch. On the contrary, the MR clutches with smaller gaps require higher input currents. The torque-mass ratio resulted for clutches with different gap sizes are shown in Fig. 3.16. The smaller gap sizes features higher torque-to-mass ratio, considering the input power varying within 0 to 2 W range. In practice, it is however difficult to achieve to very small fluids gaps. The

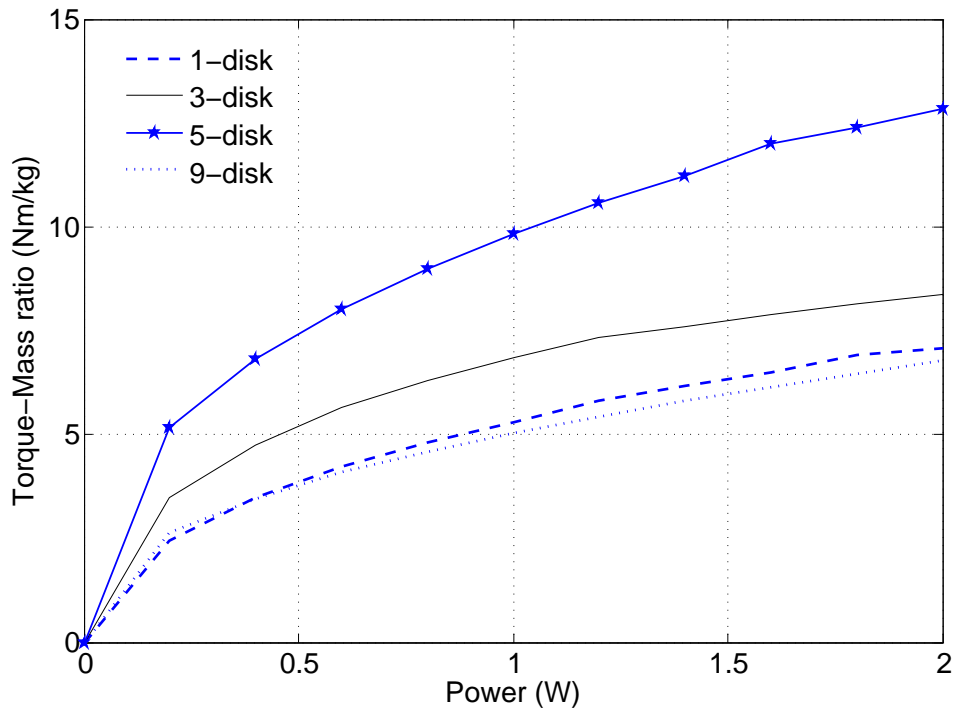


Figure 3.15: Torque-mass ratio versus input power for different output disks configurations.

Table 3.8: Comparison among disk-type MR clutches with different MR fluids gap sizes

	0.1 mm gap	0.5 mm gap	0.9 mm gap
Output torque			
[Nm]	20.25	19.78	19.62
Volume			
[ $mm^3$ ]	<b>203.01</b>	337.06	407.98
Mass			
[kg]	<b>1.38</b>	2.36	3.01
Current density			
[ $A/mm^2$ ]	1.78	1.58	<b>1.38</b>

main challenges arises when MR fluid needs to be injected through the fluid gaps.

In summary, Table 3.9 concludes the characteristics of drum, single-disk and multi-disk MR clutches.

It can be seen that among these three configurations, the drum configuration possesses

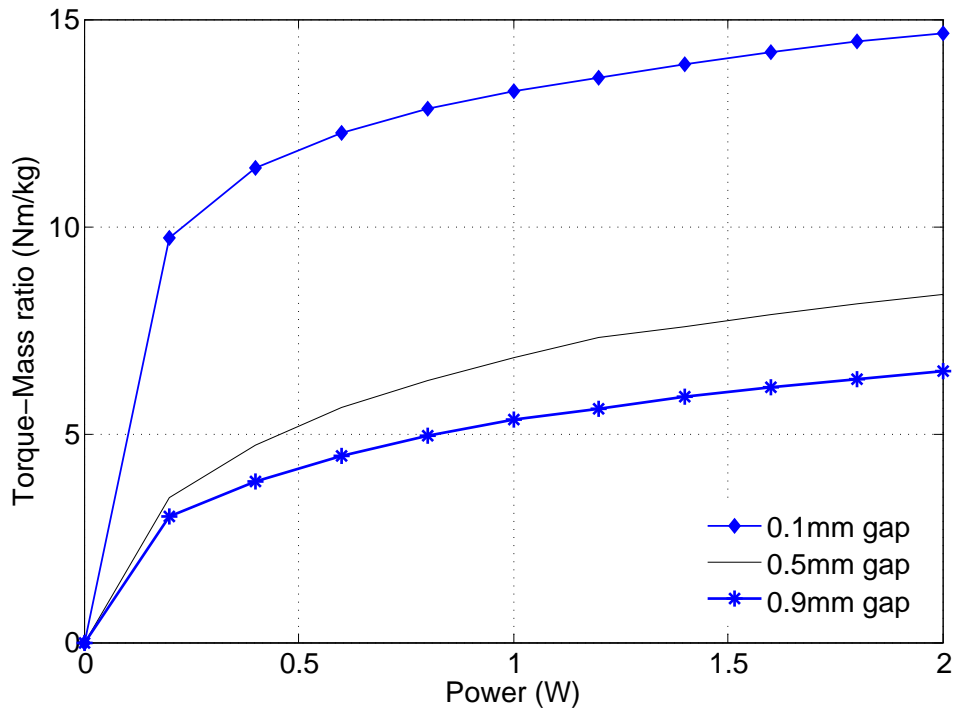


Figure 3.16: Torque-mass ratio versus to input power for different gap sizes.

Table 3.9: Conclusion of comparisons among different configurations

	Drum	Single-disk	Multi-disk
Compactness	Ordinary	Good	<b>Excellent</b>
Weight	Ordinary	Good	<b>Excellent</b>
Current capacity	<b>Excellent</b>	Ordinary	Good
Torque-to-mass ratio	Ordinary	Good	<b>Excellent</b>
Zero-current-applied torque	<b>Excellent</b>	Good	Ordinary
Output moment inertia	Ordinary	Good	<b>Excellent</b>
H-R ratio	<b>Excellent</b>	Ordinary	Good
Manufacturing	<b>Excellent</b>	Good	Ordinary

less compactness, heavier design, and larger output moment of inertia compared to other configurations. However, the drum configuration features the smallest zero-current-applied output torque as well as relatively large H-R ratio. Another advantage of drum configuration is that the manufacturing of drum-based clutches are easier in general compared to

multi-disk configurations. The single-disk configuration demonstrates middle level characteristics among other configurations. The main issue with using single-disk clutches is that they may possess a very large radius, constraining their application in specific environments. They also require the electrical component with larger current capacity. The multi-disk configuration, in turn, exhibits the best characteristics considering compactness, weight, torque-to-mass ratio, and moment of inertia. Their H-R ratios are also larger comparing to single-disk configuration, making them an alternative option for tasks requiring higher compactness. Careful attention should be paid however designing MR clutches with high number of disks. Characteristics of MR clutches can dramatically affected by increasing the number of disks, hence the number of fluid gaps. Also, increasing number of disks would result in more complicated assembling. Moreover, the fluid gap sizes can alter characteristics of multi-disk clutches, as increasing gap sizes will result in reduction in magnetic field and output torques in MR clutches.

### 3.5 Conclusion

In this chapter, an optimized design for MR clutches was presented aiming at minimizing the clutch mass for a desired torque. To this intent, several configurations were considered for MR clutches, including drum, single-disk, and multi-disk arrangements. A new objective function was proposed for optimizing the MR clutch parameters. As an important aspect of the new objective function, the physical limitations on the available electrical power and the temperature tolerances of coil wire were considered as well in the design optimization. Thorough analysis were performed to discuss characteristics of each configuration obtained by optimization. Advantages and disadvantages of each configuration were highlighted. In addition, sensitivities of the characteristics to variation of fluid gap sizes were analysed specifically for multi-disk clutches. It was concluded that smaller gaps would result in higher torque-to-mass ratio. The analysis provided in this chapter could be used in selecting proper configuration for an MR clutch and optimizing MR actuators for robots.

## Bibliography

- [1] J. Carlson and J. Sproston, "Controllable fluids in 2000 status of er and mr fluid technology," in *Actuator 2000?th International Conference on New Actuators*, pp. 126–130, 2000.
- [2] J.-H. Koo, F. D. Goncalves, and M. Ahmadian, "A comprehensive analysis of the response time of mr dampers," *Smart materials and structures*, vol. 15, no. 2, p. 351, 2006.
- [3] J. Huang, J. Zhang, Y. Yang, and Y. Wei, "Analysis and design of a cylindrical magneto-rheological fluid brake," *Journal of Materials Processing Technology*, vol. 129, no. 1, pp. 559–562, 2002.
- [4] X. Xu and C. Zeng, "Design of a magneto-rheological fluid clutch based on electromagnetic finite element analysis," in *Computer Engineering and Technology (ICCET), 2010 2nd International Conference on*, vol. 5, pp. V5–182, IEEE, 2010.
- [5] A. K. Kwan, T. H. Nam, and Y. Y. Il, "New approach to design mr brake using a small steel roller as a large size magnetic particle," in *Control, Automation and Systems, 2008. ICCAS 2008. International Conference on*, pp. 2640–2644, IEEE, 2008.
- [6] K. Gudmundsson, F. Jonsdottir, and F. Thorsteinsson, "A geometrical optimization of a magneto-rheological rotary brake in a prosthetic knee," *Smart Materials and Structures*, vol. 19, no. 3, p. 035023, 2010.
- [7] N. C. Rosenfeld and N. M. Wereley, "Volume-constrained optimization of magnetorheological and electrorheological valves and dampers," *Smart Materials and Structures*, vol. 13, no. 6, p. 1303, 2004.
- [8] K. Karakoc, E. J. Park, and A. Suleman, "Design considerations for an automotive magnetorheological brake," *Mechatronics*, vol. 18, no. 8, pp. 434–447, 2008.
- [9] E. J. Park, L. F. da Luz, and A. Suleman, "Multidisciplinary design optimization of

- an automotive magnetorheological brake design,” *Computers & structures*, vol. 86, no. 3, pp. 207–216, 2008.
- [10] Q. Nguyen and S. Choi, “Optimal design of an automotive magnetorheological brake considering geometric dimensions and zero-field friction heat,” *Smart Materials and Structures*, vol. 19, no. 11, p. 115024, 2010.
- [11] N. Guo, H. Du, and W. Li, “Finite element analysis and simulation evaluation of a magnetorheological valve,” *The international journal of advanced manufacturing technology*, vol. 21, no. 6, pp. 438–445, 2003.
- [12] Q. Nguyen and S. Choi, “Optimal design of a novel hybrid mr brake for motorcycles considering axial and radial magnetic flux,” *Smart Materials and Structures*, vol. 21, no. 5, p. 055003, 2012.
- [13] A. S. Shafer and M. R. Kermani, “Design and validation of a magneto-rheological clutch for practical control applications in human-friendly manipulation,” in *Robotics and Automation (ICRA), 2011 IEEE International Conference on*, pp. 4266–4271, IEEE, 2011.
- [14] A. S. Shafer and M. R. Kermani, “On the feasibility and suitability of mr fluid clutches in human-friendly manipulators,” *Mechatronics, IEEE/ASME Transactions on*, vol. 16, no. 6, pp. 1073–1082, 2011.
- [15] A. S. Shafer and M. R. Kermani, “Magneto-rheological clutch with sensors measuring electromagnetic field strength,” Apr. 14 2011. WO Patent/2011/041890.
- [16] A. S. Shafer and M. R. Kermani, “Magneto- and electro- rheological based actuators for human friendly manipulators,” Nov. 1 2009. United States Patent U.S. Provisional Patent, Serial No. 61/272,597. 2009.
- [17] Q. Nguyen and S. Choi, “Selection of magnetorheological brake types via optimal design considering maximum torque and constrained volume,” *Smart Materials and Structures*, vol. 21, no. 1, p. 015012, 2012.

- [18] M. Avraam, *MR-fluid brake design and its application to a portable muscular rehabilitation device*. PhD thesis, Ph. D. thesis, Université Libre de Bruxelles, Bruxelles, Belgium, 2009.
- [19] “Designing with mr fluids,” tech. rep., LORD. 1998”.
- [20] P. Yadmellat and M. Kermani, “Adaptive modeling of a magnetorheological clutch,” *Mechatronics, IEEE/ASME Transactions on*, in press, doi: 10.1109/T-MECH.2013.2292594.
- [21] D. Wang and W. Liao, “Magnetorheological fluid dampers: a review of parametric modelling,” *Smart Materials and Structures*, vol. 20, p. 023001, 2011.
- [22] R. Phillips, “Engineering applications of fluids with a variable yield stress,” 1969.
- [23] J. Carlson, “What makes a good mr fluid?,” *Journal of intelligent material systems and structures*, vol. 13, no. 7-8, pp. 431–435, 2002.
- [24] M. Jolly, J. Bender, and J. Carlson, “Properties and applications of commercial magnetorheological fluids,” *Journal of Intelligent Material Systems and Structures*, vol. 10, no. 1, pp. 5–13, 1999.
- [25] K. Karakoc, *Design of a Magnetorheological Brake System Based on Magnetic Circuit Optimization*. PhD thesis, University of Victoria, 2007.
- [26] P. Yadmellat, A. S. Shafer, and M. R. Kermani, “Development of a safe robot manipulator using a new actuation concept,” in *Robotics and Automation, IEEE International Conference on*, pp. 337–342, IEEE, 2013.
- [27] H. A. Wheeler, “Simple inductance formulas for radio coils,” *Proceedings of the Institute of Radio Engineers*, vol. 16, no. 10, pp. 1398–1400, 1928.

## **Chapter 4**

# **Design, Development, and Validation of a Mobile Robot Actuated by Magneto-Rheological (MR) Actuators**

In this chapter, the advantages of applying MR actuators to a mobile robot is discussed. As the MR actuator features relative high torque-mass ratio, the mobile robot actuated by MR actuators can have large driving force and also keep its own weight light. Moreover, the compliant characteristic of MR actuator decouples the mobile robot and the wheel. In this way, most components of the mobile robot is protected. Therefore, an actuator that consists of one motor and two MR clutches is proposed to implement on a mobile robot. The MR clutches are optimal designed to obtain a certain output torque with the minimum mass and power consumption. The structure and specifications of the mobile robot are reported in this chapter.

## 4.1 Introduction

The history of mobile robots can be traced back to the 1940s. People at first considered the mobile robot as a machine that was able to move automatically. With the development of mobile robots in recent years, the mobile robot has already attracted increasing attention. Nowadays, the mobile robot can be found in fields of research, industry, military and also in people's homes. Increasingly mobile robots are hired to perform housework, such as cleaning and gardening. While recent studies are mostly focused on the control and navigation of mobile robots, the actuation of the mobile robot is not discussed so frequently.

An electromagnetic motor is often employed in many mobile robots for their actuation [1, 2, 3, 4, 5] due to its simplicity and ease-of-use. There are various options of motors in terms of size, output torque and mass, so it is easy to find a proper motor for a specific mobile robot. Moreover, the linear relationship between the input and output of the motor makes the speed control of a mobile robot simple. However, in order to obtain larger driving force for a mobile robot, a powerful motor with a large output-torque range is required. Unfortunately, this kind of motor is always heavy and expensive. Though, the output torque of a motor can be expanded by using a big ratio gearbox after the output, the gearbox itself also carries huge mass which increases the mass of the mobile robot. To this end, the mobile robot has to endure heavy weight as long as the larger driving force is commanded. On the other hand, the output torque of motors is hard to control. Therefore, to keep a motor-actuated mobile robot stationary, a mechanism such as a brake is always needed on the robot. Consequently, some alternative actuators are proposed for mobile robots. For example, a cableless micro mobile robot was actuated by Giant Magnetostrictive Alloy (GMA) actuator was developed in [6]. The GMA is capable of expanding in the direction of the applied magnetic field. To this end, the displacement of GMA can be considered as the motion that actuated the mobile robot. While this design would get rid of cables from mobile robot, the small output from GMA actuator is only enough to drive micro mobile robot, which limits its applications. Another rubber actuator, Hydrogen Storage Alloy (HSA) was applied as actuation for an inpipe inspection mobile robot in [7]. Similar to the GMA actuator, HSA was designed to use gas pressure to expand its own length and

this displacement would also drive the whole robot. Compared with GMA, HSA features much more displacement and makes the robot lighter, but its own tube shape is not suitable for most mobile robots. The same concept of actuator was also proposed in [8]. A PZT was designed as an actuator for a mobile robot in water. The displacement of PZT is employed to control the "fin" of the mobile robot. Unfortunately, the output of this actuator is still not powerful enough to drive large-scale mobile robots.

In our previous body of work, we developed a new actuation mechanism known as Magneto Rheological (MR) actuator using MR clutches [9]. The MR clutch is a mechanism that consists of an input part, an output part, and MR-fluids gaps between input and output. In practice, the gaps would be filled with MR fluids whose viscosity can be changed by the applied magnetic field. Except MR clutches, the MR actuator also includes a motor as an active component whose output is connected with the input of the MR clutch. Once the motion from the motor transmits to the input of the MR clutch, the torque on the MR clutch's output part can be controlled by altering the magnetic field. The details and advantages of MR actuator have been reported in [9, 10, 11]. Thanks to the existence of MR fluids, the input and output of an MR actuator are actually decoupled by a compliant element, which protects both input and output parts. The torque-mass ration of MR actuator is relative higher than the other torque actuation. Also, the controllable bandwidth is much higher than the other compliant actuators. Moreover, inspecting the concept of an MR actuator, one active component (motor) is able to provide motion to an infinite number of semi-active components (MR clutches) due to the individual functions of an MR clutch. On the other hand, it has been also proved that the output torque of the MR actuator actually can be controlled even without any torque sensors[12].

The main contribution of this chapter first is the optimal design and the development of two MR clutches. The objective of the design is to obtain an MR clutch that can produce certain output torque with minimum mass and power consumption. Then a light mobile robot is developed by using these two optimized MR clutches and one motor. The MR clutches are not only the actuation but also the wheel mechanism of the mobile robot. Moreover, due to the output torque of the MR clutch is able to be precisely controlled, the MR clutch can be used as a brake as well. On the other hand, the compliance of MR fluids

prevents damages to the core part of mobile robot, such as the transmitting shaft and motor. And this compliance is able to provide infinite gear ratio which ensures the mobile robot actuated by MR actuators can run on any kinds of surfaces. The omni- direction of the mobile robot is achieved as each MR clutch is able to work separately.

The remaining of the paper is organized as follows. Section 4.2 discusses the optimal design of MR clutches and presents the specifications. Section 4.3 shows the mobile robot actuated by MR actuator. Section 4.4 concludes the paper.

## **4.2 Development of the MR actuator**

Unlike other actuation, the MR actuator can be considered as a torque actuation that is usually made of one Active component and Semi Active components. In common cases, the motor is a good candidate for the Active component which applies power and motion to the Semi Active components. On the other hand, the Semi Active component which is usually developed by using the MR clutch is able to distribute the power as a controllable output torque. The MR clutch can be divided into two functional parts and MR fluids are filled in the volume between these two parts. Either part could be mechanically assembled with the motor as the input of the MR clutch, and the other part would be considered as the output part. Once the power and motion from the Active component introduces shearing between input and output parts of an MR clutch, the torque on the output part can be controlled by altering the magnetic field inside the MR clutch. Moreover, one Active component can be employed to serve for a theoretically infinite number of Semi Active components, because each MR clutch works individually. To be a suitable Active component, the selected motor is only required to apply enough power to the Semi Active components in one actuation. However, to design and develop a good MR clutch, one needs to consider various factors: the maximum output torque, the mass of the MR clutch and the power consumption for example. To this end, the design of the MR clutch should be the most important issue during the development of an MR actuator.

### 4.2.1 Optimization design of the MR clutch

In order to employ MR actuators as the actuation of a mobile vehicle, the designed MR clutches should meet at least three requirements: small weight, high output and low power consumption. To this end, the multi-disk type is chosen as the configuration of the MR clutch [13] and the number of output disks is decided as four. Fig. 4.1 demonstrates the cross section of a multi-disk MR clutch in which a set of disks and two thicker plates are fixed on one shaft, while the other set of disks can be assemble with any component. In practice, either set of disks is able to be the input of the MR clutch; the other set becomes the output. Between every two disks in the same set, there are spacers to keep the distance. Therefore, a small gap called an MR-fluids gap exists between disks and MR fluids are designed to fill all MR-fluids gaps inside the MR clutch. To make the MR clutch more compact, the MR fluids gaps are reduced to 0.2 mm compared with our previous generations of MR clutches [14, 9]. The thickness of disks are fixed at 1 mm due to the manufacturing process. The electromagnetic coil is designed to be wound on the shaft directly. With this structure, the coil would feature the smallest radius and weight as long as the number of turns is known. However, to determine the rest of the dimensional parameters shown in Table 4.1, an optimization should be run under a certain objective function. Considering the above requirements, the objective function is proposed as:

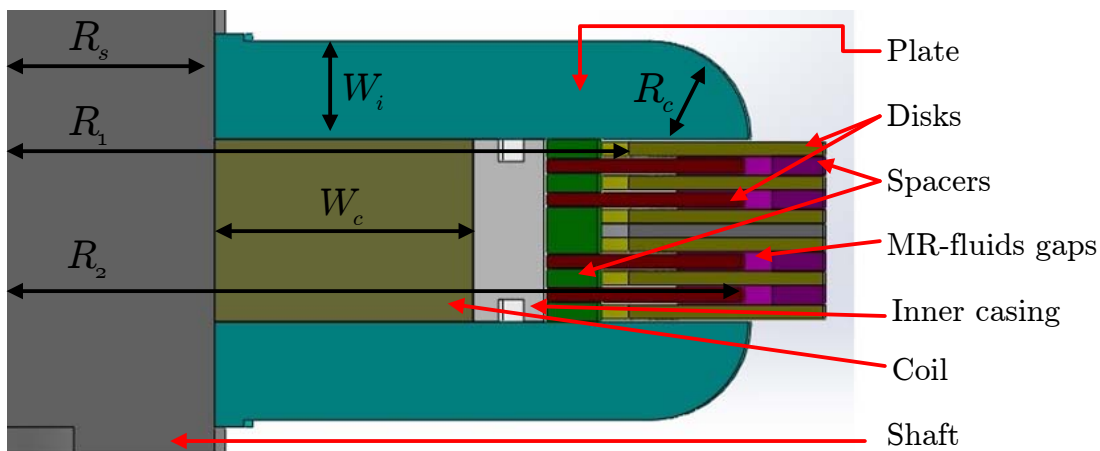


Figure 4.1: Cross section of the MR clutch without outer part.

Table 4.1: Optimized dimensional parameters of the MR clutch

Optimized Dimensions	Description
$R_s$	Radius of the shaft
$W_c$	Width of the coil
$W_h$	Width of the plates
$R_1$	Inner radius of the disks
$R_2$	Outer radius of the disks
$R_h$	Cutting radius of the plates

$$\text{Obj} = \min(W_1|T_r - T_a| + W_2M + W_3P) \quad (4.1)$$

subject to  $J_D = J_{Dmax}$

where  $W_1$ ,  $W_2$  and  $W_3$  are weighting coefficients such that  $W_1 + W_2 + W_3 = 1$ ,  $T_r$  is the desired torque,  $T_a$  is the predicted output torque of the clutch calculated by using the Bingham model,  $M$  is the mass,  $P$  is the power whose value is related to the dimension of the coil and can be obtained by using method in [13],  $J_D$  is the current density applied to the coil and  $J_{Dmax}$  is the maximum current density which is dependent on the selection of copper wires for winding coil. Applying this objective function to optimization design, the MR clutch could generate a required output torque with the smallest weight and power consumption.

Considering that the copper wires are in round shape, ideally they are aligned as a coil (see Fig. 4.2). The maximum current density can be calculated as

$$J_{Dmax} = \frac{I_{max}}{\sqrt{3}D^2} \quad (4.2)$$

where  $I_{max}$  is the maximum current that the copper wire can tolerate and  $D$  is the diameter of the copper wire. Based on the information of the maximum current of copper wires in different gauges and equation 4.2, the maximum current density of various copper wires are listed in Table 4.2. Inspecting the results, the copper wire in gauge 21 features the highest current density, which means the electromagnetic coil wound by using 21 gauge copper wires is the most powerful compared with the other coils wound in the same size but with different copper wires. To this end, 21 gauge copper wires are selected as the material for

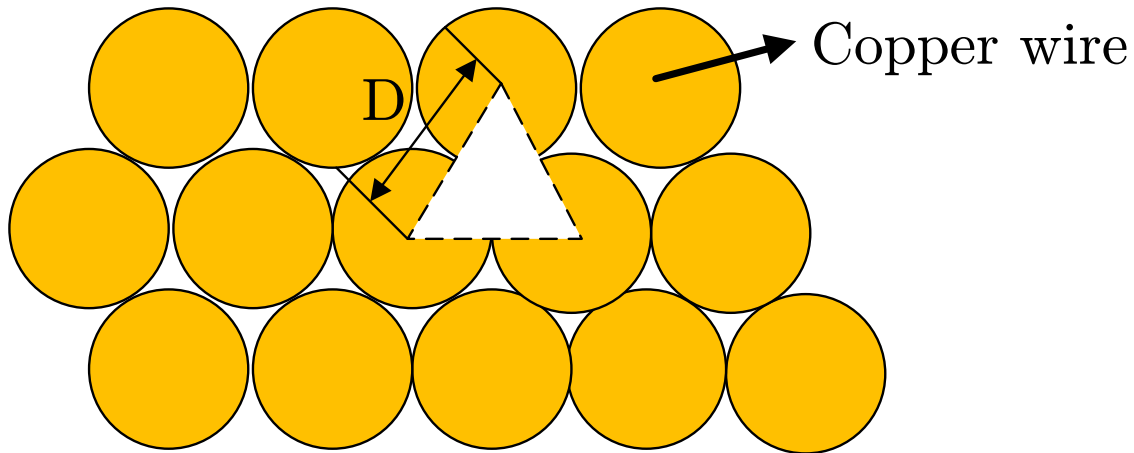


Figure 4.2: Cross section of the coil.

the electromagnetic coil. At the same time, the desired maximum output torque of the MR clutch is set as 20 Nm.  $W_1$ ,  $W_2$  and  $W_3$  are set to be 0.4, 0.3 and 0.3 respectively. Hence, the equation 4.1 can be complete with the actual numbers.

Table 4.2: Maximum current density for different gauge copper wires

Gauge of wires	Diameter (mm)	Maximum current [A]	Maximum current density [ $A/mm^2$ ]
18	1.024	16	8.816
19	0.912	14	9.721
20	0.813	11	9.613
<b>21</b>	0.724	9	<b>9.916</b>
22	0.645	7	9.710
23	0.574	4.7	8.235
24	0.511	3.5	7.753

In addition, the magnetic field distribution inside an MR clutch is related to the materials' characteristics. Therefore, the materials for the parts of an MR clutch should be determined and the information of materials should be analyzed in order to run the optimization design. Note that while the 21 gauge copper wires are chosen as the material of the coil, the materials of shaft, plates and disks in Fig. 4.1 are selected to be steel to form the magnetic circuit inside the MR clutch. However, for the sake of embedding hall

sensors to make the MR clutch behave linearly, an aluminum disk is required to be aligned with steel disks. The reasons of employing aluminum to be the material of that disk are discussed in [12]. It makes the magnetic field distribute uniformly on the disk and prevents the hysteresis affecting the reading from the Hall sensors. The inner casing, which is located between the coil and disks, is designed to separate MR fluids from the electromagnetic coil, and it is made of acrylic to ensure all magnetic flux flows through MR fluids gaps and keeps the design light. The same concerns are considered when choosing the material of spacers, making acrylic a good candidate material for them. After applying these materials' information to the considerations of optimization design, the geometrical dimensions in Table 4.1 can be optimized under the objective function 4.1.

#### **4.2.2 Mechanical Design of the MR clutch**

The application of the designed MR clutch is to drive a mobile vehicle. In order to simplify the structure of mobile vehicle, the outer part of the MR clutch which is attached to one set of disks is considered to be in the shape of a wheel. Employing the shaft and the other set of disks as the input of MR clutch, the wheel-shaped outer part would act as the output component and feature a controllable torque up to 20 Nm. To this end, the MR clutch can be considered as the actuation and also as the wheel mechanism of the mobile vehicle. The material of this part is required to be non-magnetic to prevent the leakage of magnetic field, so acrylic is used for this part as well. Moreover, the output component consists of two parts: a basin-structure shell and a cap. This structure allows assemble of all disks layer by layer, from the bottom to the top of the basin. On the other hand, MR fluids can be filled at the same time as the assembling disks, which insure the existence of MR fluids in every MR-fluids gap. The cap is located on the top of outer shell to seal the MR clutch. Fig. 4.3 demonstrates A cross section of the complete MR clutch and also the key components. Each disk has four angled fins and uses these fins to assemble with inner casing and outer shell. This angled design makes all the disks fixed in the radius direction while the pressure from the top keeps the position of the disks in axis direction. In addition, the inner and outer spacers are in the same angled shape as that of the input and output disks.

In summary, an MR clutch is developed by considering all concerns mentioned above. The specifications of the designed MR clutch are reported in Table 4.3 and the actual MR clutch is shown in Fig. 4.4.

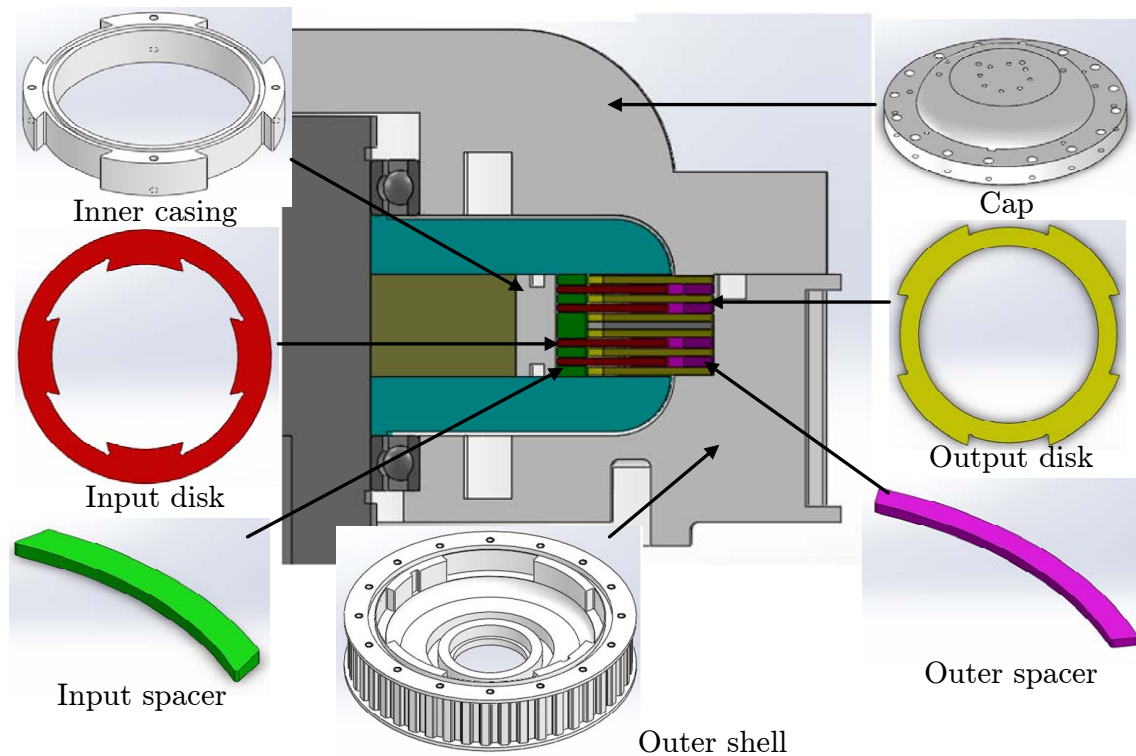


Figure 4.3: Cross section of the MR clutch.

Table 4.3: Specifications of the MR clutch

Outer diameter [mm]	149
Maximum width[mm]	62
Disk thickness[mm]	1
MR fluid gap thickness [mm]	0.2
No. of input disks	4
Maximum torque [Nm]	20
Total mass [kg]	2.2

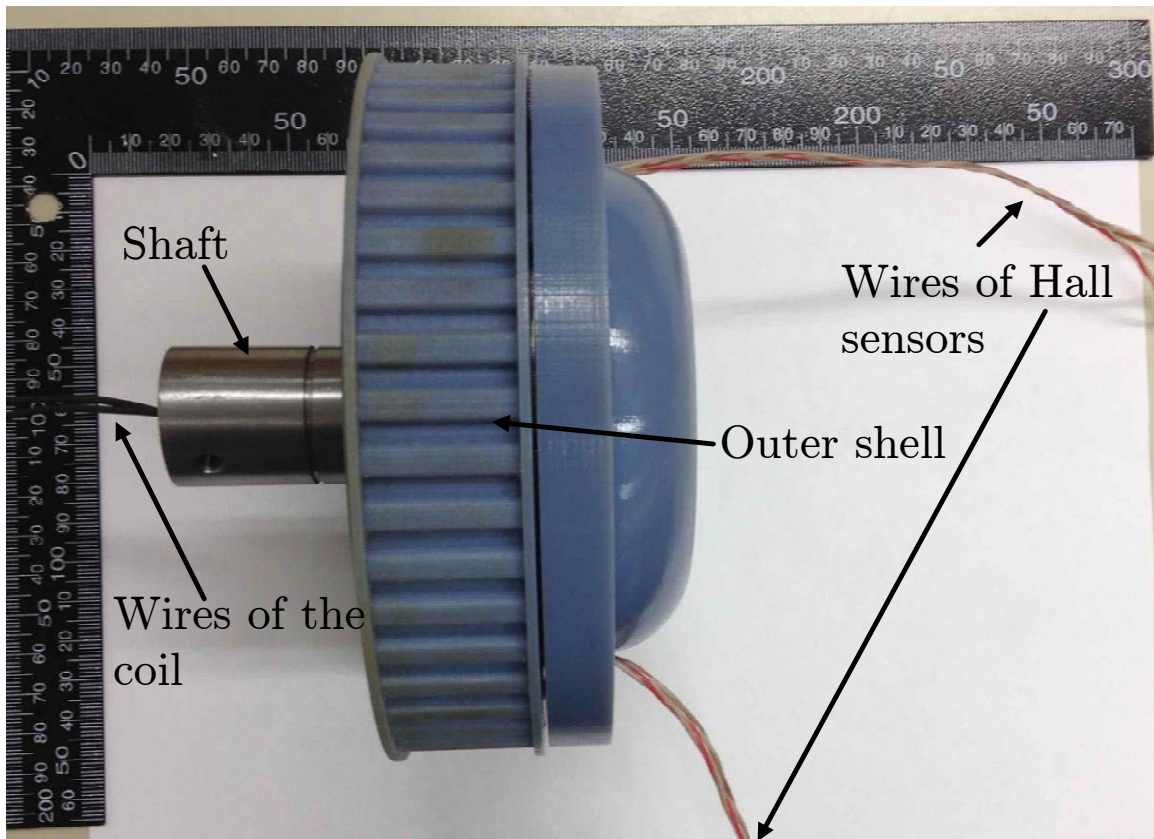


Figure 4.4: The optimal designed MR clutch.

### 4.3 Development of Mobile Robot

Fig. 4.5 shows the schematic architecture of the mobile robot. In order to demonstrate the concept effectively, an MR clutch is divided into three parts: the input, coil and output. While the inputs of two MR clutches are connected with one motor, the outputs of them are different due to the current for each coil is individually commanded by the mother board. To this end, the two front wheels are able to run in different velocities and the mobile robot can work in every direction. Moreover, the electrical devices: mother board and current drivers can keep stationary because of the use of slip rings.

The designed mobile robot has already employed the MR actuator as actuation and two MR clutches as wheel components. The structure of the mobile vehicle and its components are shown in Fig. 4.6. As observed, on the platform of the mobile vehicle, those two MR clutches are located at the rear position. Moreover, the MR clutches drive the other

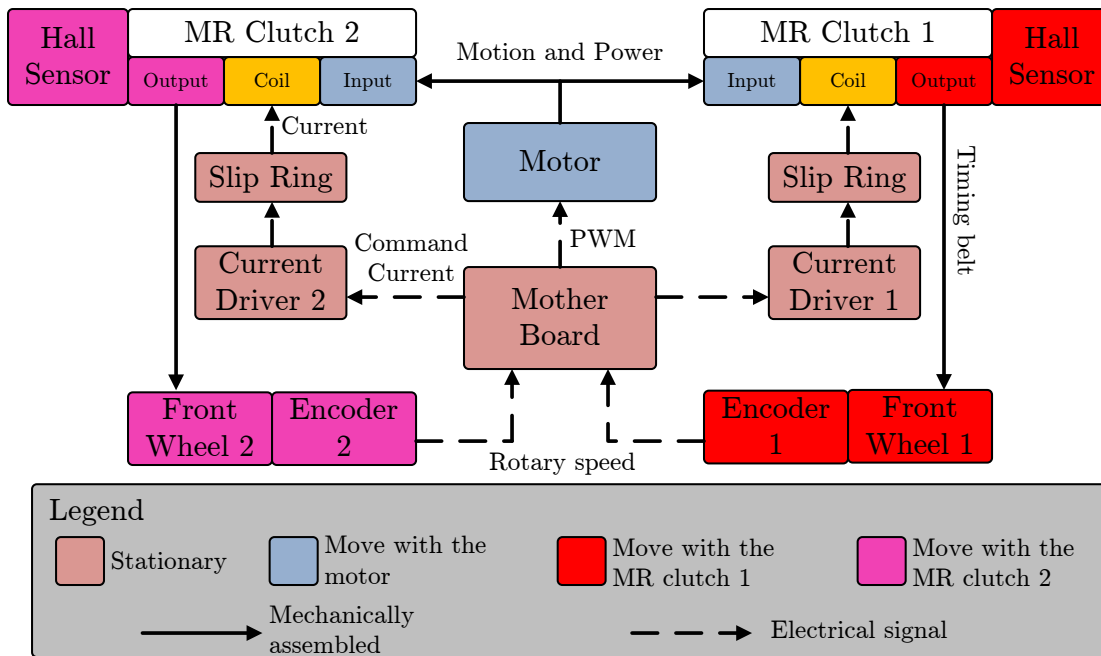


Figure 4.5: Schematic architecture of the mobile robot.

two regular wheels whose outer diameter is same as that of MR clutches in the front of the platform by using the belt transmission. A DC motor with a gearbox is settled in the middle of the mobile robot, and is employed to provide power as well as motion to both MR clutches. In order to obtain enough power to allow two MR clutches to produce the maximum torque, a belt-pulley transmission with a gear ratio is applied after the output of the motor. It should be noted that a slip ring is designed to connect copper wires from the coil with the electronic device that offers current to the coil. The slip ring is an electronic device that allows power and signal to transmit from a rotating to a stationary component. It can improve the mechanical performance and prevent the damage of wires. As mentioned above, the electromagnetic coil is fixed on the input shaft of the MR clutch and the input shaft can be rotated continuously. Therefore, employing a slip ring helps to apply currents to the coil constantly and stably.

In order to control the speed of the mobile robot, a rotary encoder is designed to be mounted on the shaft for each front wheel. Based on the information from the encoder and the outer diameter of the wheel, the speed of the mobile vehicle is easily obtained and

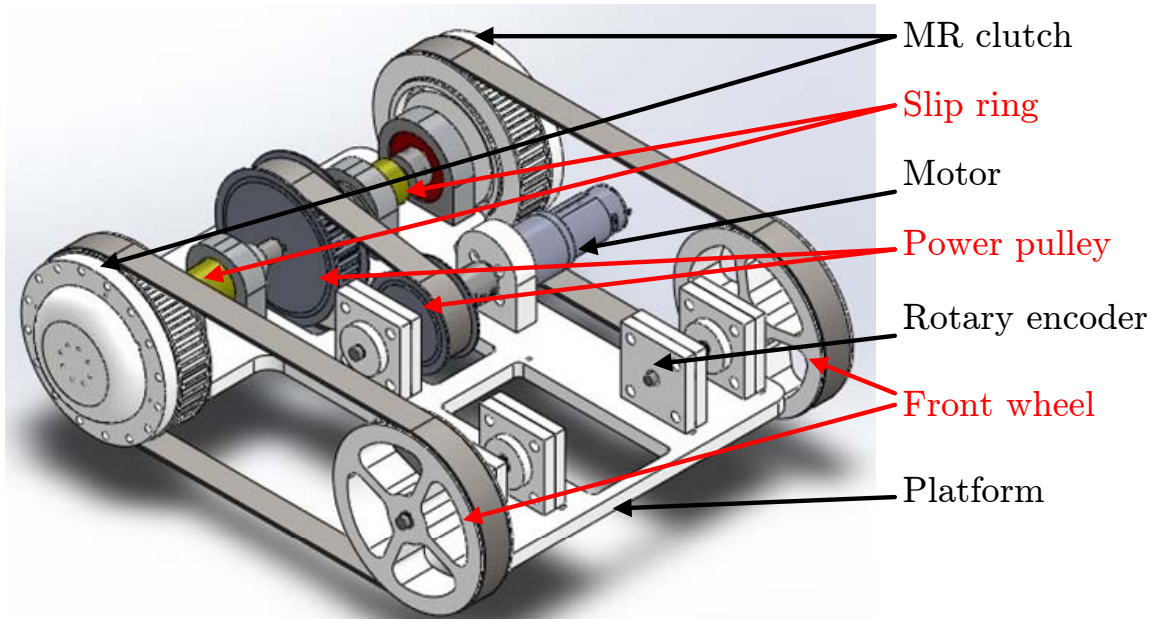


Figure 4.6: Design of the mobile robot.

controlled. Then the position of the mobile vehicle can be achieved by integrating speed with respect to time. Though the motor on the platform only works in one direction, the two clutches work individually and can control the speed on each side of the mobile robot separately. To this end, this mobile robot still features omnidirectional capability. The specifications of the designed mobile robot are reported in Table 4.4

Table 4.4: Specifications of the mobile vehicle

Maximum width [mm]	149
Maximum length [mm]	62
Ground clarence [mm]	20
Total Mass [kg]	10.2

## 4.4 Conclusion

In this chapter, the implementation of MR actuators on a mobile robot is discussed. The high torque-mass ratio of the MR actuator ensures that the mobile robot has a large driving

force and keeps the weight light. Moreover, The MR actuators can also act as brakes for the mobile robot. At the same time, the compliant transmission decouples the wheel and the other components of the mobile robot, which protects the damages to the core components. To this end, a mobile robot is designed and developed by using an MR actuator. The important candidate of the MR actuator, the MR clutch, is optimal designed by considering that generating a certain output torque with the minimum mass and power consumption.

## Bibliography

- [1] R. C. Arkin, "Motor schema-based mobile robot navigation," *The International journal of robotics research*, vol. 8, no. 4, pp. 92–112, 1989.
- [2] R. A. Brooks, "A robust layered control system for a mobile robot," *Robotics and Automation, IEEE Journal of*, vol. 2, no. 1, pp. 14–23, 1986.
- [3] R. C. Arkin, "Motor schema based navigation for a mobile robot: An approach to programming by behavior," in *Robotics and Automation. Proceedings. 1987 IEEE International Conference on*, vol. 4, pp. 264–271, IEEE, 1987.
- [4] Y. Koren and J. Borenstein, "Potential field methods and their inherent limitations for mobile robot navigation," in *Robotics and Automation, 1991. Proceedings., 1991 IEEE International Conference on*, pp. 1398–1404, IEEE, 1991.
- [5] J. R. Millan, F. Renkens, J. Mouriño, and W. Gerstner, "Noninvasive brain-actuated control of a mobile robot by human eeg," *Biomedical Engineering, IEEE Transactions on*, vol. 51, no. 6, pp. 1026–1033, 2004.
- [6] T. Fukuda, H. Hosokai, H. Ohyama, H. Hashimoto, and F. Arai, "Giant magnetostrictive alloy (gma) applications to micro mobile robot as a micro actuator without power supply cables," in *Micro Electro Mechanical Systems, 1991, MEMS'91, Proceedings. An Investigation of Micro Structures, Sensors, Actuators, Machines and Robots. IEEE*, pp. 210–215, IEEE, 1991.
- [7] T. Fukuda, H. Hosokai, and M. Uemura, "Rubber gas actuator driven by hydrogen storage alloy for in-pipe inspection mobile robot with flexible structure," in *Robotics and Automation, 1989. Proceedings., 1989 IEEE International Conference on*, pp. 1847–1852, IEEE, 1989.
- [8] T. Fukuda, A. Kawamoto, F. Arai, and H. Matsuura, "Mechanism and swimming experiment of micro mobile robot in water," in *Micro Electro Mechanical Systems, 1994, MEMS'94, Proceedings, IEEE Workshop on*, pp. 273–278, IEEE, 1994.

- [9] A. S. Shafer and M. R. Kermani, “Design and validation of a magneto-rheological clutch for practical control applications in human-friendly manipulation,” in *Robotics and Automation (ICRA), 2011 IEEE International Conference on*, pp. 4266–4271, IEEE, 2011.
- [10] A. S. Shafer and M. R. Kermani, “Magneto-rheological clutch with sensors measuring electromagnetic field strength,” Apr. 14 2011. WO Patent/2011/041890.
- [11] A. S. Shafer and M. R. Kermani, “Magneto- and electro- rheological based actuators for human friendly manipulators,” Nov. 1 2009. United States Patent U.S. Provisional Patent, Serial No. 61/272,597. 2009.
- [12] W. Li, P. Yadmellat, and M. R. Kermani, “Linearized torque actuation using fpga-controlled magneto-rheological actuators,” in *Robotics and Automation (ICRA), 2014 IEEE International Conference on*, IEEE.
- [13] W. Li, P. Yadmellat, and M. R. Kermani, “Design optimization and comparison of magneto-rheological actuators,” in *Robotics and Automation (ICRA), 2014 IEEE International Conference on*, IEEE.
- [14] P. Yadmellat, A. S. Shafer, and M. R. Kermani, “Design and development of a single-motor, two-dof, safe manipulator,”

# Chapter 5

## Conclusion and Future Works

### 5.1 Conclusion

In this thesis, first, a new way to linearize the behavior of an MR actuator is proposed and developed. Unlike the hysteretic relationship between the input current and output torque, the magnetic flux density inside the MR clutch features an one-to-one relation to the output torque. To this end, a Hall sensor that is embedded in the MR clutch is employed to collect the magnetic field information. The position of the Hall sensor is studied as well by using Finite Element Analysis (FEA). It indicates that a Hall sensor is required to be embedded in a non-hysteretic disk, so the hysteresis would not effect the reading from the Hall sensor. Moreover, the analysis also demonstrates that the magnetic flux density is not sensitive with the radius of disk. Considering these facts, a Hall sensor is fixed on an aluminum disk in the MR clutch. Theoretically, as long as the magnetic field information is obtained, the output torque of an MR clutch can be easily calculated by using the Bingham model. However, the dynamic characteristics of components, such as shaft and coil introduce the error between the actual output torque and the calculated torque from the Bingham model. Therefore, a dynamic model is studied to eliminate that error. This model is developed by using MATLAB Identification toolbox with Multi-Sine and Swept-Sine signals. The experimental results show that the estimated torque is much more accurate than those without using dynamic model. Thus, a closed-loop control scheme is developed to linearize the behavior of an MR actuator. The feedback signal of this control

scheme is the magnetic flux density acquired by the Hall sensor. Then the magnetic flux density is employed to estimate the output torque by using a proposed model that consists of the Bingham and the dynamic models. A PID controller is applied to compensate the error between the estimated and desired torques. Moreover, the whole control scheme is implemented on an FPGA circuit board that also can be embedded on an MR clutch. This design simplifies the structure of MR actuator as a linear torque actuation. The experimental results validate the effectiveness of the proposed control scheme. It proves that our control scheme can obtain competitive results compared with the results acquired by a torque/force sensor involved closed-loop control scheme. However, our control scheme is able to get rid of torque/force sensors which are usually heavy and expensive.

Second, a novel optimization design of MR clutches is proposed, and based on this optimization characteristics of MR clutches in different configurations are compared. In order to select an applicable configuration of MR clutch, the difference among configurations should be analyzed and compared, but it is difficult to summarize the characteristics. In fact, except specific parameters can be obtained theoretically, such as the output torque and dynamic range, there are various dimensional parameters uncertain before designing an MR clutch. Therefore, a reasonable optimization design is developed and dimensional parameters are determined under this optimization design, which makes all configurations of MR clutches comparable. Considering all factors that should be concerned of MR clutches, the input power and output torque are the only two parameters that can be known before designing, which are also the only two parameters in the process of the optimization. The object function of the proposed optimization aims to minimize the mass of the MR clutch with known input power and output torque. Three common configurations of MR clutches: drum, single-disk and multi-disk, are optimally designed and their characteristics, such as torque-mass ratio and friction are compared. People can select a suitable configuration based on this comparison before designing an MR clutch. Moreover, for multi-disk MR clutch, the number of disks and the MR-fluids gap size are also recognized as design considerations and their effects are reported. It indicates that for certain input power and output torque, there is an ideal number of disks to minimize the mass. On the other hand, the small size of MR-fluids gaps would dramatically make the MR clutch compact

and light, but it also require electronic devices with high current capacity.

Third, a mobile robot is accomplished by using MR actuators as actuation. To be a good candidate for mobile robot actuation, an MR clutch in the MR actuator is optimal designed by minimizing the mass and power consumption with a certain requirement of output torque. Meanwhile, the most part of MR clutch is made of plastic to keep it light and MR-fluid gaps are small to make it compact. Two Hall sensors are embedded into on clutch to make it behave linearly. Moreover a circuit board based on Bluetooth communication is mounted on the clutch as well to send the magnetic field information wirelessly. In order to simplify the structure of mobile robot, MR clutches are also designed as wheel mechanism. The omnidirectional movement of mobile robot is achieves by only employing two MR clutches and one motor, because each MR clutch is able to work individually even actived by one motor. Due to the MR actuator can be consider as an actuation whose output torque can be accurately controlled without torque sensors, the MR clutches on the mobile robot is able to act as brakes. To this end, this mobile robot can stop at a position with incline degrees even without running motor. Moreover, MR fluids inside the MR clutch provide infinite gear ratio to the mobile robot, which makes it more efficient. Lastly, the compliance introduced by MR fluids decouple the wheel and the body part of mobile robot. In this way, the core parts, such as transmitting shaft and electronic devices are safer than mobile robots which use other actuation.

## **5.2 Future Works**

### **Development of MR clutches**

In our current design of MR clutches, the Hall sensor is embedded on an aluminum disk inside the MR clutch. Though the aluminum disk provides a non-hysteretic environment to Hall sensors and makes the reading clear, the huge reluctance of the aluminum disk sacrifices the performance of the MR clutch. Compared with steel, aluminum features relative permeability as 1, which means the reluctance of one aluminum disk is thousand time to that of a steel disk. While the relative permeability of MR fluids ranges at tens, the thickness of MR-fluid gaps is much smaller than the thickness of aluminum disk. To this end,

the most part of total reluctance is determined by the aluminum disk and the value of it is huge. A simulation is performed to validate this concept. The COMSOL model in Chapter 4 is rebuilt by using 0.5 mm and 0.3 mm MR-fluid gaps and the output torque results are reported in Table 5.1. As observed, there are minor difference among those models. This result is against the conclusion in Chapter 3, which is acquired from MR clutches without aluminum disks. Therefore, if the aluminum disk can be removed from MR clutch, it would make the MR clutch more compact and lighter. An alternative way to get rid of the aluminum disk is to proposed a new design of MR clutch in which the Hall sensor can be placed in a new location, or the aluminum disk can be replaced with a disk that is made of non-hysteretic and high relative permeability material. Instead of removing the aluminum disk, a thinner aluminum disk can be used with Hall effect element, which would reduce the reluctance as well. On the other hand, the use of electromagnetic coil is very constrained at this moment. The maximum current to the coil is obtained from experience. A method to improve the effectiveness of coil is to embed a temperature sensor in the clutch to measure the coil temperature. Based on this information, the maximum current to the coil can be easily found. Though the time constant of current is small, the response time of output torque is much larger, which is related to the design of magnetic circuit. To this end, a dynamic magnetic field analysis is necessary in further study.

Table 5.1: Comparison of output torque among MR clutches with different MR-fluid gaps sizes.

Output	MR-fluid gap size [mm]		
Torque	0.2	0.3	0.5
[Nm]	19.1	18	17.1

### Control and Navigation of Mobile Robot

At this point, there is no enough time to design a specific controller and navigation plan for the mobile robot. In fact, on the mobile robot, there are rotary encoders that can be employed to achieve the speed information, and also the Hall sensors which enable to con-

trol driving force of mobile robot. To this end, the future navigation can be accomplished by controlling noth speed and driving force or either of them, Moreover, the use of MR actuator as a brake needs to be further studied.

### **Implementation of Mobile Robot**

The implementation of MR actuators on mobile robot is not so mature. Various improvements should be addressed for next generation of mobile robot. For example, the power pulley can be eliminated by using transmitting shaft directly.

# Curriculum Vitae

**Name:** Wenjun Li

**Post-Secondary** The University of Western Ontario

**Education and** London, Ontario, Canada

**Degrees:** 2011 - 2014 M.E.Sc.

Electrical and Computer Engineering Dept., Robotics and Control

Beihang University

Beijing, China

2007 - 2011 B.E.Sc.

School of Automation Science and Electrical Engineering

**Related Work** Teaching Assistant

**Experience:** The University of Western Ontario

2012 - 2014

## Related Publications:

Li W., Yadmellat P., Kermani M.R., "Linearized Torque Actuation using FPGA-Controlled Magneto-Rheological Actuators," Accepted by IEEE/ASME Transactions on Mechatronics.

Li W., Yadmellat P., Kermani M.R., "Linearized Torque Actuation using FPGA-Controlled

Magneto-Rheological Actuators,” Accepted by IEEE International Conference of Robotics and Automation (ICRA) 2014.

Li W., Yadmellat P., Kermani M.R., “Design Optimization and Comparison of Magneto-Rheological Actuators,” Accepted by IEEE International Conference of Robotics and Automation (ICRA) 2014.